Technische Universität München

TUM School of Engineering and Design

Theory to Practice: Design, Integration and Applications for an Active Distribution Grid Laboratory

Anurag Mohapatra

Vollständiger Abdruck der von der TUM School of Engineering and Design der Technischen Universität München zur Erlangung eines

Doktors der Ingenieurwissenschaften (Dr.-Ing.)

genehmigten Dissertation.

Vorsitz:

Prof. Dr.-Ing. Andreas Jossen

Prüfende der Dissertation:

Prof. Dr. rer. nat. Thomas Hamacher

Prof. Reinaldo Tonkoski Junior, Ph.D.

Die Dissertation wurde am 20.11.2023 bei der Technischen Universität München eingereicht und durch die TUM School of Engineering and Design am 19.04.2024 angenommen.

Abstract

Anthropological climate change has begun and a key mitigation measure is the drastic decarbonisation of electrical, heat and transportation sectors through renewable energy resources. This 'green transition' requires building intelligence in the active power distribution grids to control the intermittent renewable generation and the electrification of all energy sectors. Sophisticated laboratory and experiment setups are necessary to fortify and validate the operation and control ideas for these active distribution grids.

This thesis chronicles commissioning challenges and subsequent application cases of a state-of-the-art active distribution grid laboratory at the Technical University of Munich. Specifically, it investigates a distributed measurement concept, an universal observation platform using Internet of Things tool and a power hardware in the loop framework for experiment design. These individual ideas are built upon technical constraints of fidelity with a real distribution grid and prosumers, a lack of centralised computation capacity within a distribution grid, access to only local measurements and unpredictable communication delays, while fostering collaborative and simultaneous research.

Three distinct applications of the laboratory are presented to showcase its capacity as an investigative tool for active distribution grid control and operation research. The first application shows a phasor measurement unit being implemented as a pure software bundle in the laboratory through shared embedded resources. The second application is an experimental validation of an optimised operation algorithm for such grids, which had only been presented in literature as simulation with favourable assumptions. The third application is a concept of a formally verified grid frequency controller through reachability analysis, which has been recently proposed as a promising tool within power systems community. It uses the emulation features of the laboratory to recreate the dynamic response of absent machines with controllable inverters.

The collected works within this thesis provide best practices to design the control system for active distribution grid laboratory in a research institute. It also presents several first time applications of a real active distribution grid and power hardware emulators, for system test of previously simulated grid operation and control algorithms.

Zusammenfassung

Der anthropogene Klimawandel hat begonnen und eine wichtige Maßnahme zur Minderung dieses Phänomens besteht in der drastischen Dekarbonisierung der Sektoren Elektrizität, Wärme und Verkehr durch erneuerbare Energiequellen. Diese "Green Transition" erfordert die Integration von Intelligenz in die aktiven Stromverteilungsnetze, um die unstetige erneuerbare Energieerzeugung und die Elektrifizierung aller Energiesektoren zu steuern. Ausgefeilte Labor- und Versuchsaufbauten sind notwendig, um die Betriebs- und Steuerungskonzepte für diese aktiven Verteilnetze zu festigen und zu validieren.

Diese Dissertation dokumentiert Herausforderung in der Inbetriebnahme und anschließende Anwendungsfälle eines innovativen Labors für aktive Verteilungsnetze an der Technischen Universität München. Konkret werden ein verteiltes Messkonzept, eine universelle Beobachtungsplattform unter Verwendung von 'Internet of Things', und ein Power-Hardware-in-the-Loop Konzept für die Experimente untersucht. Diese einzelnen Ideen basieren auf technischen Einschränkungen in Bezug auf die realitätsgetreue Nachbildung eines realen Verteilungsnetzes und der Prosumer, einem Mangel an zentraler Rechenkapazität innerhalb eines Verteilungsnetzes, Zugriff auf ausschließlich lokale Messungen und unvorhersehbare Kommunikationsverzögerungen, während kooperative Forschung gefördert wird.

Es werden drei verschiedene Anwendungen des Labors vorgestellt, um seine Fähigkeit als Forschungswerkzeug für die Steuerung und den Betrieb aktiver Verteilnetze zu demonstrieren. Die erste Anwendung zeigt eine "Phasor Measurement Unit", die im Labor als reine Softwarelösung durch gemeinsam genutzte embedded Ressourcen implementiert wird. Die zweite Anwendung ist eine experimentelle Validierung eines optimierten Betriebsalgorithmus für solche Netze, welche in der Literatur bisher nur durch Simulation mit vorteilhaften Annahmen gezeigt wurde. Bei der dritten Anwendung handelt es sich um das Konzept eines formal verifizierten Netzfrequenzreglers durch "Reachability Analysis", welches ein vielversprechendes Werkzeug in der Energieversorgungsbranche vorgestellt wurde. Es nutzt die Emulationsmöglichkeiten des Labors, um das dynamische Verhalten von fehlenden Maschinen mit steuerbaren Wechselrichtern nachzubilden.

Die gesammelten Arbeiten dieser Dissertation bieten bewährte Verfahren für die Entwicklung eines Steuerungssystems für ein aktives Verteilnetzlabor in einem Forschungsinstitut. Außerdem werden mehrere erstmalige Anwendungen eines realen aktiven Verteilernetzes und Power-Hardware-Emulatoren für Systemtests von zuvor simuliertem Netzbetrieb und Steuerungsalgorithmen vorgestellt.

Acknowledgments

This document exists because about five years ago I decided that, doing something I enjoyed daily is maybe as good a strategy as planning years in advance. I did not know if that joy would persist till today. It does and here is my attempt to thank an overwhelming list of people for that.

I thank Prof. Thomas Hamacher for giving me the opportunity to find my way - letting me break things and allowing me the time to fix them. Above everything, showing me that idealism is not incompatible with the real world.

I thank Dr. Vedran Peric, my daily PhD mentor and closest collaborator, for teaching me how to navigate this phase of my life as a doctorate student, develop the correct research ethic and consistently providing the best feedback for my papers and presentations.

I would then like to thank my brothers, Soner Candas and Leonhard Odersky, for being an integral part of why I looked forward to a 40 minutes commute to Garching. We have taken this journey together and maybe we grew a bit because of each other. Here's to finding family in a foreign land!

To my closest CoSES companions, Daniel Zinsmeister, Franz Christange and Thomas Lickleder - this was really fun! I would gladly accept the next project of building a lab in an empty basement, if you guys are around.

My other colleagues of past and present, many of whom I regard as friends, thank you for the lunch breaks, the coffees and the beers. I cherish the fact that I met you all.

My sincerest gratitude for my friend, Erhan Sezgin with whom I did my first experiments in the lab. I am grateful to my students, especially the trio of Matthias Mayr, Martin Cornejo and Steffen Büttner, who became my co-authors for the work presented in this thesis. It is cliched, but I did learn way more from them than I could have ever taught them.

I thank the research community for accepting and also questioning my work. They have ensured that my next contribution has every chance to be better than what came before.

I am appreciative of my family's unconditional support for me to pursue my academic ambitions. Maybe I should say this more often.

Finally, I would like to mention the one person who has always, in her own way, made me a better person. To Aradhana, thank you for being you.

Contents

List of Figures

List of Tables

Chapter 1

Introduction

History shows again and again
How nature points out the folly of men

Donald Roeser

Technologies which truly transform the world, must reach a point where we stop noticing them. The invention of electricity was a milestone for humanity, but the true miracle was harnessing this natural phenomena into an useful power delivery infrastructure. There exists an elegant bond between the angular momentum of the mechanical shaft of a synchronous generator and the electrical power demanded by the loads [1]. This bond has a built-in stability and also motivates an universally available currency - the grid frequency, to monitor the health and control our grid.

Furthermore, the electric power is delivered from the central generation points to the geographically spread out loads. If we had to imagine this as a network of roads, it would be a mostly one-way traffic from the generation plants to the load centers. This property has operational and economic benefits. The grid protection services can be simplified and transformer designs can be optimized. In distribution grids, substations can forego precise monitoring along the length of individual feeders due to a known dropping voltage profile between the ends of the line. The cost of each grid equipment can be also optimized to work for an unidirectional energy flow.

The natural inertia of the power systems, the universal presence of a synchronized grid frequency and the unidirectional energy flow, have provided us with a stable foundation to streamline the variables for efficient design of the power grid. We built generation, transmission and distribution infrastructure to last for decades with little changes during their lifetime. The associated industries thrived by focusing on the logistics of the production line, with a rather incremental research and development cycle.

1.1 Evolving power grids

The required transition to a fossil-fuel free electrical grid has forced the hand of the power grid industry [2]. The founding tenets of the traditional power systems do not hold true under a high penetration of renewable resources [3]. Firstly, it introduces a stark

seasonality and diurnal intermittency into the stable generation profile of a fossil-fuel fired power plants. Next, power electronic converters must replace synchronous machines as our primary generation equipment [4]. These two changes alone, rob the grid off the inherent stability derived from a reliable base load generation and inertia of the rotating machines. Power electronic converters have no inherent electro-mechanical coupling with the grid and thus the frequency stops being a direct measure of the instantaneous mismatch between generation and load. Fig. 1.1 shows the trend in system inertia of the Great Britain power grid. It is fairly straightforward to observe that due to the increased renewable generation from 2008 till 2019, the system inertia of Great Britain grid has dropped significantly and the reliable operation limits, in red, are being breached for some days of the year, with the safety margins being reduced for a larger percentage of days.

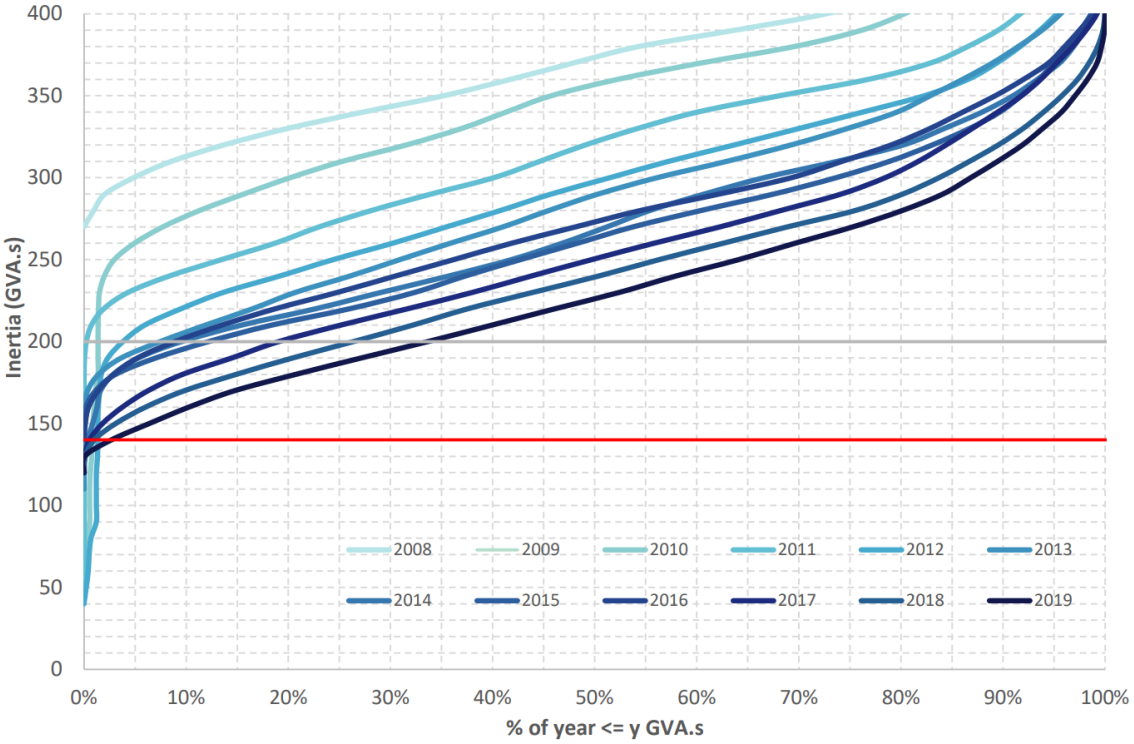

Figure 1.1: Change in system inertia due to a changing generation mix from 2008 - 2019, for the Great Britain power grid as measured by the system operator National Grid ESO [5]

Additionally, renewable generation potential is spread out across the grid. Renewably generated electricity, such as from a rooftop PV array, can be fed into the consumer loads through an inverter costing a few thousand euros. This leads to a distributed generation portfolio and the rise of the renewable distributed generation resources (DER). Combining the intermittent DERs with the power electronic converter capabilities elevates energy storage devices to critical grid component status. The notion of unidirectional energy flow is thus challenged by DERs, sector coupling and energy storage elements now being located at nodes which hosted only passive loads in the past [6].

Naturally, the transformation pathways of energy grids have become one of the top

worldwide drivers of research and innovation. The problem statement can be constructed as, *try to find ways to convert every generation unit into an emission free renewable energy source, while sacrificing as little as possible on consumer comfort and keeping step with the growing sophistication of our energy use cases.* The challenge remains significant, but we also possess new tools to combat them. For example, power electronic converters lack the mechanical inertia of synchronous machines and thus reduce the stability margins of the power grid. But their lack of inertia allows them to react much faster than synchronous machines. Power electronic converters, with the correct control strategy, can ramp up and down to maintain the previous stability margins [7].

1.2 Definitions and history

New fields of research have emerged to facilitate the transformation towards renewable energy based smart grids. Power system research groups are working on load sharing over inverters, plug and play inverter operation, advanced instrumentation for distribution grids, protection schemes for inverters, prosumer operation, demand side flexibility, sector-coupled operation, islanded grids, peer to peer energy trading and new energy markets, to name a few. Three of the research directions pertinent to this thesis are :

- Microgrids or Active distribution grids (ADG),
- Real-time (RT) computation, and
- Power Hardware-in-the-loop.

Before proceeding any further, we shall look into their definitions, research history, and the role they play in the overall goal of *green leap* taken by the power grid.

1.2.1 Microgrids / Active distribution grids

The concept of a microgrid was formally introduced in 2001 at the IEEE Winter Meeting panel on *Role of distributed generation in reinforcing the critical power infrastructure* by Bob Lasseter [8]. It was motivated by the advent of renewable energy resources and small fossil-fuel technologies such as micro-turbines under 100 kW. The paper defines microgrids as,

> A cluster of micro-sources, storage systems and loads which presents itself to the grid as a single entity that can respond to central control signals.

Since then, the microgrid concept has embraced the ADG philosophy [9][10]. Now the term microgrid is used loosely to represent any distribution grid, rendered *active* by the transformation of erstwhile passive load nodes into prosumer (*pro*ducer + con*sumer*) nodes through DERs and storage systems [11]. Coupling an electrical microgrid with the heating and transportation sectors adds a further dimension to the term. A typical microgrid representation is shown in Fig. 1.2. For consistency, we will use the term ADG in the remainder of this thesis for all instances of Microgrid/ADG references.

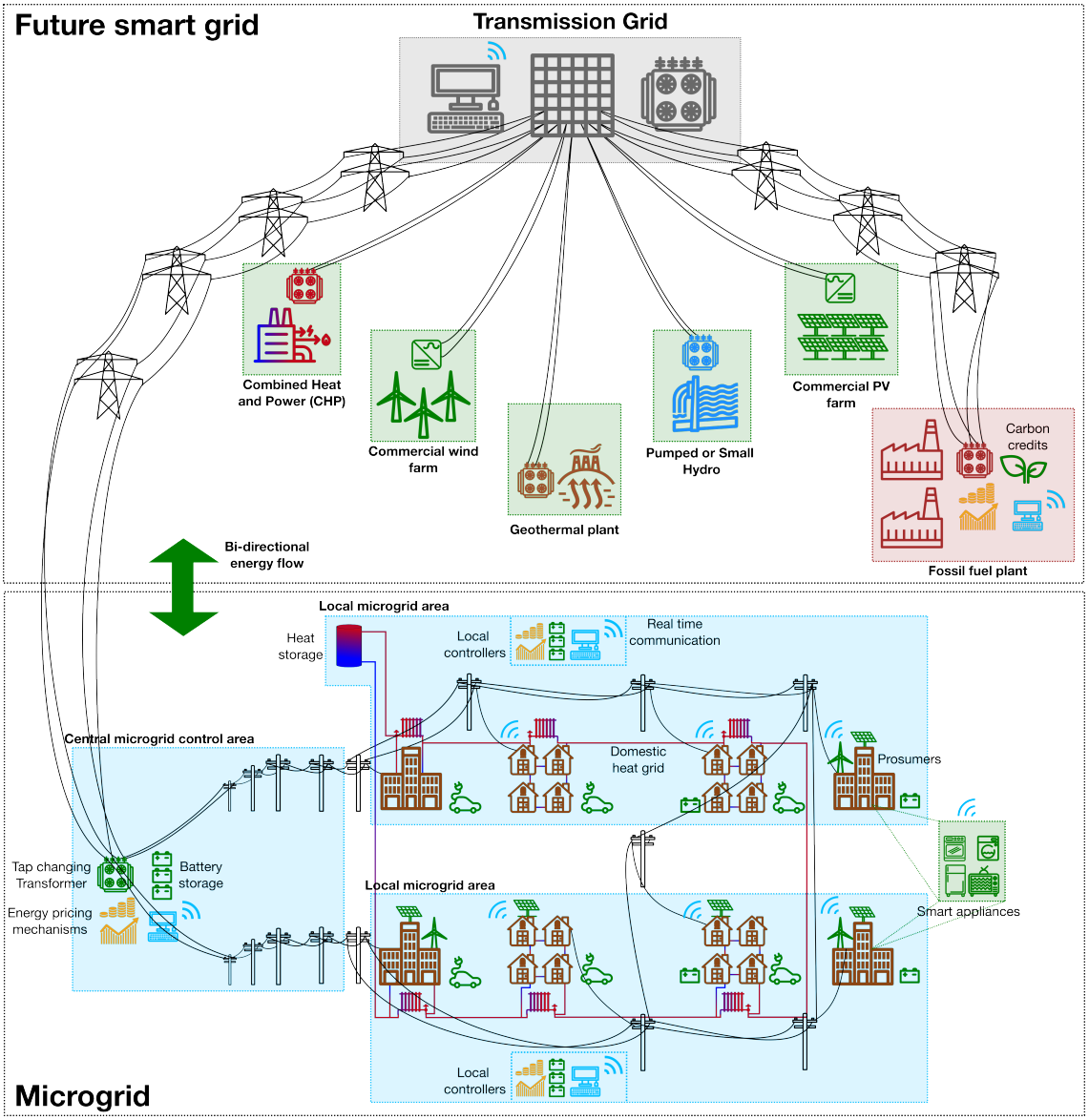

Figure 1.2: A schematic for a typical intelligent sector-coupled microgrid/ADG as popularised in literature.

ADG are also characterised by a deeper integration of information and communication technologies (ICT) as opposed to traditional power grids. This is both a necessity, due to the intermittent nature of DERs, and also a feature, to increase the quality of consumer service [12]. Each power electronic converter requires a local controller for current or voltage control. However this controller board generally has an internet connection, and can therefore receive external control setpoints. This creates an opportunity to implement optimal operation within the ADG by enabling coordination between prosumer nodes. Further extensions can also include optimised storage operation, local energy markets and smart devices, to name a few.

A key feature of the concept proposed in [8] was the nature of the interface between the

ADG and the upstream grid. The interface, also known as point of common coupling (PCC), should essentially isolate the two sides electrically but keep them coupled economically. The electrical control separation allows significant divergence from standard operation, tolerances and protection schemes inside an ADG. These adaptations are deemed necessary to accommodate the switching power electronics and reduce investment costs. The IEEE 1547, Standard for Interconnecting Distributed Resources with Electric Power Systems [13], is one such adaptation where ADG operation and reliability metrics have been adjusted as compared to a traditional power grid, to allow greater renewable deployment.

1.2.2 RT computation in Power systems

The use of computers in power system research started in the 60's. Notable among them was the work of Hermann Dommel at TU Munich in 1967 [14]. In his work, he used a computer program to calculate electromagnetic transients by programming an algorithm to integrate ordinary differential equations using the trapezoidal rule. During the turn of the 90's decade, the concept of RT computation to analyse transients was introduced in power systems [15]. It was positioned as a training tool for operational planning exercises where new operators could learn without the fear of damaging the real grid. The first commercial RT digital simulator (RTDS) was presented by RTDS Technologies in 1991 [16]. Over time, the progress in parallel processing and digital signal processing (DSP) has led to RT simulations being part of every power system research laboratory.

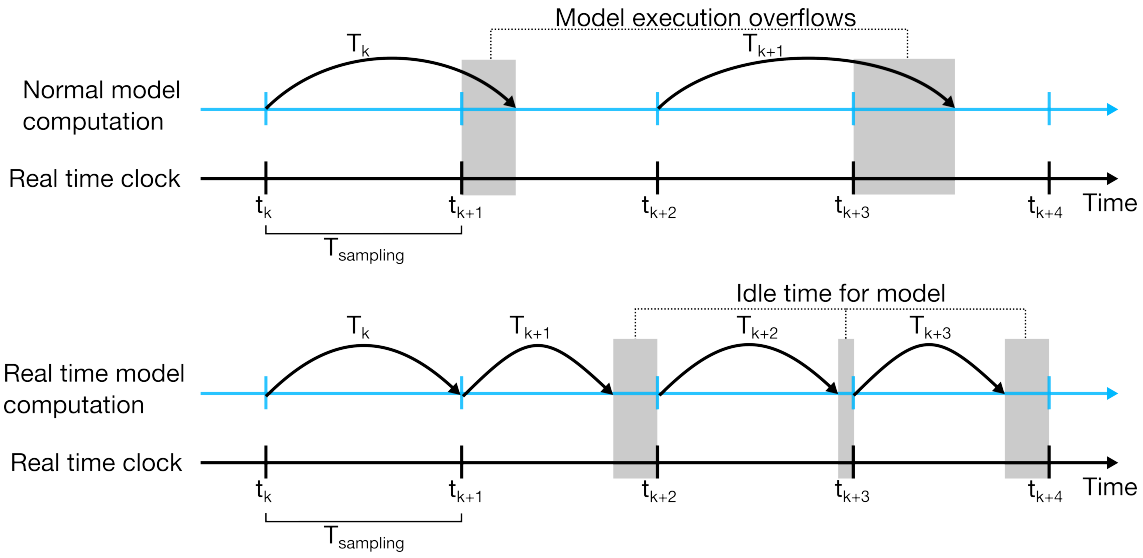

Figure 1.3: A comparison between RT and normal model execution as compared to a RT clock.

A simulation is termed as *Real-Time* if the execution time of the simulation model in a computer is shorter or equal to the model time-step [16]. In Fig. 1.3, the top graphic represents a simulation model with a given model execution time-step of $T_{sampling}$. But the processor takes more time per step to finish the model execution and this leads to overflows in execution. If the simulations are connected to a real control hardware feedback, such overflows will lead to erroneous simulation of the model. On the other hand, the

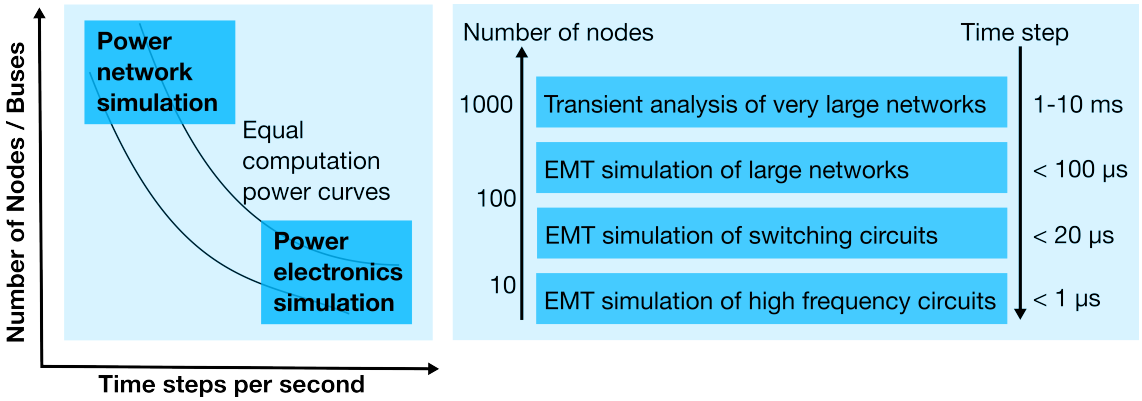

Figure 1.4: An illustration of computation requirements for different RT simulations and their typical time-steps.[16]

bottom graphic in Fig. 1.3 shows a RT simulation model being executed within the model time-step and most times leaving an idle time for the processor before the next timed execution begins. This idle time can be used by the processor for other tasks or be allotted to other RT simulation models. Most RT simulators also support parallel computing across multiple RT processor cores to handle multiple RT simulations models at the same time.

RT simulations must find the right balance between size of the model and the desired accuracy of the results, which is generally represented by time step of the simulation, as shown in Fig. 1.4. Today, one can broadly classify all RT simulations for electrical systems into two families,

1. Stability analysis simulations

2. Electromagnetic Transients (EMT) simulations

Stability analysis simulations try to encapsulate an entire grid and are useful to analyse long-term transients of the network. These are large models but the simulation time step is also kept large, as the transients below a certain timescale are neglected. EMT simulations are used to reproduce the short-term transients within the network and are needed to faithfully model power electronics devices. They model an individual device or a part of the grid with greater detail than stability analysis models and have a smaller time step for greater accuracy.

All RTDS systems have the same generic structure with minor differences due to manufacturer IPs. A general purpose host computer is used to prepare the model, deploy it on the RT hardware and observe the simulation results. Input-Output (IO) terminal cards interface the RTDS to real hardware or other computers. Multiple parallel processors and Field programmable gate array (FPGA) boards are used to run the RT simulations. FPGA boards are especially useful for EMT simulations [17]. The RTDS software environment is able to simulate high frequency switching circuits, preferably on the FPGAs, and combine them with a power system simulation running, with several orders of magnitude larger time step, on the parallel processors. FPGA boards are also used to generate switching signals for a real inverter connected to a grid simulation running on the RTDS system.

The host computer uses a standard operating system (OS) such as Windows or Linux. An application software is needed to create offline models, deploy them on the RT processor and log the signals. Some RTDS vendors use MATLAB and LabVIEW as the basis application with their proprietary functions added as an optional toolbox. Other vendors, such as Typhoon HIL, provide their own simulation environment to create the RT models. The RT processor also requires an OS, such as RTLinux or VxWorks. A Real-time OS (RTOS) is event-based, where the priority of concurrently occurring events can be dynamically reallocated to make sure certain tasks are always processed within the constraints of RT [18]. RTOS' are important for real world application where the priority of a task is not constant. As an example, consider the operating system governing the electronics in a car. The driver tries to adjust a mirror position through the central console, while applying the brakes as the car approaches a traffic stop. Clearly, safely stopping the car at the traffic stop has a higher real world priority than adjusting the mirror. Even if both the events occurred at the same time, a RTOS would prioritize finishing the braking operation within the acceptable latency while downgrading the window adjustment and allowing a variable delay in reacting to such a signal.

RT simulations provide a sensible alternative to the real systems for the early stage development of a product. However, they cannot be considered a validation step due to the lack of any real hardware or measurements. RT simulations also depend on fixed time step solvers to perform the simulations. Such solvers struggle with stiff differential equations which are common in power system differential algebraic equations (DAE)[19].

1.2.3 Power Hardware-in-the-loop

Hardware-in-the-loop (HIL) concepts were motivated in mid-90's by the rapid prototyping needs of the quickly growing power electronics industry [20][21]. The increased accuracy of solvers and computation power at hand on an embedded processor, created an opportunity for the developers to reduce the time-to-market for a power electronics based product. A device under development could be quickly validated against a model of the use case real environment on a table-top RTDS. While the RT model of the use case was not 100% accurate, it was sophisticated enough to prevent developers from chasing obvious dead-ends early in the development cycle. In the power systems community, two versions of HIL have been explored and their representative schematic is shown in Fig. 1.5,

1. Controller Hardware-in-the-loop (CHIL) and

2. Power Hardware-in-the-loop (PHIL).

In CHIL, a real controller board is connected to a simulated RT model. The real controller features can be tested by simulating specific scenarios in the RT model. The exchange of information from the real board to the RT model happens over signal voltages and thus at ultra-low power levels. In PHIL, the hardware under test (HUT) handles real power. A voltage or current source in the RT model is a real HUT. Conservation of energy is enforced at the interface between the HUT and RT model and real power is virtually exchanged with the RT environment. This is useful when the developer has access to a real power equipment but not a controlled electrical grid. A good example is show in [22]

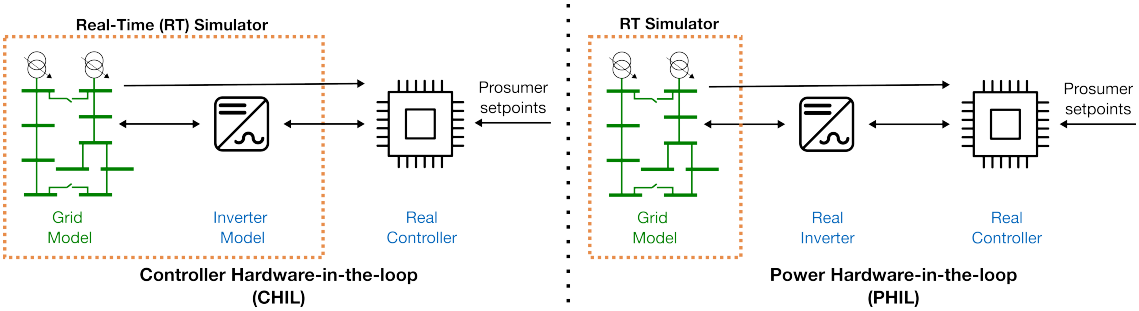

Figure 1.5: A schematic description of the differences between CHIL and PHIL test-beds.

where a real inverter is connected to a RTDS running a model of an inverter acting as a dynamic load. The interface between the HUT and RT model also links to a RT control loop which generates the setpoints for the dynamic load under certain reference directive.

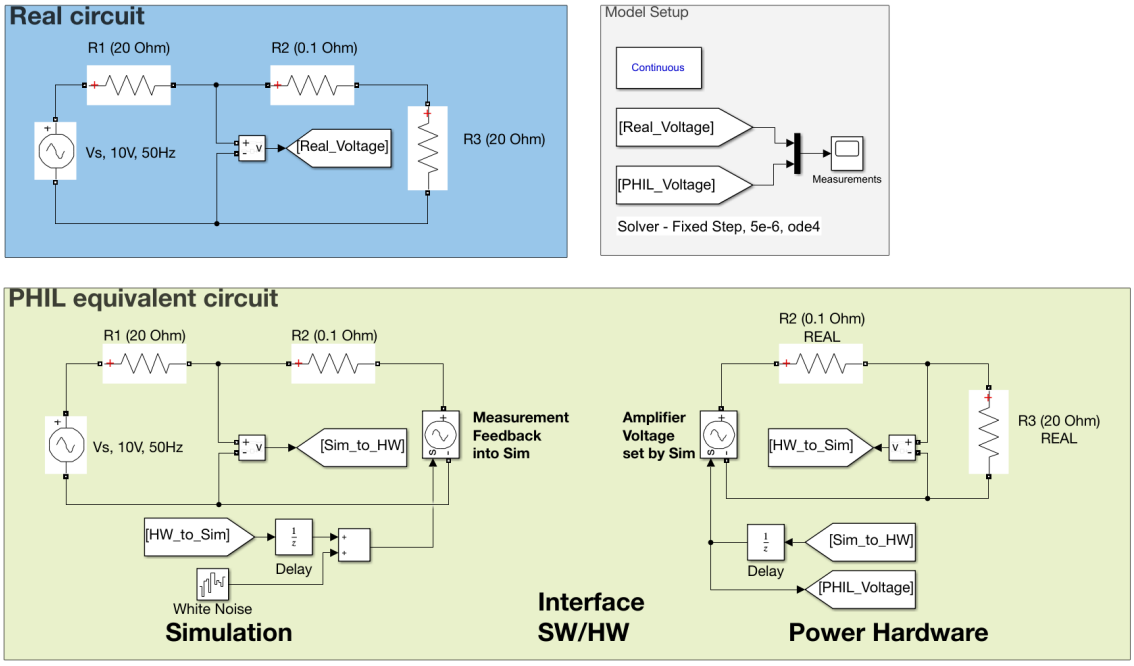

Figure 1.6: A schematic of a generic PHIL experiment for a voltage divider circuit, simulated in MATLAB/Simulink.

The design choice of the interface between HUT and RT models, also known as Interface Algorithm (IA) is the most important element of a generic PHIL setup. The ideal interface between the hardware and software domains has an unity gain, infinite bandwidth and zero time delay. In the real world, one can only go close enough to the ideal scenario and thus the interface is the seat of majority of the accuracy errors due to the unavoidable transfer delays. A stable network in the real world can be rendered unstable in its PHIL analogue form due to an non-ideal choice of IA. In [23], it was shown that for a small transfer delay and white noise over the IA, significant errors can be introduced into the PHIL analogue of the real circuit. Fig. 1.6 shows a comparison between two simulations

of a simple voltage divider where the original circuit is recreated by a PHIL equivalent circuit with 5 μs delay over the interface and a white noise signal error of $< 0.6\%$ standard deviation. The top diagram represents a real power circuit and the bottom is the PHIL analogue for the same circuit. In the bottom left circuit, the voltage seen by resistor R2, is simulated and then amplified over a power interface to be fed as voltage source into the real power hardware on the bottom right. The real measured voltage across a real resistor R3 is scaled down over the interface and fed as a signal into the software domain model on the left. This model is inspired from a similar study done in [23]. In Fig. 1.7, we see the divergence in the real and PHIL equivalent circuits, in form of phase shift and amplitude attenuation, due to this one step time delay, which can be attributed to communication overheads. Therefore beyond the optimal choice of the IA, one has to also think about compensation blocks in series for transfer delays, signal noise correction and attenuation.

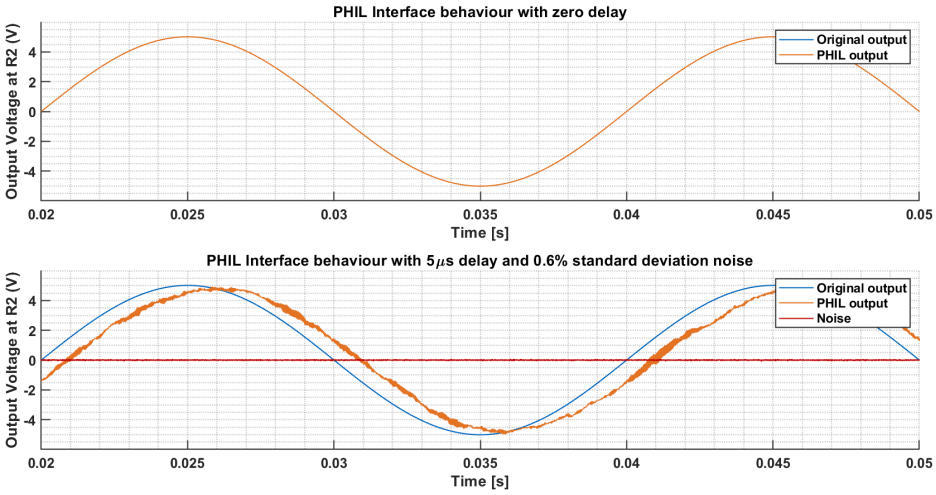

Figure 1.7: Fidelity of the PHIL equivalent voltage over the Interface Algorithm with and without a small transfer delay.

Different types of IA have been proposed in PHIL literature, some having advantages over the others for specific use cases. A list of commonly used IAs in commercial RTDS units is shown in [19]. The IA can be viewed as a connecting L or LCL filter [22]. It can also be imagined as a connecting transmission line, represented by a Bergeron equivalent model [23] or as a back-to-back converter [23]. In [24], it is shown that switched mode amplifier IAs are more suitable for voltage and current control applications. A synchronous machine IA was better suited for simulations which require a balanced three phase voltage source. A linear amplifier IA had the least time delay, simplest transfer function and the highest dynamic range but has the highest per kW cost.

PHIL experiments cannot be truly validated as the real system is not available to compare against. They can only be as accurate as their implemented RT model. They also face inevitable errors from their IAs and signal acquisitions blocks. This makes it difficult to correctly grade the accuracy of an implemented RT model, as the mismatch could arise from model errors, IA or from signal interfaces. Additionally, they carry forward the issues from standard RT simulations of difficulty in solving stiff problems, common in power

systems, using a fixed time-step solver. However, PHIL experiments remain an extremely powerful tool at the disposal of a power systems researcher for state-of-the-art dynamic analysis by subjecting the RT simulations to interact with real power hardware.

With the primary definitions and an brief study of their features out of the way, we now look at the trends within ADG research and their intersections with each other. This is an important step to appreciate the problem statement at the core of this thesis.

1.3 Dominant trends in ADG research

Over the years, 'microgrid/ADG research' has involved work done by researchers of various core competencies. It is perhaps obvious that such a tendency would emerge, given that the roots of the microgrid concept has roots in control theory, power electronics, systems-level studies, energy economics and optimisation research. One could even extend the scope towards sector-coupling and include groups working on vehicle-to-grid and heat grids. Regardless of these different directions, three distinct trends have dominantly emerged in the ADG research community. We shall look into the relevant problems within these composite trends, their tools and the boundary conditions of their work.

1.3.1 Optimised operation of ADG

The first cohesive trend arises from optimisation groups who are working towards finding the best coordination strategy to minimize operation cost of a ADG. This includes problems of optimally sizing the components of a ADG [25], increasing the participation of renewable energy resources in the final energy mix [26] and enabling greater sector coupling to reduce load peaks [27–30].

Academically, these works involve a convex or heuristics based optimisation problem. The problem reflects the constraints of, but not limited to, the generation units, storage blocks, distribution network, load foresight and weather conditions. The electrical systems are represented by drastic approximations to maintain a tractable problem. Several relaxation techniques have been proposed to morph the problem into a form which can be solved by commonly known solvers [31][32].

The inaccuracies arising from relaxation approximations are generally neglected. The assumptions in these works, generally neglect the cost of extensive instrumentation for set-points and measurements across the grid and the cost of retrofitting an entire grid infrastructure for coordination strategies. However, they are useful baseline studies to highlight the potential in intelligent operation of the currently available technologies.

The tools of choice are optimisation toolboxes, available in commonly used programming languages of MATLAB, Python and Julia. The results generally show active and reactive power output from DERs and nodal voltages from the approximated power system formulation. The validation is carried out by comparing operation costs against an uncoordinated approach, for simulation runs ranging from days to years.

1.3.2 ADG controller design

The next obvious grouping can be made over the ADG controller design community. These groups are present day iteration of the previous generations' power systems operations and control research groups. Their focuses have currently drifted towards distribution grids and from synchronous machines based power systems towards power electronics based grids [33][34].

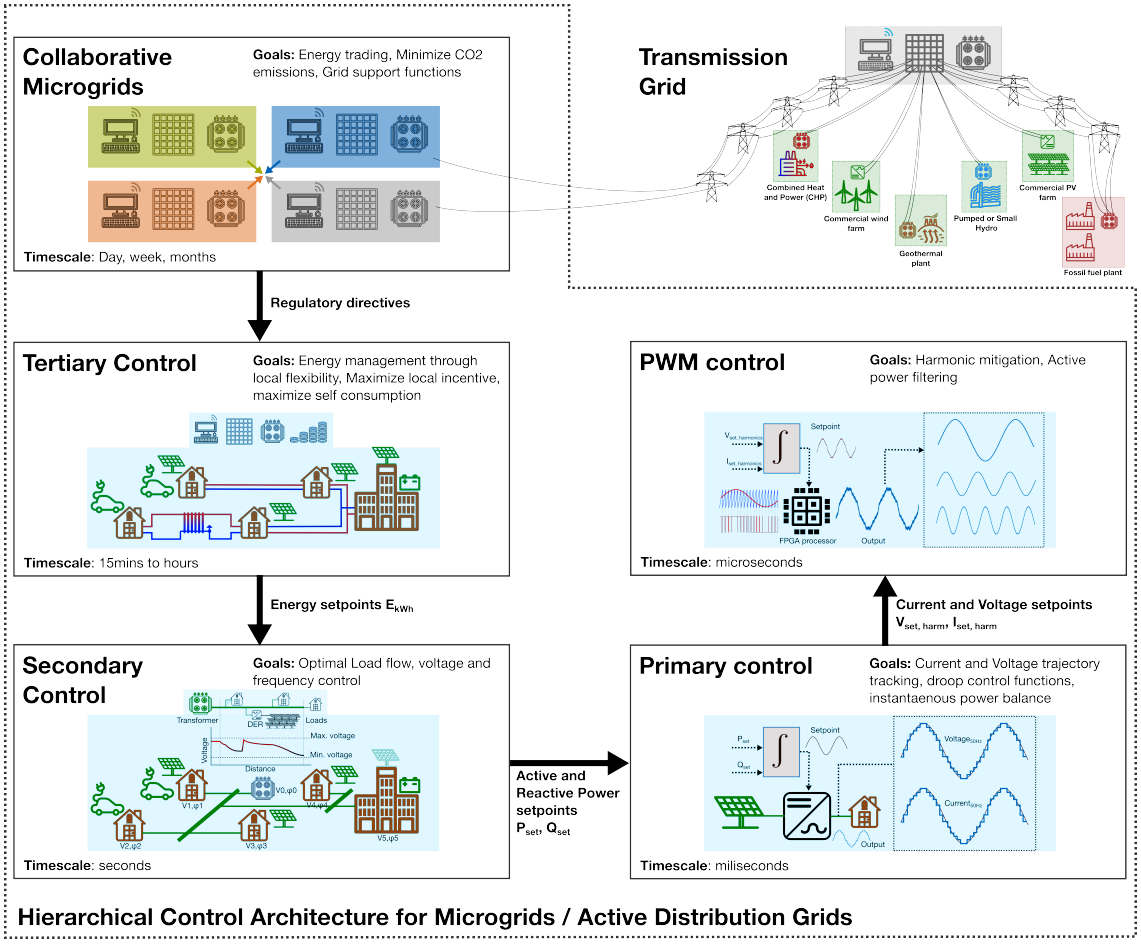

Figure 1.8: A typical hierarchical representation of an ADG primary, secondary and tertiary control design.

The transition towards ADG has introduced interesting control problems in the form of low or no inertia grids, inverter coordination, coupled active and reactive power flows due to matching R/X ratios, increased harmonics, increased short circuit current at inverters and grid synchronisation issues [35]. The electrical systems are modelled as per their DAE representations. Approximations are allowed on lumped parameters models of cables and complexity order of an inverter equivalent circuit. Community consensus has been to extend the traditional three-layered control scheme of - primary, secondary and tertiary control into ADG with additional considerations for energy storage elements, bidirectional energy flows, fast reaction from converters and distributed computation schemes. A typical

hierarchical ADG control model is shown in Fig. 1.8. ADG controller design community also extends towards power electronics research with precise inverter switching to implement harmonic mitigation [36] and active power filtering schemes [37]. Similarly, on the other end of the spectrum, collaborative microgrids with energy trading and market mechanisms are involved [38]. However, we will focus on the three standard control layers due to their higher relevance to this thesis.

Primary control strategies for ADG, re-imagine the traditional P-f and Q-V droop functions for inverter topologies [39][40]. The droop functions can be decoupled for extreme grid scenarios where either the resistive or the inductive part dominates grid impedance. The challenge lies in droop function formulation under uncertain grid impedances leading to coupled P-Q flows and robust control loops for all topologies of inverters - grid forming, grid following and grid supporting type. However, as always, the goal of primary control strategy within an ADG, is still limited to maintaining the instantaneous supply-demand balance.

The secondary controllers in ADG are aligned with traditional Automatic generator control (AGC) approaches toward bringing the voltage and frequency errors to zero by modifying the setpoints for the droop functions. Here the biggest challenge is posed by the significant increase in the number of generation units within an ADG control area. There have been reports suggesting that the deployment of distributed generation will outpace centralised generation units 5-to-1 by 2024 [41]. 83% of EU households could potentially become prosumer entities as per a study conducted by CE Delft [42]. A further investment is necessary for measurement and communication networks to link disparate DERs across an ADG to generate and propagate a secondary control signal. Decentralized secondary control strategies have been proposed under the constraints of irregular or low-fidelity communication between generators [43].

Tertiary control in ADG could also be imagined as an energy management layer which can coordinate with other ADG and propose optimal setpoints for individual DERs within the ADG [44]. An emphasis is also given on self-consumption or any other local incentive maximization [45]. In this regard, tertiary control for ADG does follow the economic load dispatch ideas of traditional tertiary control, where the cost of generation and transmission is taken into account to move towards the least cost energy mix. Naturally, this control layer is also the interface for the results from the optimisation community as we move from static and discrete steps to continuous control loops. Here a picture emerges where the two research fields of ADG control and optimisation can be combined.

The tools of choice are common simulation environments such as MATLAB/Simulink, LabVIEW, PSCAD, PSEE, PowerFactory and Modelica. The results include step responses, voltage, current and power tracking for a few seconds time horizons. The validation is carried out over standard simulations or with RT simulations.

1.3.3 PHIL validation of ADG controller

The third group of our classification has emerged as an offshoot of the power systems control design groups interested in RTDS systems. With increasing popularity of RT simulations in publications, in attempts to further bridge the gap between experiments and reality, there was an obvious migration towards experiment bed design and PHIL [46–52].

A pure software validation over RT simulation does not account for real world issues of controlling power hardware.

Notwithstanding the implementation challenges specific to ADG, there are significant hurdles to create an environment within an university premises for safe experiment design with power hardware. It brings forth the issues of high cost of installation, a critical decision to choose the right kind of hardware/software combination, real world consequences if a testing goes wrong and an increased cost of a technical crew to maintain the facilities.

PHIL validation deals with real power hardware which can be deployed on a real ADG, which, as mentioned in Sec. 1.2.1, can diverge significantly in operation and protection schemes from a conventional distribution grid. IEEE has tried to synchronize these activities by setting standards and minimum requirements for ADG components. Two relevant standards for PHIL test beds would be the IEEE 1547.4 - standard for design, operation and integration of distributed resource island systems with electric power systems [13] and the IEEE 2030.7.2017 - standard for the specification of ADG controllers [53]. However, since IEEE is not a internationally recognized standardization authority, these standards have been marketed as design guidelines for manufacturers and researchers. Their popularity is rising but their long term transition into an International Electrotechnical Commission (IEC) standard remains unrealised.

The tools of choice are a combination of commercial RTDS systems, such as OPAL-RT and dSPACE, with power amplifiers or power HUT. The style of the results is similar to the control design community papers but are now fortified with PHIL simulations. This field of research is most pertinent to the current thesis and shall be awarded the whole next section to be studied in detail and identify its associated research gaps.

1.4 PHIL laboratory test beds in ADG research

Power system laboratories in the past could not have had access to a real thermal or hydro power plant setup for experiments, due to the obvious cost and size reasons. On the other hand ADG comprise of smaller generation units which are easier to house and procure for research institutes. Secondly, as mentioned in a Sec. 1.2.1, ADG carry more ICT and fast reacting power electronic converters at their nodes. These additional components must be tested in the real world, wherever possible, since they introduce fast dynamics in a low-inertia grid. Thirdly, ADG contain too many separate DER technologies to individually and accurately model them on RT systems. Finally, there are new energy vectors such as transportation and heat being added into the mix under sector-coupled ADG concepts. These are completely different families of technologies and there is a lack of confidence on their accurate equivalent modelling in RT systems.

Extending the CHIL and PHIL test designs, ADG test-beds have embraced a combination of RTDS and PHIL approaches [54] to address the above mentioned challenges. These setups have been used to validate individual DER controllers, adequacy of relays and PMUs or staging cyber-physical attacks for resilience tests. Taking advantage of the common hardware and software elements in many of these research objectives, the PHIL validation community of ADG research has gravitated towards establishing PHIL laboratories. In

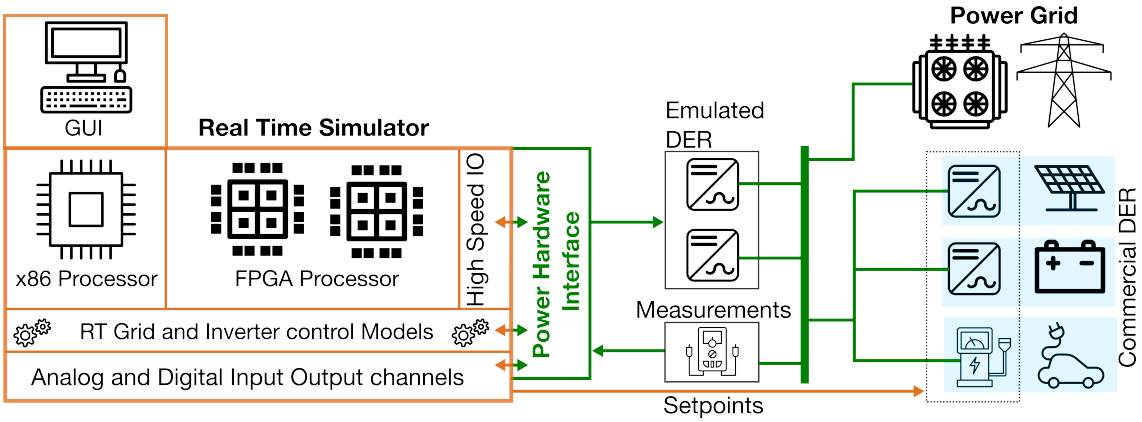

Figure 1.9: A typical schematic for PHIL laboratories for ADG research.

these laboratories, real world power equipment and communication networks are interfaced with programmable RT environments to validate a variety of research objectives.

The PHIL laboratories generally comprise of collection of DERs and their converters, connected through a power interface to a RT simulator for the grid model, top level controllers for coordination between the DERs and in some cases, FPGA controllers for switching a real or power hardware emulated inverter. A list of active laboratories in 2016 can be found in the DERlab activity report [55]. A collection of laboratories have described their setup, research direction and exemplary experiments in [19], [56–74].

In [75], a visualisation can be found regarding the collaboration among the identified smart grid laboratories. A similar survey was conducted in [76], and abundant commonality was identified through these setups. Congruity over programming languages, simulation and modelling tools and control interfaces were also noted. The resulting generic schematic for PHIL laboratories for ADG research in shown in Fig. 1.9.

1.5 Research gaps in ADG PHIL laboratories

The V-model, shown in Fig. 1.10, is an useful representation of a product development cycle [77]. The right arm of the V-model lists the Testing phase for a product's development and is a suitable proxy to describe the testing of products designed by complex system such as ADG. There are many variant of the V-model in literature, but based on the structure shown in Fig. 1.10, PHIL experiments would lie between the 'integration, test and verification' and 'System verification and validation' phase. PHIL laboratories offer tests at component level and multiple integrated components into a sub-system level. However, most PHIL laboratories would be unsuitable for a system-level testing to check the operation features, as major components of the real system, eg - the power grid, is present only as a RT model. This can be considered as a gap for ADG research where various components such as - electrical grid, heating grid, power electronics, communication systems and control systems have to be considered as a single or at least correlated system.

Beyond the similar design of PHIL laboratories, [76] also identified a list of common

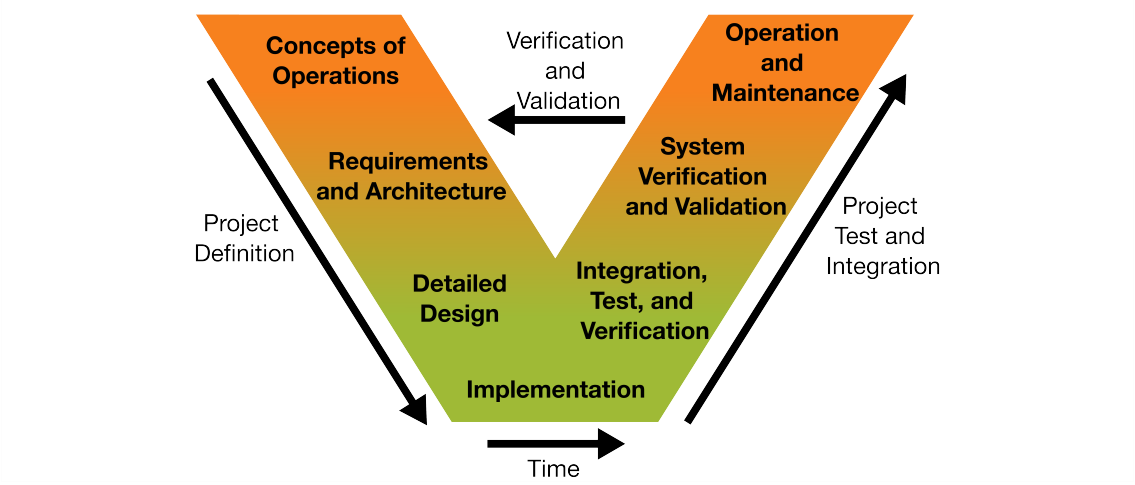

Figure 1.10: The V-model of the systems engineering process used in product development cycles.

problems for them. There was an uniform lack of visualisation screens and operator support in all of the surveyed laboratories. There was little focus on a central supervisory control and data acquisition (SCADA) platform and the use cases were too complex to be represented adequately on standard SCADA suites. Although there were generic similarities in the schemes, the final device specifications were different. The tests carried out in these labs were difficult to reproduce due to these differences. A common data format was missing to perform efficient model exchange. Building on from this preliminary assessment, a few more research gaps while using an ADG laboratory with PHIL testbeds, are highlighted in this section.

1.5.1 Accuracy of ADG RT models

PHIL abstractions are an analogue of the real world, and as explained in Sec. 1.2.3, they are never 100% accurate. This is especially true for the RT grid models with the lumped parameter blocks for cables. While power converters, relays, circuit breakers and bus bars are common in PHIL laboratories, a real and reconfigurable power grid is a rarity. Certain institutes have access to a real power grid [78] but they are rigid configuration distribution grids with real end-users. Cables and bus bars cannot be re-oriented for experiment specific layouts as this would involve interruption of service to real consumers.

The dependence on RT grid simulation models also creates a narrative that a controller in the field has access to high quality grid parameter estimates. Taking the example of the branch cable parameters, the data on distribution grid feeder length and location is either a restricted or in some cases unavailable. Therefore, in many distribution grids, the branch admittance matrix cannot be calculated to the precision levels seen in a IEEE test case used for RT simulation. If the application cases are dependent on a precision of grid parameters, the product cannot be considered market ready after a PHIL test.

1.5.2 Centralised control systems

Control systems and RT hardware for PHIL laboratories are centralised in most of the cases. This might not be a fair representation of the real world where DER entities controlled by inverters have local control boards and thus cannot carry a massive centralised intelligence on them. Some laboratories do possess separate controllers for the individual DERs but they still rely on a central access point which collects all the measurements and connects to every controller from within the RT environment. Referring to the typical laboratory schematic in Fig. 1.9, any inverter control model deployed on the RT simulator or the FPGA, typically has access to the precise output from all the measurement transducers through the IO interface of the RT simulator.

Measurements in the real world cannot be transferred at a reasonable cost and at the resolutions seen in PHIL setups, in between physically separated controllers. Furthermore, within an ADG populated by controllable prosumers, measurements like the PCC voltage, might end up being too far away to wire directly into individual controllers over low voltage signals. Additionally, there are issues of synchronisation among distributed controllers if they want to switch synchronized converters.

1.5.3 Research isolation from other pertinent groups

There is a need to bring together various core-competency groups for ADG research was mentioned in Sec. 1.3. Without this collaboration, a truly sector-coupled and intelligent ADG shall remain a pipe-dream. The first obstacle would be the lack of common assumptions among fields marked for collaboration. The consensus on acceptable modelling strategies vary depending upon the research problem.

A good example is a simple DER coordination scheme within a sector-coupled ADG, a popular research objective in *DER optimisation* or *energy system modelling* community, such as the work presented in [26]. The output is an optimal generation schedule for all DERs, commonly in hourly, half-hourly or quarter-hourly resolution for a weekly, monthly or yearly duration. General assumption for these models, consider all DERs as continuously modulating prosumers to avoid a model blow-up with binary elements. This assumption could be argued to be valid for capacity sizing, total cost estimates or any such problem dealing with aggregated resources. However, one cannot use the same assumptions for an optimal operation schedule of DERs at a few minutes or seconds resolution. Commercially available heat pumps, combined heat and power plants and heat storage cannot be controlled over the full zero to 100% loaded power modulation range. Even when they do lie in the controllable range, these devices do not behave as ideal sources which can be precisely regulated. This means that the actual economic advantage of a coordinated operation scheme in the real world might be different for two groups doing similar research depending on the time-scale of each optimised step.

Another point of contention could be the advanced component level control schemes and their validations, a popular topic for PHIL and RT simulation communities. Due to reasons ranging from safety standards, intellectual property rights and market conditions, a manufacturer would rarely allow a third-party controller to have an override on the inbuilt control schemes, which have been built to stringent functional safety standards.

Commercial DERs posses a remote controlled mode and many do support a modulation setpoint for the output power. However this setpoint is communicated through general purpose communication protocols such as Modbus, CAN bus which cannot be used for RT control loops. Therefore an active and reactive power controller such as the one shown in [79] for a battery storage cannot be implemented on commercial battery storage systems. The laboratories must design their own experimental PHIL test-beds for various DERs, for complete freedom in adjusting even the inner current and voltage loops. Therefore, the validated 'use case' pushed through by the PHIL results have limited significance as the commercial DERs are incapable of enacting them in real life.

1.5.4 Inadequate laboratory designs for collaboration

Laboratories are designed to promote reproducible results and build systems to efficiently convert an idea to published resource. University research structures allow people to collaborate for short periods for a specific publication or spend a few months as a visiting scholar. Even within the same institute, the laboratory resources must be shared and simultaneous experiments might be needed to be scheduled. Therefore, laboratory best practices must take into account the limited time window at the disposal of every researcher for a meaningful contribution.

While there are some common groupings of toolchain in use among the PHIL ADG communities, it is not a trivial expectation to have research level expertise on all of them at the same time. This basic difference prohibits people from exchanging models and research period is reduced by the learning curve one must overcome as a short-term collaborator. Extending this analogy to other fields, such as heat systems and optimisation groups, further complicates this process.

On top, design decisions that may seem completely valid from a hypothesis point of view, might be limiting on a collaboration context. A laboratory must be designed for multiple researchers to work at the same time. If there is a central control system, a deployed experiment blocks this resource for others. If all the measurements and synchronisation blocks are hosted at this central controller, even parts of the lab which are not part of the current experiment might be inaccessible for other projects. The time it takes to reset one experiment run and repeat the measurements is another crucial element to experiment design. If a run requires coordination between multiple software environments, the turnover rate between two runs is affected. The lack of a SCADA interface in many PHIL laboratories is a further pain point for efficient experiment design.

1.6 The problem statement

Following the presentation of the research gaps in PHIL laboratory design for ADG research, a few research questions can be proposed to address them. The major prerequisite however is the presence of a suitable laboratory to show the implementation of the ideas.

1.6.1 Establishment of an ADG laboratory

The establishment of such a laboratory at the Technical University of Munich (TUM) was one of the early research objectives of this thesis. Namely, the author was responsible for the installation and commissioning of the electrical power system instrumentation, PHIL interfaces for Prosumer emulation and a decentralised RT control system of the laboratory. The Center for Combined Smart Energy Systems (CoSES) at Technical University of Munich (TUM) was inaugurated in July 2019 [80] to research sector coupled active distribution grids. The laboratory serves as the validation site for the ideas proposed in this thesis.

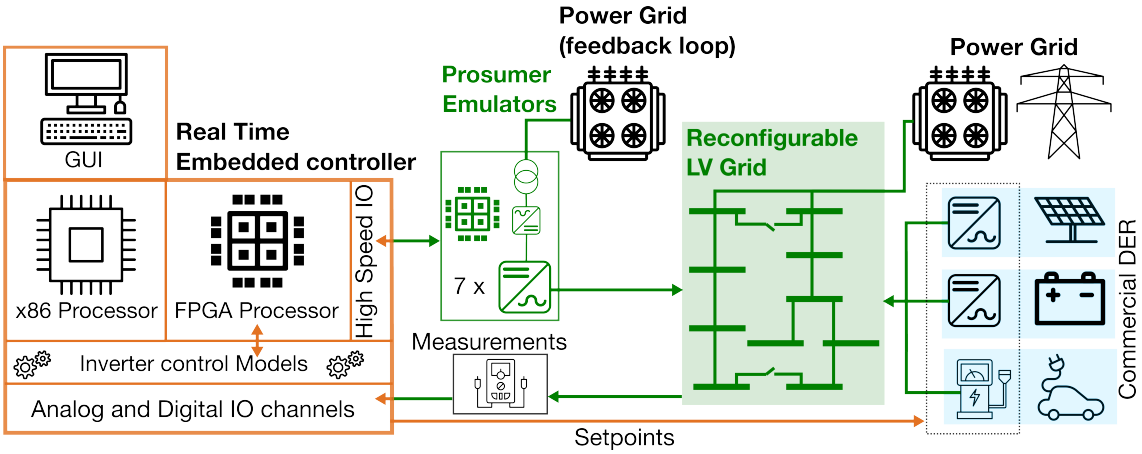

Figure 1.11: Center for Combined Energy Systems at TU Munich as an ADG facility.

The CoSES is a low-inertia, sector-coupled, low voltage power grid laboratory in TUM Garching campus, designed to investigate implementation hurdles for optimised sector-coupling technologies at the distribution grid prosumer level. Interested readers can refer to the following publications for details regarding the laboratory setup.

- Overall architecture of the sector-coupled ADG and DER capacities - [81]
- PHIL infrastructure, RT control system and detailed description of the electrical grid - [82]
- Heating and cooling grid prosumers, thermal grid controllers and detailed description of the thermal grid - [83]

A schematic representation of the lab, is shown in Fig. 1.11 and can be contrasted with the generic PHIL laboratory in Fig. 1.9. The laboratory presents an unique research landscape by combining,

- a real and reconfigurable low-voltage distribution grid,
- with a fourth and fifth generation capable district heating infrastructure [84],
- governed by a decentralised control and instrumentation architecture,
- to modulate commercial electrical and heat DERs over native remote protocols,

- alongside emulated electrical and heat DERs over precisely controllable PHIL interfaces.

1.6.2 Research questions

While many ADG PHIL laboratory facilities possess a subset of the above listed attributes, all of them are necessary to produce credible results for sector-coupled smart grids with realistic test conditions. Highlighting the various design choices for the electrical and control systems at CoSES, there is an attempt in this thesis, to address the gaps identified in Sec. 1.5. Three relevant research questions can be formulated as parts of a general question,

Q1: How should a PHIL laboratory for ADG research be established, with real prosumers, distributed control scheme, limited set of measurements,

Q2: to validate concepts on, as realistic as possible, test beds,

Q3: while promoting efficient experiment design and reduced collaboration pains?

1.6.3 Thesis outline

The thesis outline can be divided over two main chapters with a prevailing theme of setting up an ADG laboratory and using the ADG laboratory. Each chapter is comprised of three publications each which can be expanded as three individual sections within a chapter. An illustration of the chapter breakdown is provided in Fig. 1.12. The papers included in this thesis are as follows,

Chapter: ADG Laboratory Setup

Publication #1 E. Sezgin, A. Mohapatra, T. Hamacher, Ö. Salor, and V. S. Perić, "Fast harmonic analysis for PHIL experiments with decentralized real-time controllers," *Electric Power Systems Research*, vol. 211, Oct. 2022, ISSN: 03787796. DOI: 10.1016/j.epsr.2022.108493.

Publication #2 M. Mayer, A. Mohapatra, and V. S. Peric, "IoT Integration for Combined Energy Systems at the CoSES Laboratory," in *Proceedings of 7th IEEE World Forum on Internet of Things, WF-IoT 2021*, IEEE, Jun. 2021, pp. 195–200, ISBN: 9781665444316. DOI: 10.1109/WF-IoT51360.2021.9596000.

Publication #3 A. Mohapatra, T. Hamacher, and V. S. Peric, "PHIL Infrastructure in CoSES Microgrid Laboratory," in *Proceedings of 2022 IEEE PES Innovative Smart Grid Technologies Conference Europe, Novi Sad*, vol. 2022-October, IEEE PES, 2022, ISBN: 9-7816-6548-0321. DOI: 10.1109/ISGT-Europe54678.2022.9960295.

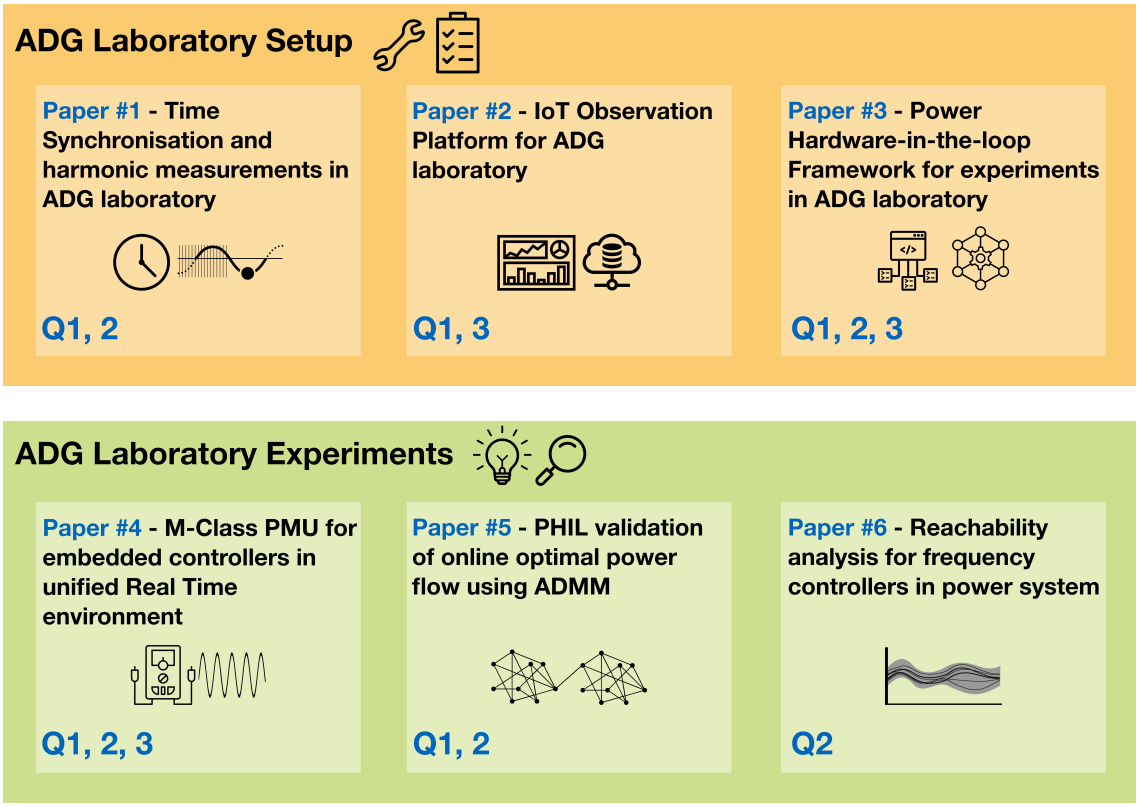

Figure 1.12: Outline of this thesis

Chapter: ADG Laboratory Experiments

Publication #4 A. Mohapatra, S. Büttner, G. Bumiller, T. Hamacher, and V. S. Perić, "M-Class PMU for General Purpose Embedded Controllers in NI Veristand Environment," in *Proceedings of 2023 IEEE Belgrade PowerTech*, IEEE, Jun. 2023, pp. 1–6, ISBN: 978-1-6654-8778-8. DOI: 10.1109/PowerTech55446.2023.10202989. [Online]. Available: https://ieeexplore.ieee.org/document/10202989/.

Publication #5 M. Cornejo, A. Mohapatra, S. Candas, and V. S. Peric, "PHIL implementation of a decentralized online OPF for active distribution grids," in *Proceedings of IEEE Power and Energy Society General Meeting 2022, Denver*, vol. 2022-July, IEEE PES, 2022, ISBN: 9781665408233. DOI: 10.1109/PESGM48719.2022.9916705.

Publication #6 A. Mohapatra, V. S. Peric, and T. Hamacher, "Formal Verification of Grid Frequency Controllers," in *Proceedings of 2021 IEEE PES Innovative Smart Grid Technologies Europe, Espoo*, IEEE PES, 2021, ISBN: 9781665448758. DOI: 10.1109/ISGTEurope52324.2021.9640096.

Furthermore, each publication can be linked to the prior listed research questions, as shown in Fig. 1.12. Thus the collection of the six publications tries to provide a satisfactory answer to the four relevant research questions for this thesis, while also outlining a way forward for future research direction. Certain subsections have been

provided with additional content outside of the publications, if there was a thematic necessity for continuity of thought or if the publication pertains to a currently continuing research objective.

Chapter 2

ADG Laboratory Setup

Truth suffers from too much analysis.

Frank Herbert

Control system setups at ADG laboratories demand thoughtful decisions in selecting measurement methods, synchronization techniques, visualization tools, and strategies for sharing results. While these factors may seem separate, together they greatly influence collaboration within a lab. For instance, if vital bus voltage data is only accessible in RT through one controller which is reserved for the current experiment, it might be potentially inaccessible by other controllers in parallel experiments. This chapter explores three aspects of synchronized measurements, adaptable visualizations, and a comprehensive experiment framework, over three connected publications.

The **first publication** introduces a new measurement concept by combining voltage and current data from separate RT controllers. This aids continuous power setpoint calculations and precise control strategies. Shifting focus, the **second publication** introduces an Internet of Things (IoT) dashboard tailored to ADG lab needs. This interface offers an abstraction for live experiments which can be modified to the taste of the researcher, depending on their field of interest. This is essential to remove the learning curve of accessing a PHIL laboratory while conducting multi-disciplinary ADG research. The **third publication**, which synthesizes earlier work, is the development of PHIL framework for CoSES ADG laboratory to guide the future experiment design in the lab. This framework is followed for all CoSES experiments, with a select few relevant to this thesis being presented in Chapter 3.

2.1 Time synchronisation in the laboratory

In power systems, precise timing sources are fundamental for synchronization, especially across geographically distant grids. These timing references typically follow coordinated universal time (UTC) and often originate from global positioning system (GPS) signals. In conventional power systems, UTC timing sources are essential for reliable measurements, situational awareness, fault analysis, and operator decision-making [90].

In ADG, the importance of synchronized timing extends to individual inverter operations. Inverter based resources need a timing source for synchronization over Phase Locked Loops (PLL) [91] and also for the Pulse Width Modulation (PWM) triggering of the semiconductor switches. Synchronized inverters are critical to maintaining harmony among prosumers for accurate power injection. In many cases, these ADG components employ power electronic devices with embedded controllers that use Analog-to-Digital converters for signal processing. These controllers rely also on internal timing chip to trigger digital signal acquisition.

Choice of hardware

The CoSES laboratory uses PXIe 8880 [92] embedded controllers in the PXIe-1065 chassis for prosumer control and measurement. Each controller comes with a PXIe-6683H Timing and Synchronization card [93], as shown in Fig. 2.1, to trigger events and synchronize the PXIe chassis clock. This synchronization is accomplished either through an external clock signal via RJ-45 with a 1588 PTP switch [94] or through a GPS connection via an SMB connector.

Figure 2.1: The NI PXIe 6683H timing and synchronisation card used in CoSES PXIe controllers. [93]

There is a special arrangement for the GPS connection, shown in Fig. 2.2, as it is inefficient to connect a separate GPS antenna to each of the six available PXIe 1065 chassis. We connected one GPS antenna to a six-way, passive signal splitter to distribute the same GPS signal to the different chassis. Based on the NI requirements, a signal strength of $-135\,\mathrm{dBm}$ to $-120\,\mathrm{dBm}$ is recommended at the input for the 6683H timing card. Due to the lengths involved in the laboratory, an inline amplifier is used to boost the signal strength at acceptable noise amplification, before passing through the splitter.

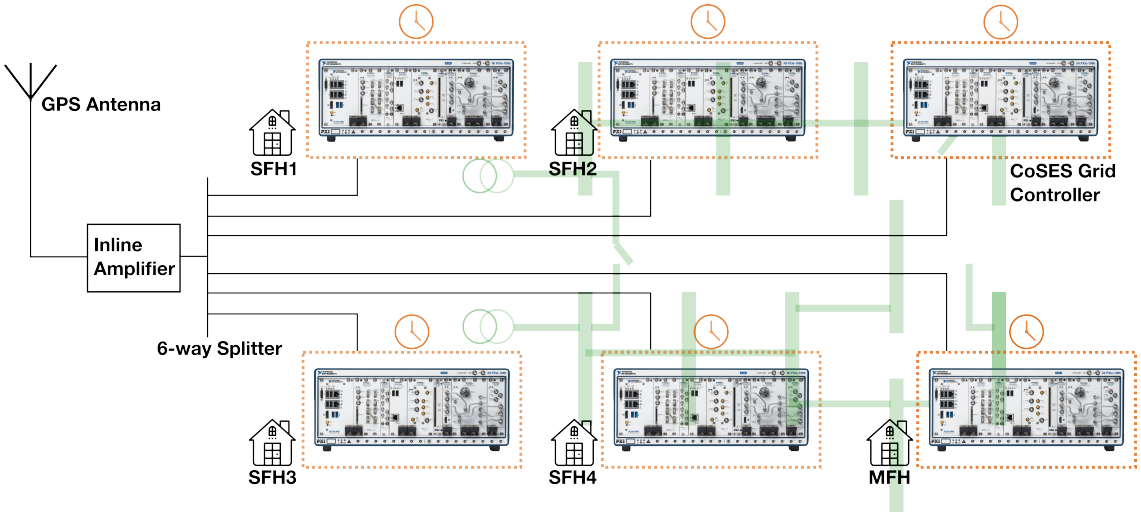

Figure 2.2: CoSES laboratory with the GPS antenna as the UTC source for PXIe chassis discipline. The position of the antenna with respect to the chassis is representational and does not reflect the distances in the lab, which are mentioned in the diagram.

Accuracy of synchronization

In [95], the authors have listed the different measurement technologies and their required accuracy for ADG operation. Within the CoSES laboratory, a phasor measurement unit (PMU) standard accuracy is needed for the prosumer synchronization and synchrophasor calculations. According to the PMU standard IEEE C37.118.2, the Total Vector Error (TVE) for the PMU synchrophasor output should be less than 1% [96]. This corresponds to a mandatory measurement clock accuracy of 31.8 μs but should be ideally under 10 μs for reliable performance across all standard mandated metrics [97]. Additionally, it has been observed that the PXIe controllers can maintain RT loop rates up to 10 kHz for prosumer control and DER emulation models. This leads to a loop delay of 100 μs for the RT models. Therefore, adhering to the PMU accuracy standard is deemed sufficient for all measurement and control needs of the CoSES laboratory.

The synchronisation quality was measured by logging the system clock offset of PXIe 8880 and chassis clock offset of PXIe 1065. The chassis clock is used for ADCs in the physical signals leaving or arriving at the controller. The system clock is used as the timing source for the control and emulation models deployed on the RT controller. An experiment was performed where the system time offset and the chassis time offset to the external timing source, GPS and 1588 PTP connected to the PXIe 6683H timing card, was recorded for 20 min at 100 Hz. The results are shown in Tab. 2.1 and guarantee that the quality of synchronisation is sufficient for PMU grade measurements and in extension for the control needs of CoSES laboratory.

Overall, a precise synchronisation exists for six embedded controllers measurements and RT model executions. These devices acquire the voltage and current measurements from the individual sensors across the laboratories. There is a necessary expectation to harmonically analyse these signals being part of an ADG laboratory. Furthermore, two out of the six controllers also send RT control setpoints for unbalanced current and voltage

Table 2.1: CoSES synchronisation clock offsets for 1588 PTP and GPS grade timing sources.

		GPS	1588 PTP
System Clock Offset	μ	$-0.024\,\mu$s	$-0.038\,\mu$s
	δ	$5\,\mu$s	$6.2\,\mu$s
Chassis Clock Offset	μ	$-0.0089\,$ns	$-0.0143\,$ns
	δ	$0.0016\,\mu$s	$0.1042\,\mu$s

from the seven Egston prosumer emulators [98]. These setpoints are transferred over an optic fiber link using the Xilinx Aurora protocol [99].

2.2 Split measurement concept (Publication #1)

A fundamental requirement within ADG, is the precise determination of power injection within the grid, which is a straightforward operation when the current and voltage measurements are inherently synchronized within a single control unit. However, complexities arise when combining a voltage measurement from a remote PCC with a local current reading. In the real world, this is similar to situations where the PCC is a considerable distance away from the local distribution unit, which is unsuitable for direct wiring of voltage measurements.

A primary concern in these situations is the measurement accuracy across these extended paths. Voltage measurements acquired remotely from the point of origin often undergo attenuation and distortion. This becomes particularly pertinent due to the harmonics in ADG. Outside the primary grid frequency voltage and current estimation, the harmonics must also be accurately identified for filtering and mitigation measures as stated in power quality standards such as the IEEE 519-2022 - Standard for Harmonic Control in Electric Power Systems [100]. The standard stipulates observation until the 50^{th} harmonic which is well within the Nyquist limit of the 10 kHz RT loop rate for the PXIe controllers in CoSES. Additionally, normal communication infrastructure does not allow the bandwidth to transfer raw measurements at their highest precision, in tens of kHz range, over practical distances. Instead, measurements are resolved to their magnitude and phase components and this data can be transferred between controllers. However, a second concern is then the often unpredictable delays from communication packet drops or variable transmission duration due to data congestion. Therefore the measurements have to be continuously corrected to manage the asynchronous communication link between controllers.

The forthcoming paper addresses these challenges through a harmonic analysis technique specifically tailored for ADG scenarios. Through frequency-shifting and filtering mechanisms, the proposed method effectively translates voltage and current measurements into magnitude and phase information. This information is subsequently transmitted across an asynchronous communication link to a remote controller, where the original waveform is reconstructed and phase compensated for the delay. The outcome is a robust approach to synchrophasor accuracy [13] of handling measurement points over multiple controllers with communication latency. An experimental validation is provided at CoSES laboratory. Two distinct PHIL experiments, in grid-connected and island mode operations,

are conducted and show the technique's versatility for accurate power control and grid synchronization.

Publication #1 - Fast harmonic analysis for PHIL experiments with decentralized real-time controllers

Authors - Erhan Sezgin, Anurag Mohapatra, Thomas Hamacher, Özgül Salor, Vedran S. Perić

Publication - Electric Power Systems Research, Volume 211, October 2022

Digital object identifier - `https://doi.org/10.1016/j.epsr.2022.108493`

Author	**Contribution**	**Tasks**
Erhan Sezgin	40%	Conceptualization, Methodology, Formal analysis, Software, Writing – original draft
Anurag Mohapatra	40%	Conceptualization, Methodology, Validation, Software, Writing – original draft.
Thomas Hamacher	5%	Supervision, Funding acquisition
Özgül Salor	10%	Supervision, Writing – review and editing
Vedran S. Perić	5%	Supervision, Project administration, Writing – review and editing

Electric Power Systems Research 211 (2022) 108493

Contents lists available at ScienceDirect

Electric Power Systems Research

journal homepage: www.elsevier.com/locate/epsr

Fast harmonic analysis for PHIL experiments with decentralized real-time controllers☆

Erhan Sezgin [a,*], Anurag Mohapatra [b], Thomas Hamacher [b], Özgül Salor [c,d], Vedran S. Perić [b]

[a] Department of Electrical and Electronics Engineering, Kafkas University, Kars, Turkey
[b] CoSES, Munich School of Engineering, Technical University of Munich, Munich, Germany
[c] Department of Electrical and Electronics Engineering, Kyrgyz-Turkish Manas University, Bishkek, Kyrgyzstan
[d] Department of Electrical and Electronics Engineering, Gazi University, Ankara, Turkey

ARTICLE INFO

Keywords:
DFT
Distributed control
Frequency shifting
Power hardware-in-the-loop
Prosumers

ABSTRACT

This paper proposes and implements, a harmonic analysis technique used in microgrids for inverter power control when measured voltage and current signals are passed over a communication link with considerable latency. Using frequency-shifting and filtering techniques, the measurement is converted to magnitude and phase information and passed over an asynchronous communication link to another controller, where the original waveform is recovered with delay compensation. The method allows accurate power calculations and grid synchronization over distributed prosumer controllers. The proposed method can work at different execution rates, depending on real time (RT) workload, and is shown to be robust against step changes, harmonics and communication delays. The method is demonstrated with two PHIL experiments at the CoSES, TU Munich lab in grid connected and island mode.

1. Introduction

Fully controllable and dispatchable, power electronics based distributed energy resources (DERs) have shown a great potential for more efficient and reliable grid operation. Combined with the advent of Information and Communication Technology (ICT) for power systems and flexibility offered through sector coupling, the literature on central and local control of prosumer oriented, multi energy systems has grown rapidly. Accurate and fast measurements in a prosumer microgrid are an important domain of research in multi energy systems. Within this broad topic, the location of the measurements with respect to the location of the controller is of particular interest.

An increase in individually controlled prosumers can lead to situations where the relevant point of common coupling (PCC) voltage might not be available on-site. The PCC voltage is important to accurately calculate power injection from the prosumers and it is generally taken at the distribution grid node behind the PCC. In the context of an optimized microgrid, each prosumer contributes individually and collectively towards maintaining the grid node voltage within limits. However, multiple prosumers can be physically too far removed to send direct measurements of the PCC voltage, as seen in a schematic in Fig. 1.

The Center for Combined Smart Energy Systems (CoSES) at TU Munich was established to research sector coupled, low-inertia, active distribution grids [1]. It emulates multiple fully controlled electrical and heat prosumers in a local grid, based on Power Hardware-in-the-Loop (PHIL) philosophy, to represent a real-world multi-energy grid and eliminates the need for real-time (RT) simulators. In CoSES, the grid voltage measurements are acquired at a controller separate from the prosumer controllers. Each prosumer has its own embedded controller which decides the local power injection. While the current is measured locally at the prosumer bus, the voltage of the upstream distribution grid node is missing. The instrumentation cabling length between the location of the voltage measurements and the prosumer controllers makes it impossible to hard wire the measurements directly.

☆ The work of Erhan Sezgin was supported by the Council of Higher Education of Turkey within the scope of YÖK-YUDAB project. The work of Anurag Mohapatra was supported by the German Federal Ministry for Economic Affairs and Climate Action through the project "OSkit - Optimierte Sektorkopplung in Quartieren durch intelligente thermische Prosumernetze" under Project number 03EN3032A. The work of Vedran S. Perić was supported by Deutsche Forschungsgemeinschaft (DFG), Germany through the project "Optimal Operation of Integrated Low-Temperature Birdirectional Heat and Electric Grids (IntElHeat)" under Project number 450821044. The construction of the CoSES laboratory was supported by Deutsche Forschungsgemeinschaft (DFG), Germany through the project "Flexible reconfigurable microgrid laboratory" under Project number 350746631.

* Corresponding author.
E-mail address: sezginerhan@kafkas.edu.tr (E. Sezgin).

https://doi.org/10.1016/j.epsr.2022.108493
Received 3 October 2021; Received in revised form 11 April 2022; Accepted 2 July 2022
Available online 14 July 2022

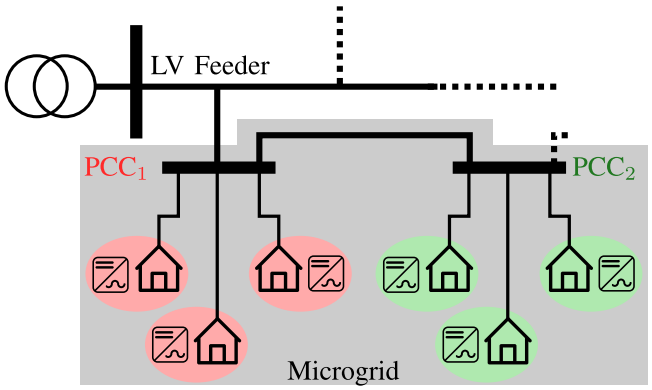

Fig. 1. Microgrids at Low Voltage (LV) level with individually controlled prosumers (the control area of each prosumer is seen in and) can be located too far away from PCC for direct wiring of voltage measurements.

Therefore, continuous voltage measurements required as feedback for prosumer power injection control must be sent over an asynchronous communication link. To avoid loss of information, it is prudent to perform harmonic analysis on the voltage and send the magnitude and phase values over the communication channels to local prosumer controllers. The harmonic analysis models must also be accurate and show quick convergence. Furthermore, the control philosophy in CoSES requires the controllers to carry compiled RT models for prosumer emulation, energy management systems and DER control. Hence the signal processing must be easy to implement, to allow capacities for the RT operation of the lab.

In this paper, we present the development and implementation of a harmonic analysis and power measurement within the aforementioned constraints of the CoSES lab. To the best knowledge of the authors, there has been no previous work on voltage measurements collected at different controllers to calculate a RT feedback for PHIL control. We use a method involving frequency-shifting and filtering to continuously calculate the magnitude and phase components of the measured signal. We time-stamp the signal at the sending end controller and compensate for the communication delay on the receiving end of the prosumer controller. The prosumers, which are emulated over bi-directional inverters, require sample-by-sample setpoints of the reference current for a specific power injection. We recover the voltages as waveforms, using the transferred magnitude and phase information, and calculate the continuous current setpoints for the prosumer. We test our algorithm for accuracy through step changes and additional harmonics on the grid voltage, while maintaining constant power injection from a prosumer.

The remainder of this paper is organized as follows. In Section 2, we introduce the proposed methodology for the measurements and power calculation. Relevant literature on similar approaches is presented and analyzed for their suitability for our use case. In Section 3, we explain the electrical prosumers and the RT control structure for the decentralized controllers in our lab. In Section 4, we validate our methodology and then use it for two PHIL experiments to demonstrate its usefulness in the lab.

2. Methodology

The IEEE standard defines, power as the continuous multiplication of voltage and current waveforms [2]. Active power is further defined as the integration of this multiplication, averaged over certain whole number multiples of the fundamental frequency. In this paper we are concerned with the active power associated with the fundamental frequency which is also known as positive sequence power in some literature. In a practical sense, the positive sequence power is the useful power used in electrical appliances, devices and components used for power delivery. Therefore, our proposed method should primarily estimate the fundamental frequency in measurements and if needed, other harmonic orders for specific PHIL experiments.

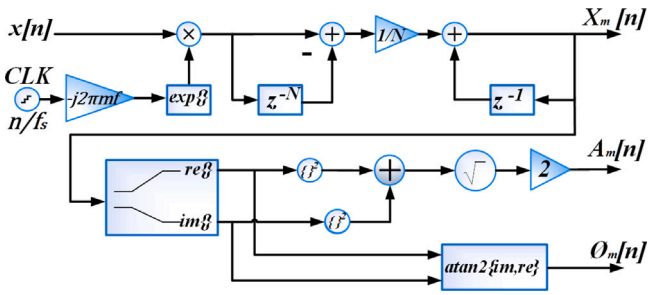

Fig. 2. Proposed harmonic analysis method.

Stationary AC electrical signals can be expressed using a line spectra model, where signals have constant frequencies, with magnitudes and phase angles for each frequency. Discretizing the time with a sampling frequency f_s, an AC signal is obtained as given in (1),

$$x[n] = \sum_{m=1}^{l} A_m cos\left(\frac{2\pi m f n}{f_s} + \phi_m\right), \tag{1}$$

where f is fundamental frequency. Here $x[n]$ has harmonic components with orders of m ($m \in [1, l]$), amplitudes A_m and phase shifts ϕ_m.

The literature on harmonic analysis is well established. These are generally, Discrete Fourier Transform (DFT), Fast Fourier Transform (FFT) [3], Discrete Wavelet Transform (DWT) [4], Second Order Generalized Integrator (SOGI) [5] and Kalman Filter (KF) [6] based methods. However, their suitability for RT experiments for control feedback must be assessed. For our application of PHIL control in microgrids, we are looking for an method which is feasible in RT, is robust against step changes or harmonics and can preferably work with continuous signals.

DFT based methods are common in Power quality (PQ) applications. However FFT analysis is computationally superior over DFT and feasible in RT applications. Yet, both methods still calculate all harmonics limited by sampling frequency and thus are computationally expensive for online applications. Buffering the signals to reduce burden is not suitable as this increases the convergence time of the estimates. Another issue is the change of signal and time localization of the estimates within large buffers. DWT based methods promise to be suitable for these changes but again the computation burden is drastically increased for RT applications [4]. KF based methods are robust against non-stationary signals [6], but the computation burden makes it infeasible for RT applications. SOGI based methods have the required computation efficiency for RT use and do not buffer the signal [5]. However, they do not outperform FFT type algorithms in convergence after step changes. KF and SOGI type methods also need a priori information on harmonic content and thus perform poorly in presence of unexpected harmonics.

2.1. Proposed method

We propose an approach where the measurements are subjected to amplitude modulation with synthetic complex exponential references followed by filtering. A block diagram representation of this proposed method is shown in Fig. 2. This concept is also known as, frequency-shifting and filtering [7], Coulon Oscillator [8], Quadrature Amplitude Modulation [9] or Complex Exponential Modulation [10,11]. They all involve shifting the required frequency component to 0 Hz for best results on the filtering step that follows. The complex exponential reference can be produced continuously from the RT controller clock signal. This gives us the benefit to timestamp without time localization issues, transfer and recover the estimated signals in other controllers. A

Moving Average (MA) filter generates a single coefficient in each step of the calculation. These coefficients hold the magnitude and phase information of the frequency component we wanted to estimate, as shown in (2),

$$X_m[n] = \frac{1}{N}\sum_{i=n-N+1}^{n} x[i]e^{\frac{-j2\pi mfi}{f_s}}. \tag{2}$$

In (2) the samples of $x[n]$ is multiplied with the corresponding element of the synthetic complex exponential reference along time and N-point MA filter is used to extract the parameters of mth harmonic component. N stands for the fundamental period of the $x[n]$ signal and it is directly affected by the components of the signals itself.

The proposed algorithm can be used on fundamental and any harmonic component of the signal. But N can also be chosen as multiples of the fundamental period to gain better frequency resolution. Such an averaging operation in (2) requires summation over N points. This is a recursive calculation, where the average value is changed by en-queuing and de-queuing elements. To reduce the number of sum operators on this function, the average values can be calculated by using consecutive elements of modulated signal. To make this possible a former coefficient obtained from the signal is written as given in (3),

$$X_m[n-1] = \frac{1}{N}\sum_{i=n-N}^{n-1} x[i]e^{\frac{-j2\pi mfi}{f_s}}. \tag{3}$$

Subtracting (3) from (2) gives us (4),

$$X_m[n] = X_m[n-1] + \frac{1}{N}\left(x[n]e^{\frac{-j2\pi mfn}{f_s}} - x[n-N]e^{\frac{-j2\pi mf(n-N)}{f_s}}\right), \tag{4}$$

which defines the coefficients for each harmonic recursively. This averaging concept is known in literature as Cascaded Integrator-Comb (CIC) Moving Average Filter [12].

Using the coefficients calculated by (4), magnitude and phase angles of the harmonic components can be calculated as given in (5a) and (5b), respectively:

$$A_m = 2\times\sqrt{\Re(X_m[n])^2 + \Im(X_m[n])^2}, \tag{5a}$$

$$\phi_m = \arctan 2(\Im(X_m[n]), \Re(X_m[n])). \tag{5b}$$

Waveforms for $x_m[n]$ can be calculated by combining real and imaginary parts of the coefficients with corresponding complex terms of the modulation signal as shown in (6a), or as in (6b),

$$x_m[n] = \Re(e^{\frac{-j2\pi mfn}{f_s}})\times\Re(X_m[n]) + \Im(e^{\frac{-j2\pi mfn}{f_s}})\times\Im(X_m[n]), \tag{6a}$$

$$x_m[n] = A_m\cos(\frac{2\pi mfn}{f_s} + \phi_m), \tag{6b}$$

where the calculated magnitude and phase angles are combined with the instantaneous time and a sinusoidal function. The approach in (6b), proves to be better in a distributed computation environment. A block diagram representation of the two methods is shown in Fig. 3.

This proposed algorithm is similar to calculating equivalent coefficients with Modulated Sliding Discrete Fourier Transform (mSDFT) [13] under certain circumstances. mSDFT is a stable and computationally efficient algorithm which has been used in other RT applications [14,15].

Processing rate and time synchronization

Typically, decomposed signals are reconstructed at the same sampling frequency. The RT controllers in CoSES can be used for a variety of control and regulation tasks. It is therefore preferable to have models which can operate at different sampling rates to manage the RT workload. Both the harmonic estimation and recovery models as proposed in this paper can be run at independent rates. Thus, the harmonic estimation model can be run at a low rate, to accommodate the burden of one model for each of the LV buses. On the recovery side, the models can be run at a higher rate to generate precise setpoints for prosumer emulators.

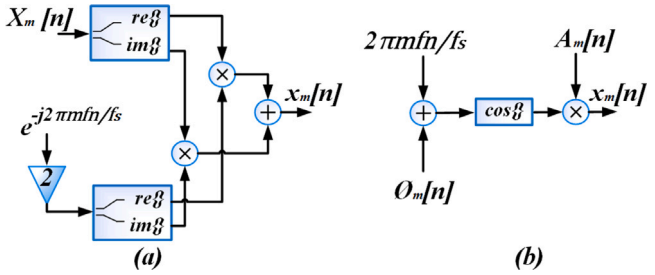

Fig. 3. Methods to generate waveforms from results of (4) and (5).

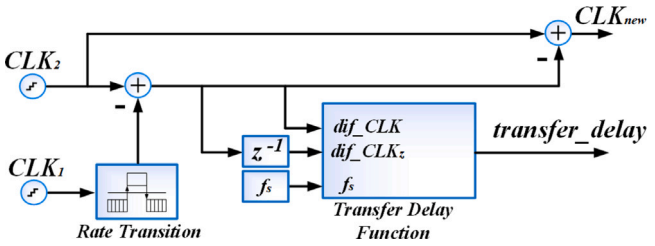

Fig. 4. Compensation of transfer delay to aid recovery of signals.

Time synchronization between multiple RT controllers is required for our approach to make sure the timestamps on sending and receiving end of the voltages are comparable. However in distributed PHIL applications, we cannot necessarily ensure that models start execution across two controllers at the same time, even though the clocks are synchronized. In other words, two model clocks can have the same rate of change but show different time due to the initial phase shift. Therefore a transfer delay function is introduced, explained in Algorithm 1, which takes the sending and receiving end timestamp as input. It produces a new clock signal for the recovery model and calculates the correct transfer delay between the two ends. A block diagram for the whole delay compensation block is shown in Fig. 4.

Algorithm 1 Transfer delay function

persistent variables
  $missing$, $checker$, $counter$;
end persistent variables
if $isempty(counter)$ **then**
  $counter \leftarrow -1$; $checker \leftarrow 0$; $missing \leftarrow 0$;
end if
if $|dif\_CLK - dif\_CLKz| > 10^{-9}s$ **then**
  if $checker = 0$ **then**
    $counter \leftarrow counter + 1$;
  else
    $missing \leftarrow missing + dif\_CLK - dif\_CLKz$;
  end if
else
  $checker \leftarrow 1$;
end if
$transfer\_delay \leftarrow counter/f_s + missing$;

2.2. Contribution

In summary, the contribution of from our proposed method can be listed as follows:

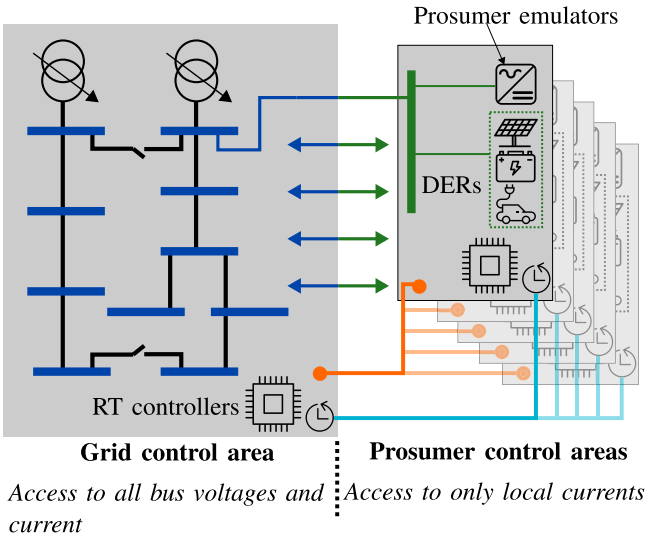

Fig. 5. CoSES electrical grid with the five prosumers. Prosumer buses ■ can be flexibly connected to any LV grid bus ■. An asynchronous communication link ■ connects different control areas within the lab. The controller clocks are synchronized ■ through a 1588 PTP ethernet link or through GPS.

- Since actual timestamp of the independent computation device is included in the calculations, it is easy to synchronize the measurements processed on independent devices in a decentralized/distributed environment.
- Decomposition and reconstruction models can be run on independent controllers using the local timestamps.
- Decomposition and reconstruction models can be run with different data processing rates to use RT resource effectively and gain higher precision on waveforms, if permitted.
- Compared to SDFT and recursive DFT calculations, the proposed method produces phase shifts (ϕ_m) on each sample rather than ($\frac{2\pi m f n}{f_s} + \phi_m$) (5b). This removes the need to use further reference signals to get the actual phase shift at each computation step.

3. Laboratory setup

CoSES is structured as a small microgrid with coupled electrical and heat sectors for five prosumers. The electrical part of the lab is of particular interest for this paper and is shown as a schematic in Fig. 5. On the left side, we see the CoSES LV grid, made of 70 mm^2 and 95 mm^2 three-phase four-core power cables sections, with a total length of approximately 2 km. The length of cable and connection pattern between the ten LV buses can be changed to fit any specific grid structure for an experiment. Two tap changing transformers connect the lab to the Munich LV grid. Two extra circuit breakers are also provided to couple the transformer buses and to create a meshed grid, respectively [1].

Prosumer emulators

Each of the five prosumers' bus has access to local DERs and a bi-directional inverter, which doubles as the prosumer emulator. These are part of the Egston COMPISO System Unit (CSU) [16], which acts as the PHIL component for CoSES. The Egston CSU at CoSES consists of seven 4-leg inverter cabinets which share the same DC bus. They serve as programmable bi-directional energy flow devices to emulate prosumer behavior. The Egston CSU can inject currents up to 5 kHz and thus can also be used as an active power filter in the grid.

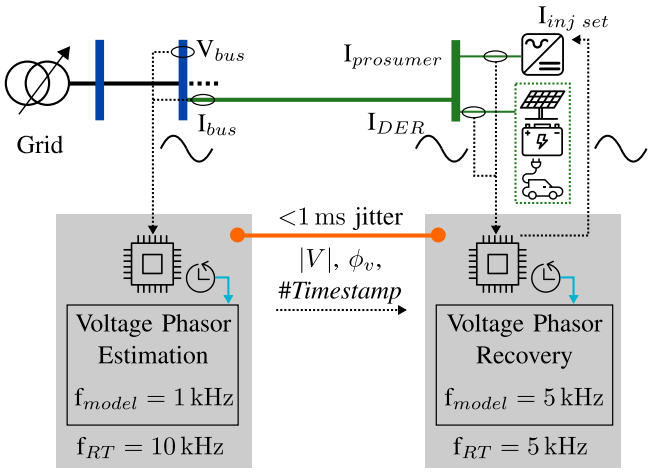

Fig. 6. Schematic representation of the grid synchronization and injection power measurement concept in CoSES.

Controllers

CoSES uses National Instruments (NI) hardware, PXIe-8880, and software, NI Veristand [17], for RT control systems of the electrical grid. Each of the five prosumers have a local RT controller and the sixth controller is located inside LV grid switchroom. The controllers act as a general purpose RT computer and have embedded systems capabilities through additional IO cards. They can also send injection setpoints to the Egston CSU through a SFP link. Within CoSES, they operate at either 5 kHz or 10 kHz RT target rate during HIL experiments. An asynchronous communication ring, shown in orange in Fig. 5, called Reflective Memory Network (RMN) is used to make data recorded or computed in any distributed controller available at other controllers under a 1 ms jitter. The software environment, NI Veristand, accepts compiled models from tools such as MATLAB/Simulink, LabVIEW, SimulationX and Python. The environment can run models at different execution rates, access field measurements and map IOs between models and hardware.

Time synchronization between RT controllers

Synchronization is an integral part of any HIL test bench with distributed control. However, as explained in Section 3, it attains a higher significance in CoSES due to the voltage and current measurements for a prosumer being split over at least two controllers, one local and the other in the LV Grid switchroom. RT Controllers in CoSES are synchronized through the NI-6683H timing and sync card, which slots into the PXIe chassis. The card provides synchronization over the 1588 Precise Time Protocol (PTP) or through a GPS antenna, as seen in cyan in Fig. 5. The HIL model clocks are thus synchronized to around 5 µs, as measured over experiments. A further synchronization is required for the PHIL emulator, Egston CSU, as it has a separate FPGA controller per cabinet. This is achieved over the SFP link, through a 4 µs strobe signal, which makes the Egston CSU clock a slave to the RT controller clocks. Thus, a laboratory wide time synchronization is achieved for measurements, PHIL emulators and RT controllers.

Sensors

A total of 246 current and voltage measurements are made in the CoSES electrical grid through LEM transducers [18]. These measurements are wired to the nearest relevant RT controller and are acquired at the controller target rate. As shown in Fig. 5, the grid control area has all the LV bus measurements and these are wired to the RT grid controller. At the prosumer level, the local currents from Egston CSU and DERs are wired to the local RT prosumer controller.

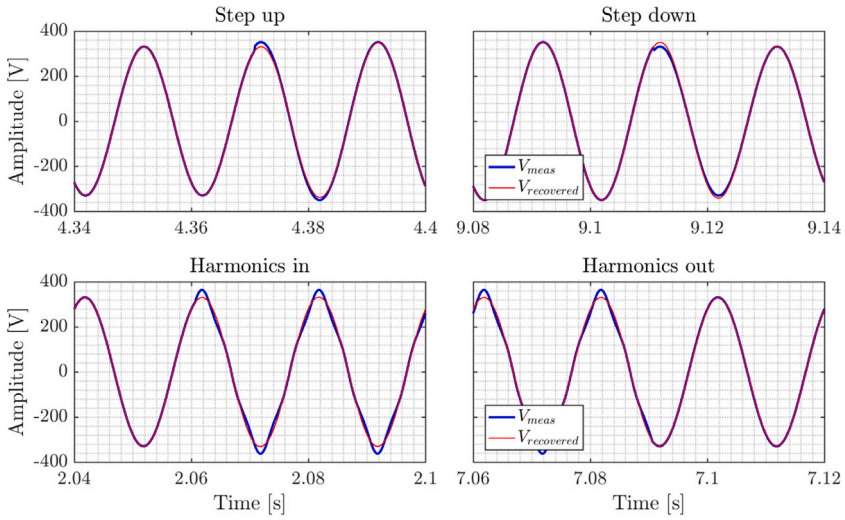

Fig. 7. Validation of recovered waveform under step and harmonic changes.

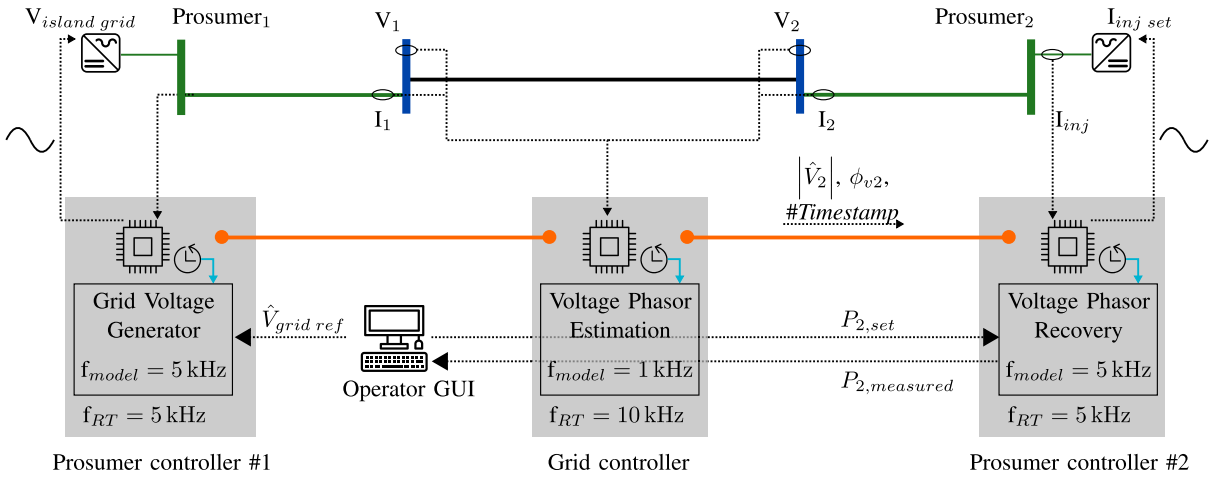

Fig. 8. Schematic of the PHIL experiment for constant power injection under step change or distortion of grid voltage in islanding mode. Prosumer#1 acts as the grid forming inverter and Prosumer#2 as grid following inverter with a fixed active power setpoint. Grid controller measures and analyzes the voltages.

4. Experimental validation and analysis

A schematic of the distributed measurements being used for grid synchronization and injection power calculation is shown in Fig. 6. The voltage of the LV bus (PCC) is measured at the grid controller, shown on the left. This analog measurement is fed to a phasor estimation model running at a specific execution rate. The output of this model, $|V|$ and ϕ_v, is sent out over the orange asynchronous link to the downstream prosumer's local controller, as seen in Fig. 6 on the right. These outputs are also timestamped at the grid controller. The prosumer controller, which is given a power setpoint by the operator, uses the transferred data as inputs for phasor recovery model, running at a specific execution rate. Since the controller clocks are synchronized, this model corrects the communication delay by comparing the incoming timestamp from the grid controller to its current controller time using the idea from Fig. 4. The model then outputs the current setpoint waveform, to be fed sample-by-sample to the Egston CSU. The injected power of the prosumer as a whole can be measured at the grid controller or individually from the Egston CSU and DERs at the local prosumer controller.

4.1. Validation of phasor estimation and recovery method

We first validate the phasor estimation and recovery models, shown in Fig. 6, with measurements in an island mode with a controlled voltage source. The models use the algorithm as mentioned in Section 2.1. The island grid voltage from one LV bus, is measured at the RT grid controller and then analyzed at 1 kHz to estimate the $|V|$ and ϕ_v. This is transferred to a prosumer controller, which recovers the voltage, at 5 kHz, as a waveform after delay compensation. Both the measured and the recovered voltages are logged individually in the two separate controllers. The results are plotted in Fig. 7 with the x-axis values being the local timestamp from the controllers at the point of logging.

In Fig. 7, we see the models reacting to a step change in the voltage amplitude from 330 V to 350 V and back. It can be seen that convergence between the recovered and measured waveform is achieved in approximately one cycle. In Fig. 7, 3^{rd} and 5^{th} harmonics are added to the island grid voltage. The harmonic magnitude is taken at 5% of the fundamental amplitude. The recovered voltage is unaffected as it is able to distinguish the fundamental component of the distorted measured signal. The results shows accuracy, quick convergence and robustness of the estimation and recovery models against changes in the measured voltage.

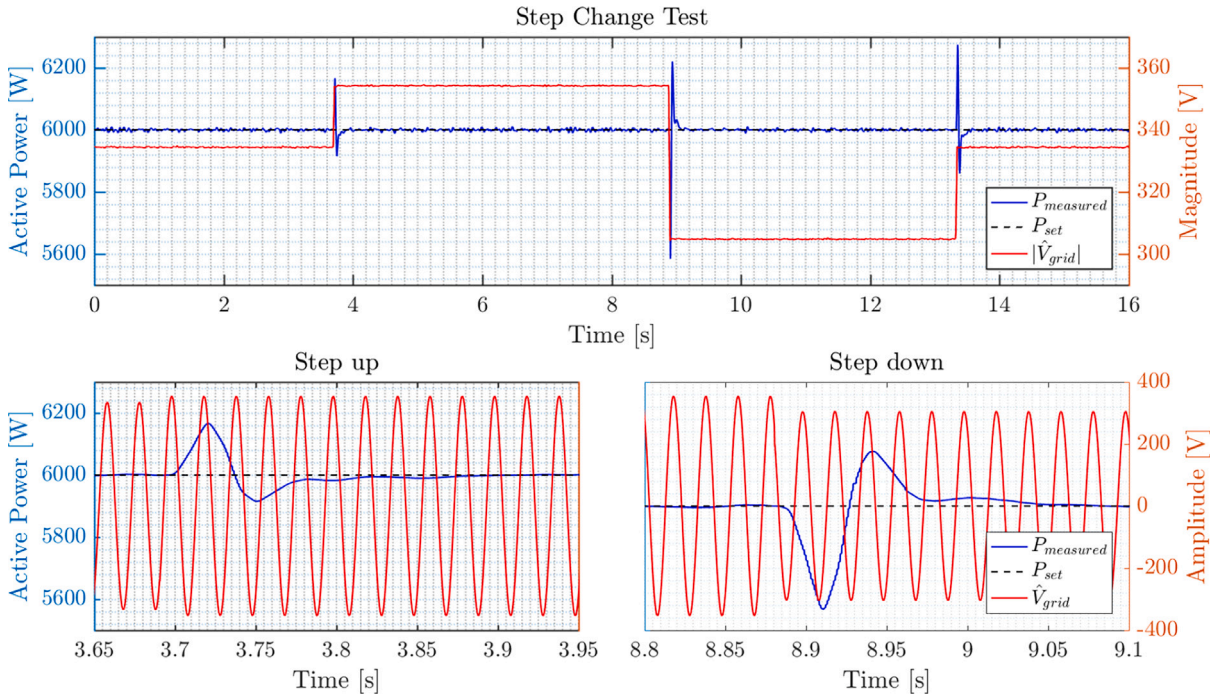

Fig. 9. Step change test on voltage with power control loop.

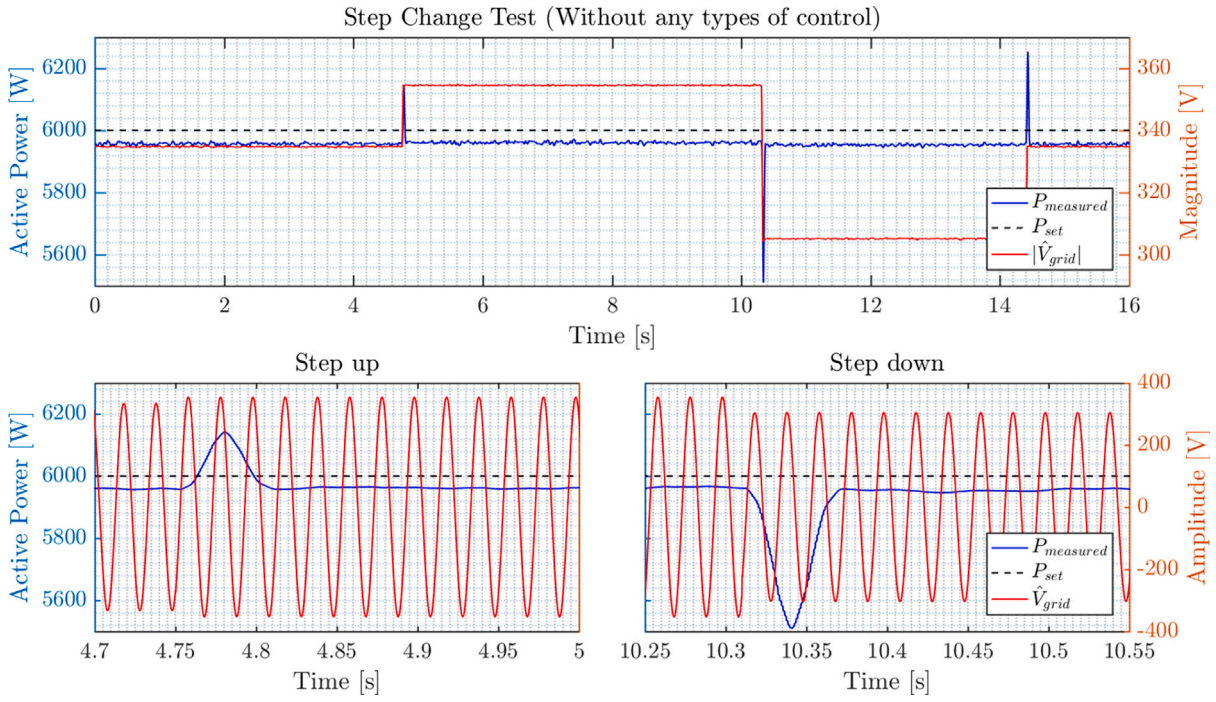

Fig. 10. Step change test on voltage without power control loop.

4.2. Implementation as a tool in PHIL experiments

Two PHIL experiments are conducted using the distributed measurement concept validated in the previous section. In Fig. 8, we use Prosumer#1 to act as a grid forming inverter with a $\hat{V}_{grid\ ref}$ given through the operator GUI. The same GUI also sends an active power setpoint $P_{2\ set}$ to Prosumer#2 which acts as a grid following inverter. The injected power from Prosumer#2 is also sent back to the GUI for logging. The grid voltage is analyzed in the Grid controller and sent to the Prosumer#2 controller, to calculate the correct $I_{inj\ set}$ for constant $P_{2\ measured}$ regardless of the change in $\hat{V}_{grid\ ref}$. As the Egston CSUs always consume some amount of reactive power based on the active power reference, the injected active power does not exactly coincide with the reference in most cases. Therefore a PI-based controller is used to modify the setpoint slightly to achieve exact injected active and reactive power. As this power control loop affects the convergence rate of the measurements, we show two sets of result, one with and one without the power controller.

In Figs. 9 and 10 we see the results as $\hat{V}_{grid\ ref}$ is changed from 330 V to 350 V, then to 300 V, and back to 330 V with a constant $P_{2\ set}$ = 6 kW.

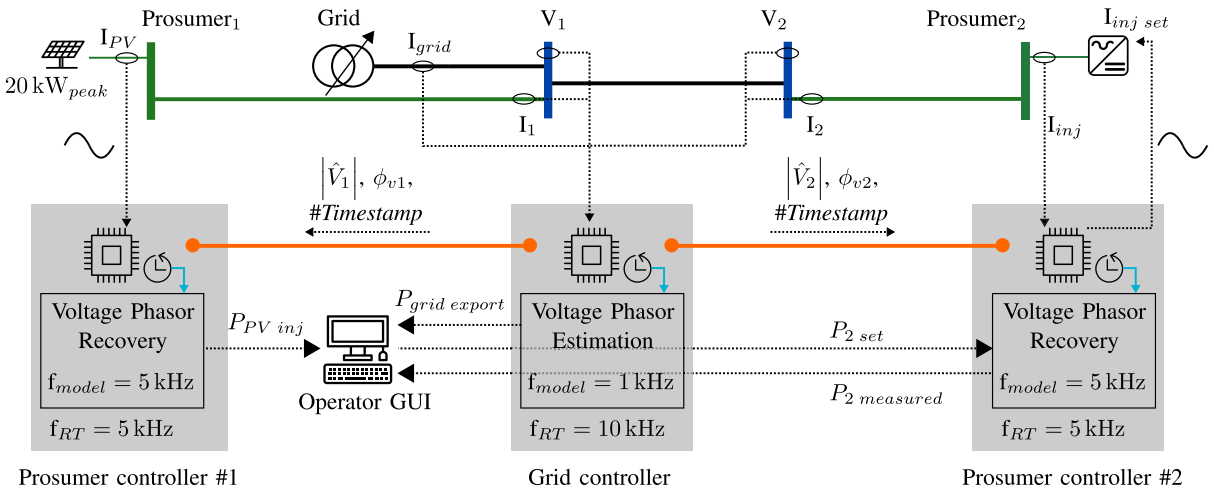

Fig. 11. Schematic of the PHIL experiment for matching the PV production as a dynamic load to make net export zero in grid connected mode. Prosumer#1 is connected to 20 kW$_{peak}$ PV and Prosumer#2 is programmed as a dynamic load with a power setpoint. Grid controller measures and analyzes the voltages.

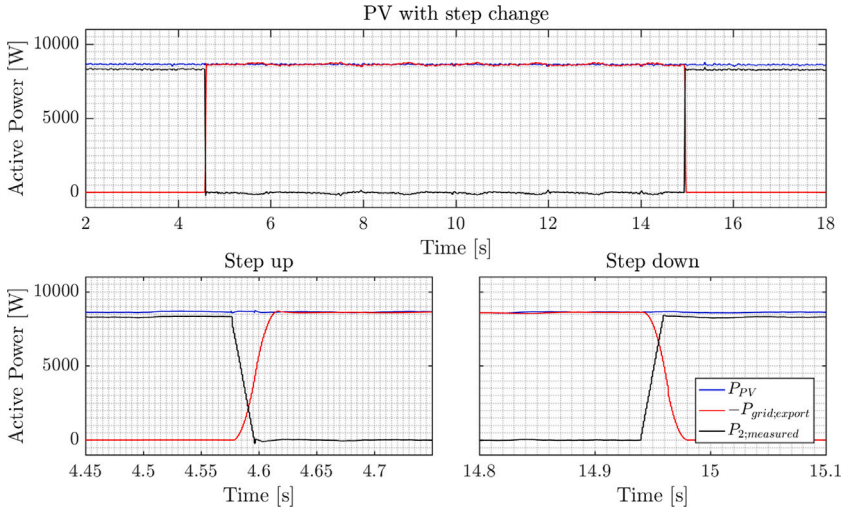

Fig. 12. Grid export with Prosumer#2 matching the PV power.

In Fig. 9, we see that the $P_{2\ measured}$ converges to $P_{2\ set}$ in around 6 cycles of the fundamental. We then turn-off the power controller and repeat the measurements in Fig. 10. Now the $P_{2\ set}$ and $P_{2\ measured}$ have a constant steady state error. However, the power measurement converges inside 2 cycles of the fundamental. These results are consistent with the convergence rate of Fig. 7, as the extra cycle is being used by the moving average part of the power measurement block.

We conduct a further PHIL experiment to minimize net grid export due to excess PV generation and the schematic is shown in Fig. 11. The LV buses are now connected to the Munich grid and thus the controlled prosumers must be synchronized using the information from the measurement models. The grid controller, as usual sends the measured voltages, V_1 and V_2, of the two LV buses to their respective downstream prosumer controllers. It additionally measures the exported power to the upstream Munich grid. Prosumer#1 measures the local DER power from the PV. This power is sent as $P_{2\ set}$ to Prosumer#2, which emulates a dynamic load to consume the total PV power. The load is measured as $P_{2\ measured}$ and sent to the operator GUI. We begin the experiment with Prosumer#2 turned off, switch it on during the experiment and turn it off once again towards the end.

In Fig. 12, we see the results logged on the operator GUI. Initially, the entire PV power is being exported to the grid. The exported power is slightly below the PV power due to the losses in the LV grid. When Prosumer#2 is turned on, it starts consuming the PV generation and the grid export starts to drop. As the power control loop is active the dynamic load exactly matches the PV generation and the grid export has dropped to zero. The transition takes approximately 40 ms or two cycles, which is again consistent with the results from Fig. 11. The same behavior takes place is reverse when the Prosumer#2 is then turned off.

5. Conclusion

We identified a gap in the distributed PHIL control literature, where all the relevant measurements are not directly wired to one controller. In the real world, an increasing number of prosumers on the LV grid may not have direct voltage measurements from PCC due to distance limits. We propose a frequency-shifting and filtering based fundamental signal analysis and recovery method between RT controllers connected to an unifying clock source, such as GPS. This method can work with variable delay between the sending and receiving end. We validated the proposed algorithm on a PHIL test-bed and then showed that it can be readily used in a variety of PHIL experiments in islanded and grid connected mode. The tool is now being used in the CoSES lab for all PHIL experiments.

CRediT authorship contribution statement

Erhan Sezgin: Conceptualization, Methodology, Formal analysis, Software, Writing – original draft. **Anurag Mohapatra:** Conceptualization, Methodology, Validation, Software, Writing – original draft. **Thomas Hamacher:** Supervision, Funding acquisition. **Özgül Salor:** Supervision, Writing – review & editing. **Vedran S. Perić:** Supervision, Project administration, Writing – review & editing.

Declaration of competing interest

The authors declare that they have no known competing financial interests or personal relationships that could have appeared to influence the work reported in this paper.

References

[1] V.S. Perić, T. Hamacher, A. Mohapatra, F. Christiange, D. Zinsmeister, P. Tzscheutschler, U. Wagner, C. Aigner, R. Witzmann, CoSES laboratory for combined energy systems at TU munich, in: 2020 IEEE Power Energy Society General Meeting, PESGM, 2020, pp. 1–5.

[2] IEEE standard definitions for the measurement of electric power quantities under sinusoidal, nonsinusoidal, balanced, or unbalanced conditions, 2010, pp. 1–50, IEEE Std 1459-2010.

[3] J.W. Cooley, J.W. Tukey, An algorithm for the machine calculation of complex Fourier series, Math. Comp. 19 (90) (1965) 297–301.

[4] J. Barros, R.I. Diego, M. de Apraiz, Applications of wavelet transform for analysis of harmonic distortion in power systems: A review, IEEE Trans. Instrum. Meas. 61 (10) (2012) 2604–2611.

[5] P. Rodriguez, A. Luna, I. Etxeberria, J.R. Hermoso, R. Teodorescu, Multiple second order generalized integrators for harmonic synchronization of power converters, in: 2009 IEEE Energy Conversion Congress and Exposition, 2009, pp. 2239–2246.

[6] A.A. Girgis, W.B. Chang, E.B. Makram, A digital recursive measurement scheme for online tracking of power system harmonics, IEEE Trans. Power Deliv. 6 (3) (1991) 1153–1160.

[7] Z. Shuai, J. Zhang, L. Tang, Z. Teng, H. Wen, Frequency shifting and filtering algorithm for power system harmonic estimation, IEEE Trans. Ind. Inf. 15 (3) (2019) 1554–1565.

[8] S. Tnani, M. Mazaudier, A. Berthon, S. Diop, Comparison between different real-time harmonic analysis methods for control of electrical machines, in: 1994 Fifth International Conference on Power Electronics and Variable-Speed Drives, 1994, pp. 342–345.

[9] A.E. Kibar, O. Salor, Harmonics analysis of power signals using quadrature amplitude modulation, in: 2016 24th Signal Processing and Communication Application Conference, SIU, 2016, pp. 1937–1940.

[10] E. Sezgin, O. Salor, Analysis of power system harmonic subgroups of the electric arc furnace currents based on a hybrid time-frequency analysis method, IEEE Trans. Ind. Appl. 55 (4) (2019) 4398–4406.

[11] E. Sezgin, Development of New Frequency and Time-Frequency Analysis Approaches on Power System Signals and Their Implementation on Hardware-In-The-Loop Framework (Ph.D. thesis), Gazi University, Ankara,Turkey, 2020.

[12] R.G. Lyons, Understanding Digital Signal Processing, 3/E, Pearson Education India, 2004.

[13] K. Duda, Accurate, guaranteed stable, sliding discrete Fourier transform [DSP tips & tricks], IEEE Signal Process. Mag. 27 (6) (2010) 124–127.

[14] P. Romano, M. Paolone, An enhanced interpolated-modulated sliding DFT for high reporting rate PMUs, in: 2014 IEEE International Workshop on Applied Measurements for Power Systems Proceedings, AMPS, 2014, pp. 1–6.

[15] C.M. Orallo, I. Carugati, S. Maestri, P.G. Donato, D. Carrica, M. Benedetti, Harmonics measurement with a modulated sliding discrete Fourier transform algorithm, IEEE Trans. Instrum. Meas. 63 (4) (2014) 781–793.

[16] Egston power product portfolio, 2021, https://www.egstonpower.com. (Accessed 03 September 2021).

[17] National instruments, 2021, https://www.ni.com. (Accessed 03 September 2021).

[18] LEM Europe GmbH, 2021, https://www.lem.com. (Accessed 03 September 2021).

Concluding remarks on the publication

The contribution introduces a fundamental signal analysis and recovery method based on frequency-shifting and filtering, allowing smooth communication and synchronization between RT controllers linked to a central clock source like GPS. This method is adaptable to variable delays between transmission and reception, enhancing its practical usability. This is particularly relevant due to the growing number of prosumers on the low-voltage grid who lack direct voltage measurements from the PCC because of distance constraints.

We thoroughly validated the proposed algorithm using a PHIL test-bed, confirming its accuracy, quick convergence, and robustness against varying measured voltage. Additionally, we applied the method to various PHIL experiments in both islanded and grid-connected modes. By incorporating actual timestamps from independent computational devices, the method easily synchronizes measurements processed in decentralized or distributed environments. This empowers us to execute decomposition and reconstruction models on independent controllers using local timestamps, even at varying data processing rates. Moreover, our method negates the need for extra reference signals to obtain phase shifts, distinguishing it from sliding discrete Fourier transform (SDFT) and recursive discrete Fourier transform (DFT) calculations.

Two distinct ADG experiments, one each in grid connected and islanded mode, were conducted using the proposed measurement concept. The first ADG experiment focused on constant power injection under step changes or grid voltage distortion in island mode, with power measurements converging within two fundamental cycles, in line with theory. The second ADG experiment aimed to align PV production as a dynamic load to achieve net zero export in grid-connected mode, demonstrating a transition from consumption to generation within approximately 40 ms or two cycles, consistent with expectations.

In conclusion, this research introduces a practical technique to address a gap in distributed PHIL control scenarios where essential measurements aren't directly accessible. The method has been in use for all experiments in the CoSES lab operations, underscoring the practical value of the work.

2.3 IoT observation platform (Publication #2)

Effective management and visualization of the measured and calculated data points is a vital task in establishing an ADG laboratory. The interdisciplinary nature of CoSES research draws practitioners from fields beyond traditional power systems. Facilitating collaboration in this environment requires abstracting lab setups and results to suit the researcher's needs. This calls for a tool that presents lab experiments at a glance and allows result monitoring, irrespective of the researcher's location—whether within the lab or remote.

Although the CoSES RT control environment, VeriStand [101], supports basic operator screens and graphical data visualization, it falls short in long-term data management aligned with current best practices [102]. Leveraging IoT-based services and applications addresses these gaps, providing a robust approach to data handling for labs like CoSES. The complexity arises from the various sensors, embedded systems, smart devices, and protocols that span energy systems. Additionally, making data access easy and enhancing

user experiences with time-series measurements are priorities. Therefore the focus is on creating an intuitive, user-friendly platform for experiment monitoring with minimum learning curve.

This led to the development of an IoT dashboard, aiming to offer robust monitoring within the CoSES ADG lab using open-source tools, accessible for researchers across fields. An IoT dashboard was created using InfluxDB 2.0 as a timeseries database and Grafana for visualization. This dashboard can be customized and accessed via web browsers, either locally or remotely. This provides a way to analyze experiment data without needing intricate knowledge of the PHIL setup. The effectiveness of the tool is demonstrated through a practical experiment with a CoSES prosumer, and the results are detailed in this paper.

Publication #2 - IoT Integration for Combined Energy Systems at the CoSES Laboratory

Authors - Matthias Mayer, Anurag Mohapatra, Vedran S. Perić

Publication - 2021 IEEE 7th World Forum on Internet of Things (WF-IoT), 14-31 July, 2021

Digital object identifier - `https://doi.org/10.1109/WF-IoT51360.2021.9596000`

Author	Contribution	Tasks
Matthias Mayer	50%	Methodology, Investigation, Software, Visualisation, Writing - original draft
Anurag Mohapatra	40%	Conceptualization, Methodology, Supervision, Visualisation, Writing - original draft
Vedran S. Perić	10%	Project administration, Writing – review and editing

IoT Integration for Combined Energy Systems at the CoSES Laboratory

Matthias Mayer
Department of Electrical and Computer Engineering
Technical University of Munich

Anurag Mohapatra
Munich School of Engineering
Technical University of Munich

Vedran S. Perić
Munich School of Engineering
Technical University of Munich

2021 IEEE 7th World Forum on Internet of Things (WF-IoT) | 978-1-6654-4431-6/21/$31.00 ©2021 IEEE | DOI: 10.1109/WF-IoT51360.2021.9596000

***Abstract*—Combined Smart Energy Systems (CoSES) microgrid lab at TU Munich has a large number of measured and calculated data points which need a robust tool to monitor and visualize. Furthermore, the tool should be simple to use among microgrid researchers from different fields of study. Based on these requirements, an IoT dashboard using open-source tools for experiment monitoring and visualization is developed for the CoSES microgrid lab. The solution uses InfluxDB 2.0 as a time-series database and Grafana for the visualizations. The dashboard can be easily customized and is both locally and remotely accessible from any modern browser. This enables the researcher to analyze the experiment data without detailed knowledge of the Power hardware-in-the-loop setup. A demonstrative experiment is conducted using one CoSES prosumer to verify the toolchain and the results are shown in the paper.**

I. Introduction

The Center for Combined Smart Energy Systems (CoSES) at TU Munich was established to research sector coupled, low-inertia, active distribution grids required for the future sustainable energy systems. The lab is realized as a small microgrid, with electrical and heat subsystems, with close integration of information and communication technology (ICT). It contains six fully controllable electrical and heat prosumers, based on Power-Hardware-in-the-loop (PHIL) philosophy, which can emulate a real world multi energy grid and thus eliminating the need to model them using real-time simulators. Detailed hardware specifications for the lab can be found in our previous publication [1].

One aspect of ICT usage in multi energy systems, such as CoSES, is the acquisition, logging and visualization of the generated data in real time. These have been characterized as part of the Internet of Energy (IoE) concept. IoE features the extension of microgrids with reliable, bidirectional and high speed communication networks for monitoring and control purposes [2]. Research institutions and industries have further used this potential, as highlighted in [3]. In CoSES, our focus is an easy-to-use monitoring and observation platform for our experiments. To this end, the presence of a variety of sensors, embedded systems, smart devices and protocols, over the different energy systems adds to the complexity of the problem. Finally, the ease of access to the data and enhanced user experience in handling the time-series of measurements are also of significance. The research within CoSES is vastly inter-disciplinary and thus attracts practitioners from fields outside the traditional power systems community. To facilitate collaboration, it is crucial to be able to abstract the lab and the results to the relevant level of detail based on the researcher's need. Therefore, a tool is needed to present the lab and its experiments at a glance and to monitor results for the systems of your interest, from your own desk either within the lab building or elsewhere.

IoT paradigms offer an elegant solution to these needs where we can consider our prosumers or devices as intelligent nodes. This can extend widely used connectivity and seamless integration concepts from the web towards the distributed embedded controllers for heat and electrical grid in the CoSES smart grid [4].

This paper presents an IoT dashboard, developed with open source tools, for CoSES. This tool can be used to monitor experiments in real-time and trend the previous results for analysis. It extends the sensor measurements and calculated data points, from models in the PHIL setup, to a time-series database. This database backup can be visualized quickly by the user for analyses, comparing different runs of the same experiment, trend high-level alarms and events or observe physical phenomenons over a wide-range of timescales.

The remainder of the paper is structured as follows. In Section II we explain the general control philosophy of CoSES. Then in Section III, we introduce the IoT toolchain to connect to this control network. A demonstration experiment is presented in Section IV to show how the dashboard visualizes the lab and the concluding statements are provided in Section V.

II. CoSES Control Philosophy

The control architecture of CoSES is based on the following three key features,

- *Modelling freedom* - Researchers working on PHIL test benches in CoSES, must have the option to work with the modelling and simulation tool of their choice to design operation and control strategies.
- *Time scales synchronization* - Control models in CoSES have widely different time scales based on energy system and model objective. They need to be synchronized to maintain real time causality through data exchange between models.
- *Commercial device protocols* - PHIL test benches should be open to commercially available smart grid components, and therefore industry standard communication

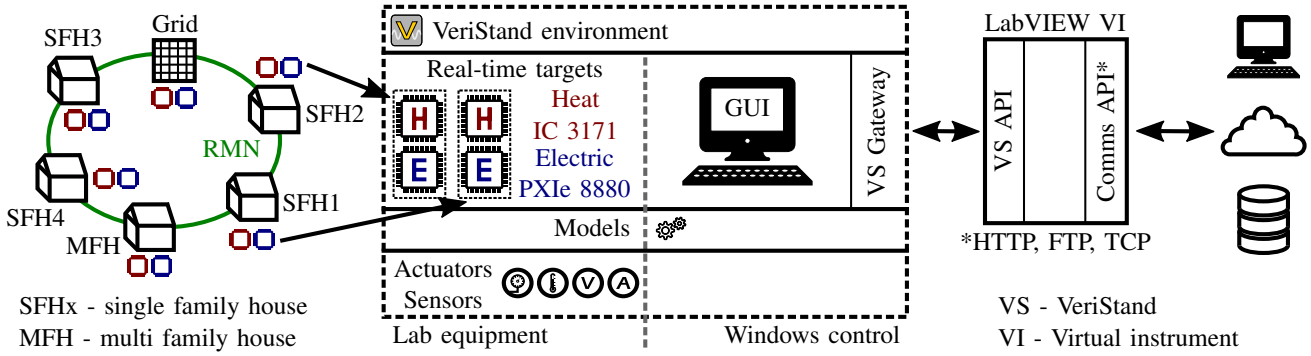

Fig. 1. Control schematic for CoSES Microgrid Lab.

protocols, to ensure the research is easily implemented in a real world scenario.

CoSES uses National Instruments (NI) hardware and software to realize the real-time control system within the lab. A schematic of the implementation is shown in Fig 1. Six PXIe-8880 embedded controllers are used as distributed real-time control agents for the electrical grid and six IC-3171 are similarly used for the heat grid. An optic fiber ring called Reflective Memory Network (RMN) is used to make data recorded or calculated at any distributed agent available everywhere within the network within 1 ms. This can be seen in the left part of the Fig. 1.

NI VeriStand is a software environment for real-time PHIL applications and can be deployed over general purpose computers and embedded controllers [5]. In the central part of Fig. 1, an example CoSES project with two prosumers is shown and the role of VeriStand is emphasized. Measurements for current, voltage, temperature, pressure, flows and counters are acquired within VeriStand through associated NI input-output (IO) cards. The rate of signal acquisition is different for different energy systems. PHIL operation set points are generated in prosumer control and grid emulator models and relayed back to the hardware from VeriStand through the same IO cards. These PHIL models are compiled using a variety of tools, not limited to, MATLAB/Simulink, LabVIEW, SimulationX and Python. VeriStand is able to synchronously deploy these models to the real-time embedded controllers in the lab and Windows PCs in the control room. The environment is capable of handling the different toolchains used for the models, their different execution rates and mapping IOs in-between models and hardware. On the Windows PC in the control room, a rudimentary operator screen with configurable user interface (UI) is also provided. This can be used to interact with the experiment in real-time and for low level monitoring of the results.

The right side of Fig. 1, shows how the VeriStand environment can be opened to the general data processing and communication protocols. LabVIEW is a graphical programming language by NI which is used as a backend unit for many other NI software [6]. VeriStand offers an Application Programming Interface (API), in a LabVIEW toolbox, which connects to a gateway on the control room Windows PC. This API can be used to read from and write into channels for both models and hardware, within a deployed real-time project. A LabVIEW virtual instrument (VI) can combine the VeriStand API with any other toolboxes for standard communication protocols. This creates a powerful tool to interact with the PHIL test bench from virtually any platform or over any protocol.

III. CoSES as an IoT Network

As mentioned in Section II, VeriStand offers rudimentary support for operator screens, graphical viewing of data and control panel widgets to interact with the hardware. However it is not meant for long term visualization and data handling in a manner consistent with state-of-the-art ideas on data management. IoT based services and applications offer the ease of usage and robust handling of data which can be useful for a lab like CoSES.

A. Network Architecture

The lab consists of actuators and sensors connected to controllers on the same switch. Therefore, as explained in Section I, the setup can be re-imagined as an IoT network with each house being an intelligent node. Through the VeriStand API, it is also possible to couple the PHIL infrastructure with an open-source analytics and monitoring platform. This can be supported by a time-series database and also enable remote viewing of the experiments.

A schematic of the CoSES IoT setup is shown in Fig. 2 and is divided into three sections - lab equipment, local network and cloud network. In the lab, the CoSES prosumers send measurements through sensors and receive set points from the embedded controllers. Within a single VeriStand project, the embedded controllers for each prosumer, run synchronously with their respective PHIL models. In the local network, a VeriStand instance running on the control room Windows PC is also part of the same project. In CoSES, there are approximately 1000 different channels which are either measured or calculated in VeriStand. As already explained in Section II and shown in Fig. 1, a LabVIEW VI for data logging can connect to the PHIL project using an API and then broadcast the channels to a time-series database using standard protocols. The data is stored into a time-series database and read by a local observation tool with a dashboard. A short

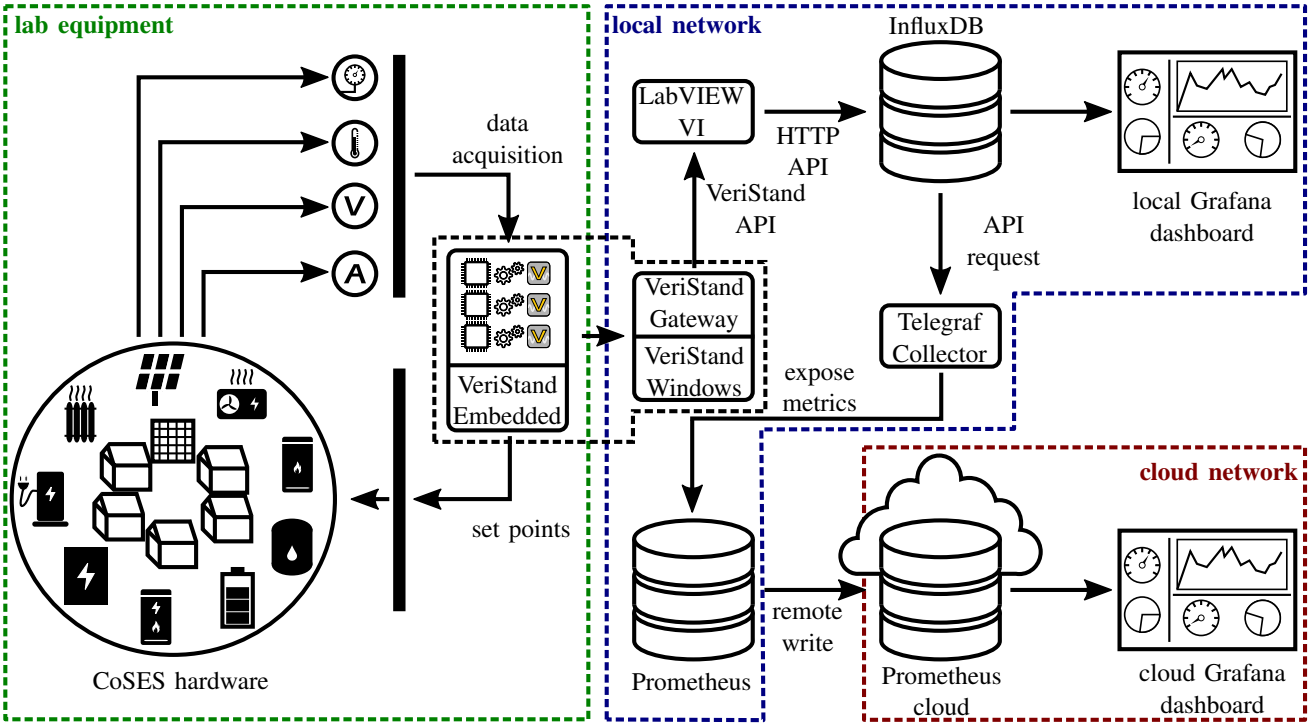

Fig. 2. CoSES laboratory control schematic with the IoT toolchain and dashboard.

term copy of the data is created, within the local network, in a real-time metrics database provided by a cloud observation tool. In the cloud network, this temporary copy is read by a cloud counterpart and associated with a remotely hosted dashboard. Thus a solution is proposed for both local and remote monitoring of the lab over any modern browser.

B. LabVIEW VI for Datalogging

A LabVIEW VI, as seen in Fig. 2, is the intermediary between the measurements and the time-series database in the local network. LabVIEW also offers an HTTP API toolbox which can execute standard methods such as POST and GET. These are used to transfer the data from the VeriStand channels to an InfluxDB 2.0 database [7]. InfluxDB 2.0, is a time-series database designed to handle the volume of timestamped data generated within projects like CoSES. It is also compatible with popular observation platforms as an additional benefit.

However, before the data can be transferred to a database, it has to be first logged from the channels with certain flexibility in choosing them and their frequency of logging. The mandatory inputs and the VI user interface is shown in Fig. 3. The bottom part of Fig. 3 shows some channel values received from VeriStand and the top half shows the response from the HTTP API. The Algorithm 1 shows the data logging idea in brief. The VI takes the location of the InfluxDB time-series database, the IP and port address and token credentials to write into the database as inputs. These do not need to be changed in subsequent runs unless the database itself is changed.

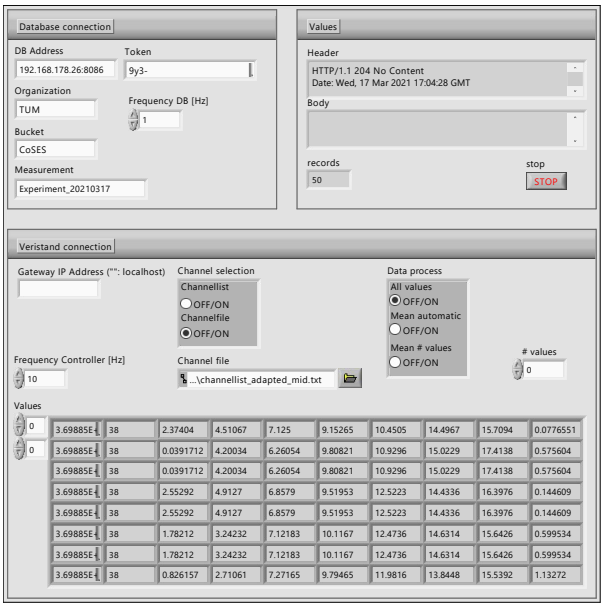

Fig. 3. User interface of LabVIEW VI for datalogging.

The VI must be provided with a channel list, which is obtained from the VeriStand signal mappings and can be exported directly as a text file. The next input is the frequency f_c, which determines the rate at which the VeriStand API requests new data from the channels. If this rate is too fast, the API would not have finished processing the previous batch before the new read/write request is initialized leading to duplicate values. Finally, the frequency f_{db} must be provided, which determines the rate at which the buffered data is written

Algorithm 1: LabVIEW VI for datalogging pseudo code.

```
Controller ← IP address, channels, f_c;
Database ← IP address, port, token, f_db;
r ← f_c / f_db;
while !stop do
    while i < r do
        read channel values;
        store data in array;
    end
    send values to InfluxDB;
end
```

into the database. All the data can be transferred to the database as it is or can be optionally averaged using two modes made available in the VI. The automatic mode averages over all the buffered data and in the manual mode the user can set averaging range as an integer between 1 and the frequency ratio, r. For example, if f_c = 10 Hz, f_{db} = 1 Hz and the manual averaging is set to 5, it will send two entries per second per channel into the database whereas the automatic averaging will send one entry per second per channel. This is helpful for very long experiments, lasting multiple days, where even a 5min precision of data is acceptable.

A nested while loop structure is at the core of the VI. The inner loop collects the specified channel values from the controller at f_c rate and buffers them in two arrays - a two dimensional data array and a single dimensional timestamp array. Individual columns in the data array are used for each individual channel which fills up in every execution. Normally, a time-series database such as InfluxDB 2.0 would automatically generate its timestamp when entries are updated. However to synchronize the entries with the lab, the system time from the controllers is read as a further channel from VeriStand and used to timestamp the signals. When the inner loop index, i, reaches the frequency ratio, r, the arrays are combined to a string and passed through the HTTP POST method to InfluxDB 2.0 as a new entry. Once the data insertion is finished, the inner loop restarts and the process is repeated until the experiment is stopped or an unexpected error occurs.

C. Visualization of the data

A powerful visualization tool is needed to exploit a time-series database for analysis and observation. Since the use case is in research, an open-source tool is always preferable due to the community around it and access to the source code if necessary. A variety of free open-source software exist for this purpose. Grafana was the most suitable for CoSES as it accepts around 30 different data sources, has many visualization plugins, is well documented and has a robust growing community [8]. Grafana can run locally on the PC to generate dashboards on any modern browser on a localhost address. The Grafana server runs as an executable on the local PC and is configured with a .ini file and the browser UI. The InfluxDB 2.0 database is arranged as sets of measurements associated with an experiment label. Grafana can perform queries on this database and visualize the stored metrics on its dashboard UI.

The Grafana dashboard is developed using panel plugins available in the tool. The dashboard allows the operator to choose between the tracked experiment and subsequently, the available data sets for each experiment is populated in a drop down list with check boxes. Thus previous experiments can be analysed with the full dataset and experiments currently underway update the plots as new data arrives. The minimum rate of data refresh is set in the Grafana .ini file and the actual rate can be set by the operator on the dashboard based on need. The default value is at 5 s and this can be lowered depending on how fast the queries can get executed. Ultimately the ideal refresh rate and the maximum viewing window, depends on the amount of data being visualized at once and the computational resources of the PC used by the operator.

D. Remote access to the dashboard

The localhost dashboard limits the observation within the CoSES building network. For internet based viewing we run Grafana Cloud which uses the Prometheus time-series database [9]. Automatic transfer of measurements from the local InfluxDB 2.0 database is enabled through the metrics collector service, Telegraf [10] and a local Prometheus database instance as shown in Fig. 2. In this setup, Telegraf sends an API request to the local InfluxDB 2.0 and receives the new measurements back. It then converts the data to a format compatible with Prometheus and exposes them on a localhost port. The local instance of Prometheus keeps listening on this port and records the new data. Later, a periodically executed remote write command extends this data to a Prometheus cloud instance which is linked to the Grafana Cloud services and its associated dashboards. Although user accounts are needed to access the cloud services, a snapshot of the dashboards can be hosted on a separate web server and be refreshed periodically. Thus a truly public platform can be created to observe the CoSES experiments as they take place from anywhere in world. This allows researchers to share live results with collaborators and enhances the possibilities through an online presence.

IV. Experiment and results

A simple experiment, shown in Fig 4, was setup to demonstrate the aforementioned IoT tools and the dashboard. On the electrical grid, two room heaters, a cooking plate and an electric drill were added as single phase loads. For the heat grid, a condensing boiler was used as the heating source combined with a domestic hot water storage facility. Although CoSES contains six electrical and heat prosumers, for simplicity reasons, only one was used for the experiment in this paper. This does not diminish the results as the dashboard and the associated tools can be extended to the other prosumers with no extra work provided every controller has its respective PHIL models.

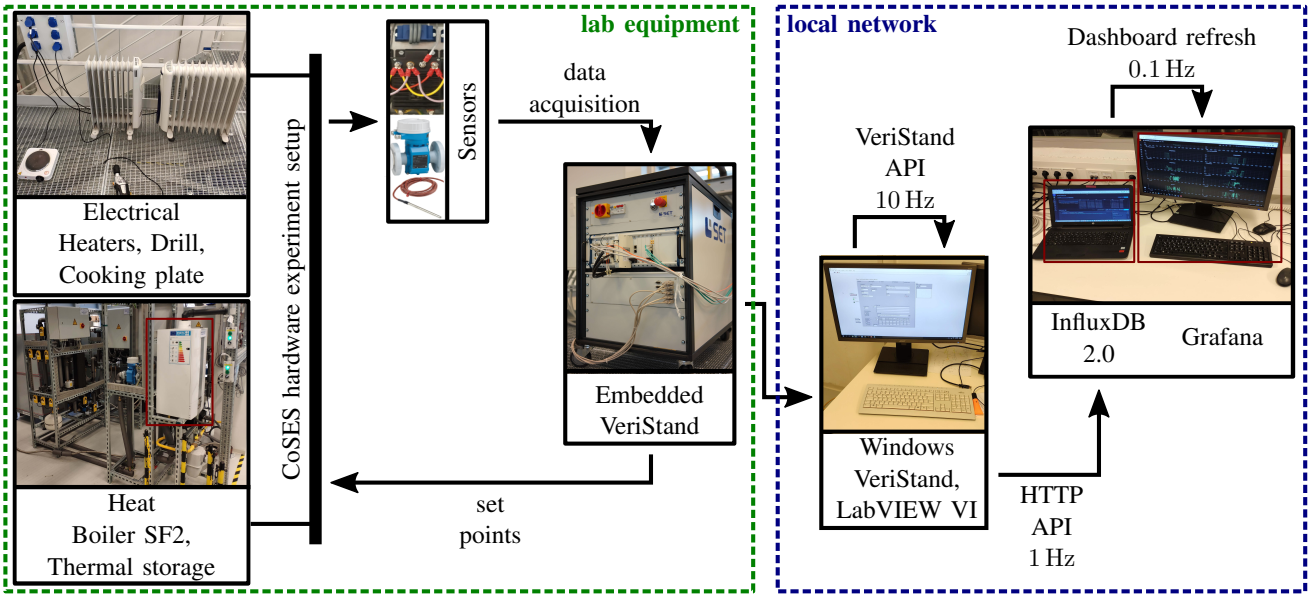

Fig. 4. Experiment setup for IoT dashboard demonstration in the CoSES laboratory.

TABLE I
DETAILED EXPERIMENT PARAMETERS.

	Electrical grid / **Heat grid**
Equipment	2 x 2 kW room heater, 1 x 1 kW cooking plate, 1 x Electric drill
	1 x 20 kW_{th} Condensing boiler 800L Thermal storage
Sensor	4 x LEM LF 210-S/SP3 Current transducers 4 x LEM CV 3-1000 Voltage transducers
	10 x PT-100 4 wire, temperature sensors 2 x Promag E 100, flow sensors
Data acquisition card	NI PXIe 4303, AI card
	NI REM-11100, AI card (Flow) NI 9216 RTD, cRIO AI card (Temperature)
Embedded Controller	PXIe-8880, Pharlap RTOS Target rate - 10 kHz
	IC-3171, Linux 64-bit Target rate - 100 Hz

Three phase current and voltage measurements were acquired for the electrical grid. Water flow and temperatures were measured in the heat grid. The boiler loading and control models were deployed through VeriStand on the IC-3171 embedded controller. The models to resolve raw current and voltage into fundamental components and calculate active and reactive power was deployed through VeriStand on a PXIe-8880 controller. Remaining details on the experimental setup is provided in Tab. I. In the control room, VeriStand on Windows, LabVIEW VI, InfluxDB 2.0 and Grafana dashboard on Google Chrome are all running on local network computers.

A fifteen minutes measurement duration is shown in the resulting local dashboard in Fig. 5. On the top the user can provide the *Measurement* name and the desired channels with the *Field* selection. This drop down list keeps itself updated with the time-series database. The screen refresh rate can be set on the top right corner of the dashboard. This can go as low as specified in the .ini file but high refresh rate can lead to spotty graphics as the local PC resources could get maxed out. In the example shown in this paper, we chose a 10s refresh cycle as the optimum.

In the first row of the dashboard shown in Fig. 5, user instructions and the current status of the experiment is provided. It also shows if VeriStand execution is happening in real-time through the HP count. When this count is non-zero, it signifies that the target rate is too fast and the execution loops are taking longer than specified in reality. In the second row, three charts show the metrics corresponding to the heat grid. The boiler heating power, which follows a constantly changing set point, is shown on the left side. Temperature measurements at different levels in the hot water storage tank are shown in the center graph and the water flow rate out of the boiler is displayed on the right. All electricity data generated during the experiment is observed with the remaining charts. The two heaters are connected to phase A and B. Their thermostat regulation is shown in the current magnitudes plot. Phase C is connected to the cooking plate and the drill, which can be seen as a discontinuous patterns on the blue curve in the current magnitudes plot. The third row shows active power metrics of the experiment. The left shows an instantaneous comparison of the three phases. The right is a stacked plot of the single phase active powers. The left plot on the fourth row shows the grid voltage during the experiment. The reactive power is shown in the bottom right plot which is being substantially contributed by only the electric drill.

The remote viewing dashboard was not presented in the results as the output window looks identical to the local dashboard. The dashboard in Fig. 5, is one of the many possible permutations an operator can make using the visualization

Fig. 5. Local Grafana Dashboard, showing the metrics of the experiment in Fig. 4.

plugins available in Grafana. We have used the standard and the clock plugins. Ideally, multiple dashboard would be setup in a single experiment by the operator and observed as separate tabs in the browser.

V. Conclusion

The CoSES lab at TU Munich with its PHIL and ICT components runs on a distributed control and data acquisition platform which need a powerful observation and monitoring software. This paper presented an open-source visualization tool for CoSES based on IoT paradigms. This tool works alongside the distributed control philosophy of the lab and thus allows the lab to function with the same freedom as before. A live dashboard, viewed from the browser tab of any local PC, is presented, which encapsulates the key measurements per experiment for the operator to monitor or analyze. A remote dashboard is also made available with limited history, to access from anywhere over the internet. The tool removes the necessity to intricately understand the control architecture and the NI toolchain to visualize an experiment. This could promote exchange of ideas and accessibility of the lab in the interdisciplinary microgrid research community.

Acknowledgment

The work shown in this paper was supported by the Deutsche Forschungsgemeinschaft (DFG) under the project number 350746631. Vedran S. Perić was additionally supported by the DFG project number 450821044.

References

[1] V. S. Perić et al., "CoSES Laboratory for Combined Energy Systems At TU Munich", *2020 IEEE Power Energy Society General Meeting (PESGM)*, Montreal, QC, Canada, 2020, pp. 1-5, doi: *10.1109/PESGM41954.2020.9281442*.

[2] E. Kabalci, and Y. Kabalci, *From Smart Grid to Internet of Energy*, Academic Press, London, UK, 2019.

[3] Y. R. Kafle, K. Mahmud, S. Morsalin and G. E. Town, "Towards an internet of energy," *2016 IEEE International Conference on Power System Technology (POWERCON)*, 2016, pp. 1-6, doi: *10.1109/POWERCON.2016.7754036*.

[4] N. Bui, A. P. Castellani, P. Casari and M. Zorzi, "The internet of energy: a web-enabled smart grid system," in *IEEE Network*, vol. 26, no. 4, pp. 39-45, July-August 2012, doi: *10.1109/MNET.2012.6246751*.

[5] *VeriStand 2018*, National Instruments, 2018.

[6] *LabVIEW*. National Instruments, 2018.

[7] *InfluxDB 2.0*. InfluxData Inc., v2.0.3, 2020. Available: https://docs.influxdata.com/influxdb/v2.0/

[8] *Grafana: The open observability platform*, Grafana Labs, 7.3.7, 2021. Available: https://grafana.com/

[9] *Prometheus Monitoring system & Time series database* , v2.24.1, 2021. Available: https://prometheus.io/

[10] *Telegraf Open Source Server Agent*, InfluxData, 1.17.2, 2021 Available: https://www.influxdata.com/time-series-platform/telegraf/

Concluding remarks on the publication

The paper meets a key need within the CoSES lab at TUM, where the combination of PHIL and ICT components provide an opportunity for the development of an open-source visualization tool adhering to IoT principles. This tool aligns with the lab's distributed control philosophy, enabling continued flexibility of experiment design. Through a live dashboard accessible via local PCs' browser tabs, operators can monitor and analyze key experiment measurements. Additionally, a remote dashboard with limited history offers online access, eliminating the need for intricate understanding of the control architecture and NI toolchain to visualize experiments.

An experiment showcased in the paper introduced single-phase loads to the electrical grid, including room heaters, a cooking plate, and an electric drill. For the heat grid, a condensing boiler served as the heating source, paired with a thermal storage unit. The experiment was conducted through the NI VeriStand project environment within the lab. The Grafana dashboard exhibited a 15-minute measurement duration. The CoSES lab is re-imagined as an IoT network, existing within the VeriStand control architecture. The Grafana monitoring ecosystem connects to this architecture via the LabVIEW API for VeriStand. Employing an HTTP API from LabVIEW facilitated POST and GET methods for interaction with the InfluxDB 2.0 database. On the lab's control room PC side, a LabVIEW VI was crafted to initiate data capture for the Grafana dashboard. This VI includes options for signal selection, capture rates, and moving average settings for time-series. These functionalities prove especially beneficial for extended experiments spanning multiple days, where a 5-minute data precision suffices.

The presented IoT-based visualization tool enhances operational efficiency within the CoSES lab by simplifying the experiment insights' accessibility and encouraging interdisciplinary collaboration within the wider research community. The seamless integration of control architecture, monitoring ecosystems, and data management through open-source tools presents a promising avenue for advancing ADG research.

2.4 CoSES PHIL framework (Publication #3)

The previous two publications have dealt with two specific issue regarding synchronised and accurate measurements and a live observation platform for an ADG laboratory. We now revisit the general question - What features must be present within an ADG laboratory designed for research institutions? The following Table 2.2, tries to list some of the expected features in an inexhaustible list. Such a laboratory configuration opens options for, to name a few - validating RT control concepts, using embedded intelligence for new grid services, and building data-driven models based on real DER behavior. All of this is achievable while engaging with prosumers, using distributed control schemes, localizing measurement wiring, operating on realistic test beds, and designing efficient experiments to simplify collaboration.

The next publication focuses on generalising the PHIL infrastructure in the CoSES laboratory at TUM for experiment design. The core idea is presenting a control system framework for PHIL test-beds with distributed RT controllers through the NI VeriStand environment. This framework combines RT computation with options for secondary and

Table 2.2: Desirable Hardware and Software features for an ADG laboratory.

Hardware Requirements	Software Requirements
Emulation instead of Simulation - Use real DERs, prosumers and grids. Emulate using powered test beds to mimic dynamic response for that which cannot be represented with real hardware.	**Free choice of toolchain** - Researcher's time must be used to work with the tools and not on learning the tools.
Flexible grid configuration - No single topology is suitable for all experiments. ADG Laboratory should be flexible to change cable lengths, re-order the buses or change the prosumer locations.	**Multiple timescales** - Control architecture must be cognizant of the orders of magnitude difference in time constants for grid control tasks.
User-friendly reconfiguration procedure - Flexible configurations should also be easy to implement and electrically safe without constant intervention in the field through a qualified electrician.	**Distributed instrumentation** - ADGs cannot centralize computation in one location. A practical test bench should follow the same principles.
Minimize power losses - Full load ADG experiments cannot be carried out without a power feedback loop.	**Open to commercial protocols** - ADG lab should be open to industry communication protocol and remote interfaces to test DERs in real-world conditions.

tertiary control. The result is a RT control environment with an API facilitating connection to computation tools and algorithms. Two experiments are presented to validate PHIL and demonstrate the proposed control framework's utility in exploring ADG research themes.

As a consequence to this experiment design structure, a clear distinction exists among hardware emulation, dynamic RT simulation models, and static simulation or optimization models. This structured approach allows abstraction, with one layer emphasized as the primary research focus and others represented through standardized models. The paper also highlights the potential of this abstraction in investigating ADG research questions.

Publication #3 - PHIL Infrastructure in CoSES Microgrid Laboratory

Authors - Anurag Mohapatra, Thomas Hamacher, Vedran S. Perić

Publication - 2022 IEEE PES Innovative Smart Grid Technologies Conference Europe (ISGT-Europe), 10-12 October, 2022

Digital object identifier - https://doi.org/10.1109/ISGT-Europe54678.2022.9960295

Author	Contribution	Tasks
Anurag Mohapatra	70%	Conceptualization, Methodology, Investigation, Validation, Software, Visualisation, Writing – original draft
Thomas Hamacher	10%	Supervision, Funding acquisition, Resources, Writing - review and editing
Vedran S. Perić	20%	Supervision, Project administration, Writing – review and editing

2022 IEEE PES Innovative Smart Grid Technologies Conference Europe (ISGT-Europe) | 978-1-6654-8032-1/22/$31.00 ©2022 IEEE | DOI: 10.1109/ISGT-Europe54678.2022.9960295

PHIL Infrastructure in CoSES Microgrid Laboratory

Anurag Mohapatra
Technical University of Munich
Munich, Germany
anurag.mohapatra@tum.de

Thomas Hamacher
Technical University of Munich
Munich, Germany
thomas.hamacher@tum.de

Vedran S. Perić
Technical University of Munich
Munich, Germany
vedran.peric@tum.de

***Abstract*—This paper describes the implementation of Power hardware-in-the-loop (PHIL) infrastructure of the CoSES laboratory at TU Munich. We present a control system framework for PHIL test-beds with distributed real-time controllers, using NI Veristand environment. This framework combines real-time computation with software in charge of secondary and tertiary control. The arrangement works as a real-time control environment, with an API access for connection to computation tools and algorithms. Two experiments are presented to validate the PHIL performance and to demonstrate the use of proposed PHIL control framework in investigation of an Optimal Power Flow (OPF) algorithm.**

***Index Terms*—Smart energy systems, Microgrid, Smart grid, Power hardware-in-the-loop, Laboratory infrastructure**

I. Introduction

Microgrids at low voltage (LV) level featuring fully controllable prosumers connected to renewable energy sources, have emerged as key players in energy sector transition pathways. Microgrid control philosophies, among others, rely on flexibility and load shifting capacity offered through sector coupling with heat and transportation networks. Furthermore, a high penetration of Information and Communication Technology (ICT) and decentralised control strategy in power systems are needed to strengthen the adoption of renewable microgrids in a wide scale. Microgrid research, therefore, focuses on small-scale, reliable multi-energy systems with limited dependence on the wide area synchronous grids through high concentration of local renewable energy resources.

Research into multi-energy microgrids with prosumer capabilities requires interdisciplinary approaches over traditional electrical power system fields. A few attempts have been made to create research facilities with a LV active distribution grid and interface them with real-time simulators and power amplifiers [1], [2], [3], [4] . These labs use detailed grid models with SCADA tools and specialise in investigating a niche field such as, grid resilience, environmental impacts on DERs, among a few. Another approach seen in this field is the concept of living labs, where research facilities have access to a public grid servicing many real customers [5], [6]. This ensures high quality data from the test network but there is an obvious limitation to the extent a real grid can be tampered for research purposes. Therefore, one can position a gap, where there is a need for a fully controllable, LV grid but with capacity to emulate real prosumers. The Center for Combined Smart Energy Systems (CoSES) at Technical University of Munich (TUM) was established to address this gap by providing capability to emulate a small multi-energy microgrid with fully controllable electrical, heating and transportation network.

The overall concept of the lab for the electrical, heat and communication grid, was introduced to the research community in [7]. However, a detailed design of the PHIL infrastructure and a clear pathway to conduct experiments using the facilities were omitted. In this paper, we present design motivation and precise implementation scheme of the CoSES electrical grid, PHIL test-beds and the associated control architecture. We also present a PHIL framework to unify optimisation and real-time emulation domains, with an access to standard APIs and minimal discrimination for the choice of programming tool-chain. Furthermore, we show results from two experiments to validate the PHIL infrastructure and a demonstration of the research directions of the laboratory using the proposed PHIL control framework.

The PHIL framework with the NI Veristand environment connects real time computation with offline simulation and optimisation algorithms. Notwithstanding the specific NI toolchain, researchers in other facilities can use the schematic of this framework to extend the results popular in multi-energy energy system modelling communities, to DER and PHIL control schemes with distributed controllers. This can help bridge the gap between simulations and experimental results, which is essential to instill confidence in the proposed ideas and develop them for real world applications. Similarly, while the lab has specific hardware, it is our hope that the adopted design and control philosophy of the multiple complex and distributed PHIL test beds, can be helpful for the community in developing similar laboratories.

The remainder of the paper is organized as following. Section II provides the philosophy behind the design choices in CoSES electrical grid and a description of the PHIL hardware. Section III provides the philosophy behind the control system design in CoSES, a description of the RT environment and associated hardware, with an emphasis on the PHIL control framework. Section IV shows two PHIL experiments as an

The construction of the CoSES laboratory was supported by Deutsche Forschungsgemeinschaft (DFG) through the project "Flexible reconfigurable microgrid laboratory" under Project number 350746631. The work of Vedran S. Perić was supported by DFG through the project "Optimal Operation of Integrated Low-Temperature Bidirectional Heat and Electric Grids (IntElHeat)" under Project number 450821044.

example use of the laboratory, which uses the control framework and equipment introduced in the previous section. We conclude in Section V, with a brief summary of the work.

II. CoSES electrical grid

In this section we present the design of the CoSES electrical infrastructure, followed by a detailed explanation of the LV grid, PHIL infrastructure and DERs as represented in Fig.1.

A. Philosophy

The electrical grid design of CoSES is based on the following key features,

1) Emulate and not simulate: Use of Real-Time (RT) simulators for detailed grid models, requiring validation, is the dominant trend in power systems laboratories. However, CoSES uses an actual grid, prosumers and Distributed energy resources (DER), wherever possible. Concepts that cannot be represented with the real hardware are emulated with test beds to mimic the dynamic response.

2) Flexible grid configuration: A laboratory for microgrid experiments should possess the following flexibilities in grid configuration: 1) switching between radial or meshed topology, 2) changing cable lengths, 3) re-ordering of buses, 4) flexible prosumers location, 5) variable DER capacities, and 6) grid or islanded mode.

3) User friendliness in changing configurations: The flexibility in grid arrangement must be easy to implement. Experiment specific configurations like, the location of prosumers, DERs and grid topology must be electrically safe to change for a researcher without LV electrician qualifications.

4) Minimize power losses for full load experiments: A microgrid can be rated at more than $100\,\mathrm{kVA}$ and such power cannot be realistically consumed in a laboratory for long duration. Therefore, to conduct continuous PHIL experiments at rated current and voltages, a power circulation loop into the supply grid must be established through the lab.

B. Grid

The CoSES electrical system is described in the Fig. 1. Two tap changing transformers connect a LV cable network, spread over a maximum of 10 buses, to the Munich city grid. The power cables have a total length of approximately $1.8\,\mathrm{km}$ and are distributed over 12 cable sections which can be connected between two arbitrary LV buses. The cables are four core NYCWY cables with cross-sections of $70\,\mathrm{mm}^2$, $95\,\mathrm{mm}^2$, and $150\,\mathrm{mm}^2$. The grid topology can be altered by changing the cable lengths between two buses. Radial and meshed topology can be accomplished using the circuit breaker labeled CB2 in Fig. 1. If needed, the grid can also be split into two separate radial distribution grids by opening CB1 and CB2 in Fig. 1. A separate $630\,\mathrm{kVA}$ transformer is used to provide a current feedback path for PHIL experiments. This allows the lab to perform experiments at the rated power levels of a LV distribution grid, while consuming only the power equivalent of the losses on the lines.

As mentioned in [7], the lab is designed as 4 single family houses (SFH) and one multi family house (MFH) connected together in a distribution grid of flexible topology. For the electrical grid, each of these houses is realised as a LV distribution board which can be connected to any of the 10 LV buses. This affords great ease and flexibility in moving the prosumer nodes across the grid for scenario studies within the same experiment context.

C. Prosumer buses

CoSES offers five prosumer nodes, represented as houses, and each of them has access to PV, battery storage, electric car chargers, prosumer emulators and a coupling to the heat network. They are labelled as Single family house (SFH) or Multi family house (MFH) in Fig. 1, while the detailed structure of a prosumer is shown with an inset image of the SFH2.

1) Prosumer emulators: The Egston COMPISO System Units (CSUs) work as the PHIL emulators in CoSES [8]. The Egston CSUs are series of seven 4-leg inverters, which share the same DC bus and can emulate bi-directional prosumer behaviour. The inverters can individually generate or consume up to $100\,\mathrm{kVA}$ at LV grid voltage, and have a combined load capacity of $230\,\mathrm{kVA}$ taken over all seven inverters. They can inject harmonics up to $5\,\mathrm{kHz}$ and can be programmed as active power filters. They can also be configured as voltage or current source inverters, which allows the lab to either operate in island or grid connected mode. Five CSUs are connected to the prosumer nodes as shown in Fig. 1. The remaining two CSUs are directly connected to the LV grid at Bus B5 and B8. These can emulate two extra prosumers in CoSES, shown as MFH2* and MFH3* in Fig. 1.

2) DER: Each prosumer node in CoSES, in addition to the Egston CSU emulators, has a possible connection to photovoltaics (PV) - 2 x $5\,\mathrm{kW}$ & 1 x $10\,\mathrm{kW}$, batteries - 2 x $13\,\mathrm{kWh}$, electric vehicle (EV) chargers - 2 x $22\,\mathrm{kW}$, and household plugs. These connections are shown for SFH2 in Fig. 1. To allow for maximum flexibility in connecting prosumer nodes to resources, a CEE [9] connector switchboard design, shown on the left in Fig. 2, is implemented for PV-battery systems and EV chargers. Thus, every prosumer can have a variety of DER capacities depending on the experiment requirements. A short cable with CEE connectors at both ends can be used to move a prosumer node to any bus within the CoSES grid, as can be seen in the cabinet image on the right in Fig. 2. The design for the DER and prosumer patch cabinet, makes it safe and user friendly to rearrange the resource within CoSES grid.

III. Control and instrumentation

In section we present the CoSES PHIL framework using the real-time control and instrumentation devices in the lab. The choice of the hardware and software is motivated by a desire to unite models from a variety of toolchains and combine real-time control with optimisation outputs or near-real-time processes. The controllers are also chosen to respect real-world limitations of physical locations, distances and commercial communication technologies. This is followed by a detailed

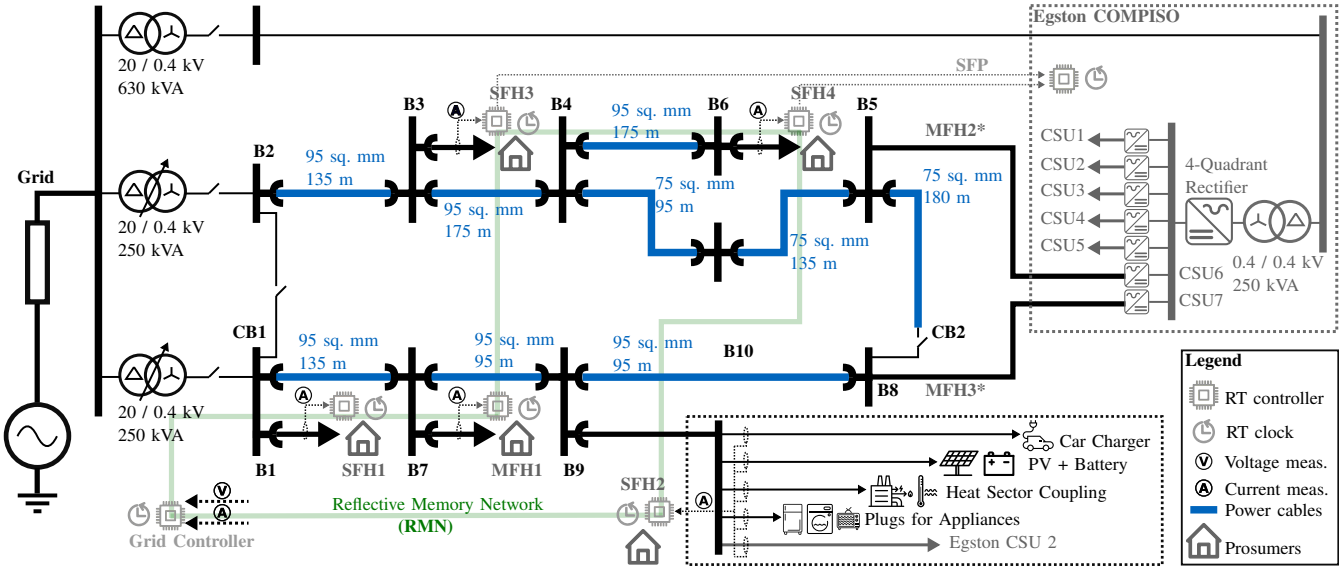

Fig. 1. Schematic representation of CoSES electrical and control infrastructure being used as a PHIL test bench.

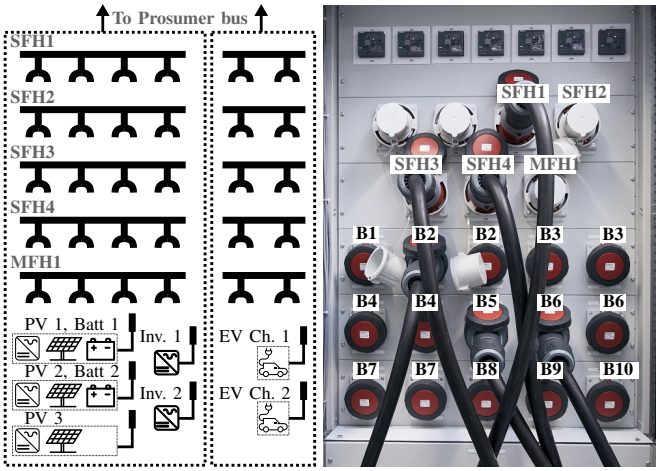

Fig. 2. DER (left) and Houses (right) connection cabinet

explanation of the control hardware, real-time environment, experiment design and instrumentation as shown in Fig.3.

A. Philosophy

The control philosophy of CoSES is based on the following guiding principles,

1) Free choice of toolchain: Researchers should be able to use different control design or power system simulation software, according to their individual preference, to foster co-operative work in an interdisciplinary field.

2) Multiple timescales: The time constants of power control and current control loops can vary by orders of magnitude. Furthermore, static simulations and optimization models for energy management systems must be incorporated to PHIL experiments to validate microgrid control schemes.

3) Distributed instrumentation and computing: Microgrid operation and prosumers should be monitored and controlled by a set of independent Real-Time (RT) resources, communicating with each other, as opposed to the centralised approach used in traditional power system test benches. This is important as DERs enabled prosumers can be spread over a geography too big for direct wiring of all measurements and real-time control from a central controller.

4) Open to commercial protocols: PHIL test benches for microgrid research should be open to industry standard protocols and interface with commercially available smart grid components, to ensure easy replication in real world scenarios.

The control philosophy of CoSES is represented in Fig. 3 and the individual components are explained further in subsequent sections.

B. Controllers

CoSES uses a National Instruments (NI) hardware and software ecosystem to realise the RT multi-energy grid control system environment. For the electrical PHIL experiments, each of the five prosumer nodes are provided with a PXIe-8880 embedded controller for the local prosumer control and measurement tasks. An extra controller is provided for the CoSES LV grid buses to collect bus voltage and branch current measurements. The controllers run the PharLap OS and are compatible with a variety of Input/output (IO) cards. The locations of the controllers is shown in Fig. 1. Within CoSES, the controllers operate at either $5\,\mathrm{kHz}$ or $10\,\mathrm{kHz}$ RT target rate for PHIL experiments. An asynchronous communication ring link, the Reflective Memory Network (RMN), is used to transfer data from one controller to another within $1\,\mathrm{ms}$ delay, as shown in Fig. 1 and 3. This setup allows a distributed RT control scheme for PHIL experiments, where grid measurements, monitoring, and prosumer current injection can be separated into different RT targets.

Distributed computation resources also allow for multiple experiments to be conducted simultaneously. The RMN asynchronous link transfers data from RT targets independently

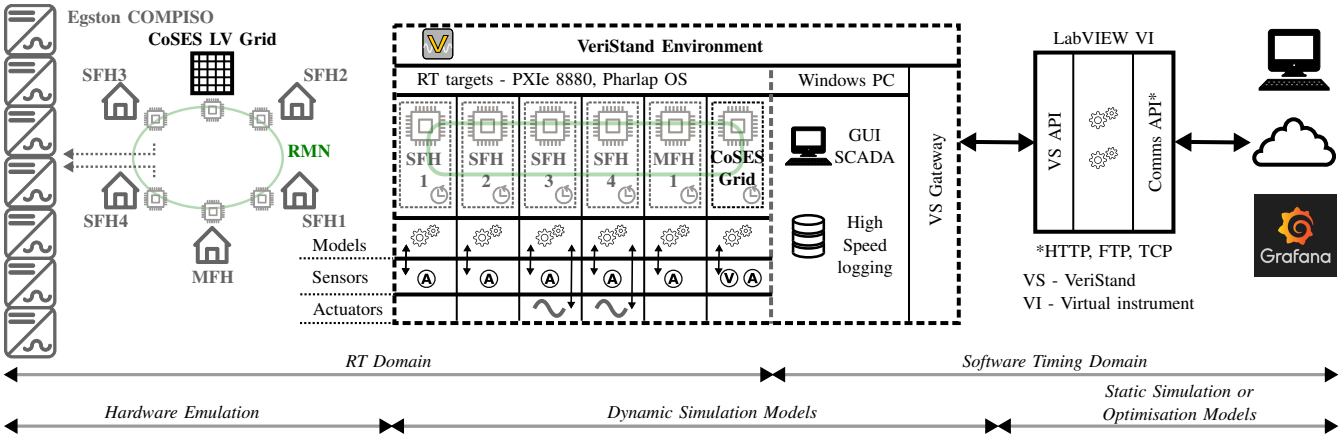

Fig. 3. CoSES PHIL control framework: PHIL testbeds (left), RT hardware and software (center), LabVIEW API access to external software (right).

from the experiments. Thus multiple PHIL experiments can take place simultaneously by sharing the LV grid measurements over the RMN.

Current or voltage setpoints are sent to the Egston CSUs, acting as prosumer emulators, through a SFP link IO card connected to the RT controllers. This card is available in SFH3 and SFH4 controllers, as seen in Fig. 1 and 3. Each card can provide setpoints to maximum four CSUs. The setpoints are transferred as sampled points to the Pulse width modulation controller of the Egston CSU. The control algorithm in the RT target converts the power setpoints to continuous waveform and sends them over to the CSU at $4\,\mu$s intervals.

NI VeriStand (VS) [10], is used as the RT software environment for PHIL applications in CoSES and is represented in the center of Fig. 3. VS can be deployed over Windows PCs and embedded RT targets running PharLap or NI Linux RT OS. Researchers can prepare their control models using a variety of tools, not limited to, MATLAB/Simulink, LabVIEW, Dymola, C, C++ and Python. VS accepts the compiled models as .dll or Functional Mock-up Interface (FMI) file. Once compiled, the models can be assigned to any RT target within the CoSES network. VS lists and maps IO from other RT targets, included in the project, using the RMN feature, albeit at a maximum $1\,\mathrm{ms}$ delay. Models can be run at different execution rates using a decimation of the RT target rate.

The VS project is configured, deployed and monitored over a Windows Host PC. A rudimentary GUI can be configured as an operator control screen to interact with the PHIL experiment and log results. High speed logging, up to the RT target rate, is possible for all transient measurements. VS offers an API for LabVIEW, .NET and C# to interact with the deployed VS project from external software. Although this connection is not RT, it can be used to transfer setpoints from an optimization routine, cloud database, a co-simulation or an energy management system with commercial communication protocols. This methodology is leveraged to develop an open-source IoT platform based monitoring and logging tool for CoSES in [11].

C. Measurements

CoSES uses a total of 246 Hall effect and closed loop fluxgate transducers for current and voltage measurements respectively in the lab [12]. The grid RT target collects all bus voltages and branch currents, while the prosumer RT targets generate appropriate control action of DERs and the Egston CSU. Since the measured bus voltage phase and magnitude information are required for closing a feedback control loop, the measured signals are passed from the grid RT controller to the Prosumer RT target over RMN. The communication delay over RMN must be corrected to maintain synchronization to the grid using PLL. This distributed measurement concept has been shown in [13] along with validation of the harmonic estimation and recovery methods.

Time synchronization between RT targets is integral for accurate measurements and feedback loops in PHIL test benches with distributed control schemes. The RT targets in CoSES are synchronized with the NI-6683H timing and synchronization card. The card offers synchronization over a 1588 IEEE Precise Time Protocol switch or through an external GPS antenna. Both of these methods are available in CoSES for the PHIL experiments. The Egston CSUs carry an on-board FPGA controller, which must also be synchronized with the CoSES controllers for power injections in grid connected mode. The SFP link between CoSES controllers and the Egston CSUs strobes at $4\,\mu$s. This property is used to make the CSU on-board clock a slave to the SFP strobe. Thus, a laboratory wide time synchronization is achieved over six RT targets and the on-board controllers of the seven CSU cabinets.

IV. Experiments

We present results of two typical experiments in this section to highlight the performance of CoSES PHIL setup. In the first part we demonstrate the precision and response of the Egston CSUs as PHIL agents. In the second part we conduct an online optimal power flow (OPF) based re-dispatching of three CSUs, while three others emulate pre-defined load profiles. This experiment leverages the tenets of the CoSES PHIL framework in combining an offline optimisation algorithm

with real-time control of inverters. It comes with an option to change the algorithm underneath the generation setpoints or inverter control strategy in a quick and efficient manner.

A. PHIL validation

The Egston CSU for SFH3 is used for the validation of the PHIL capacities in CoSES. In this experiment, we provide a pure $50\,\mathrm{Hz}$ sine wave and a signal with harmonics as a reference current for the Egston CSU and compare it the produced waveform from the power amplifiers. We operate the CSU at SFH3 as a current source inverter, as shown in Fig. 1, for unbalanced three phase references. The inverter is connected at bus B3 while bus B1 is connected to the public grid. The grid synchronous inverter current references are generated from user defined active power setpoints, voltage measurements and PLL at Bus B3. All other prosumer nodes are disconnected for this experiment. In Fig. 4, we see the fundamental and harmonics current setpoint tracking by the Egston CSU at SFH3 for phase A. A harmonics toggle switch is used to introduce 3^{rd} and 5^{th} order components to the current injection. The amplitude of harmonics is chosen to be 12.5% of the fundamental magnitude. It can be seen that the signal reproduction is accurate and the jump from purely fundamental to fundamental with harmonics reference is near instantaneous. The total harmonic distortion (THD) and magnitude values, provided in the Tab. I, show very close reproduction of the signal through the PHIL components.

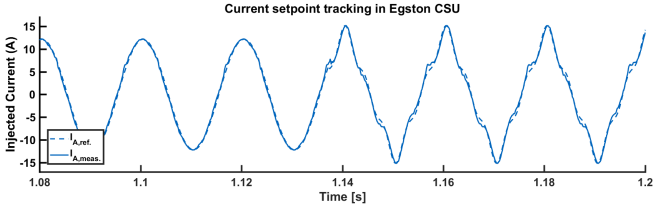

Fig. 4. PHIL validation results - harmonics and setpoint tracking

TABLE I
THD AND MAGNITUDES FOR PHIL VALIDATION

	Pure 50Hz Injection		**50Hz with Harmonics Injection**	
	Reference	Measured	Reference	Measured
THD %	0.03	2.21	17.40	17.49
$\lvert I_{50Hz}\rvert$ (A)	12.13	12.14	12.13	12.14
$\lvert I_{150Hz}\rvert$ (A)	-	-	1.497	1.463
$\lvert I_{250Hz}\rvert$ (A)	-	-	1.488	1.493

Fig. 5 shows the unbalanced three phase active power injection from the Egston CSU at SFH3. Phase A is held constant at a $2\,\mathrm{kW}$ generation, while the phases B and C switch between generation to load and vice-versa within the observation window to highlight a dynamic prosumer emulation. It can be see that the three phases can track their respective power setpoints independently and are suitable for unbalanced distribution grid emulation. In the bottom left of Fig. 5, a $8\,\mathrm{kW}$ power swing on phase C, from generation to load behaviour, is achieved. The instantaneous power changes within 10% of the cycle, and the averaged power takes up to two cycles to settle to this change. The bottom right of Fig. 5, shows the change in the current waveform with respect to the bus voltage at Phase B. As the Egston CSU transitions from generation to load, we see a near instantaneous change in phase difference shift from $180°$ to $0°$.

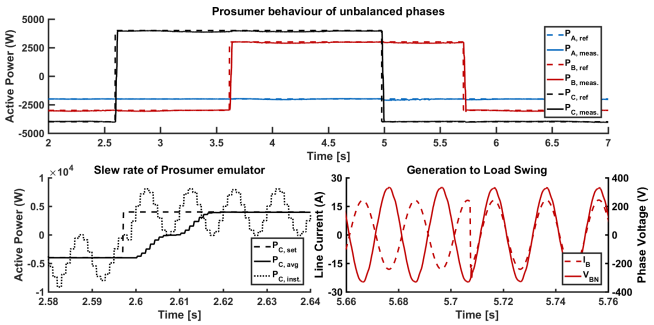

Fig. 5. PHIL validation results - prosumer operation

B. Online Optimal Power Flow (OPF) on CoSES PHIL

In this experiment, we use six Egston CSUs - three as generators and three as loads - divided in two clusters, as seen in Fig. 6. The two clusters can be imagined as two separate microgrids, which do not freely share information with each other. Only the electricity price at the ends of the interconnecting node is available to both the clusters. The load CSUs receive their setpoints from a time series of an unbalanced three phase demand profile. The generator CSUs receive their setpoints from the local cluster control and OPF algorithm. The RT target at SFH3 and SFH4 control the power injections in Cluster #1 and Cluster #2 respectively. The RT target for the LV grid, measures power at the LV buses and provides PLL references to the Egston CSUs over the RMN network. Two separate Windows PC are used to deploy the VS projects, one each for RT target at SFH3 and SFH4, to represent the two clusters. The PCs run an ADMM OPF algorithm, split in two halves, and they communicate with each other over a TCP link. The algorithm receives the measured power at the load buses and directs the generation injection power after an optimization step. We use JSONs to exchange the node prices over the TCP link. The VS LabVIEW API is used to transfer data across the static optimization and RT emulation domains. Further explanation of the methodology can be found in [14].

In the top row of Fig. 7, we show the comparison of generation mix of phase A for the two cases, Case #1 with OPF and Case #2 without OPF, for the same load profile. The experiment runs for $550\,\mathrm{s}$. The generator nodes are initially programmed to provide self-sufficiency for the local cluster as a primary control and keep the exchange of power between the two clusters, P_{tie}, at zero. In Case #1, the MFH3* generator completely provides for Cluster #1 while MFH2* and SFH4 provide for Cluster #2. Case #2 re-dispatches the three generators to minimise the total cost through online OPF, which reduces the generation from Cluster #1 and increases

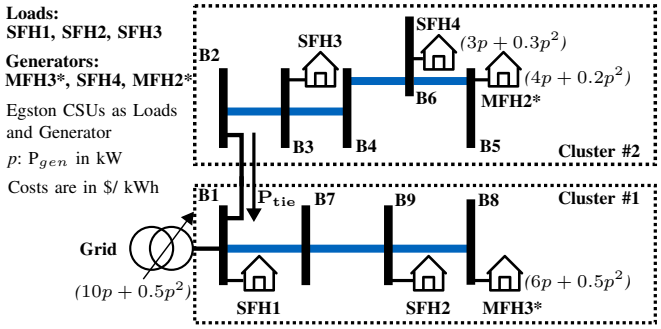

Fig. 6. PHIL experiment for OPF validation with two clusters. The *generation costs* are mentioned adjacent to the generators within parentheses.

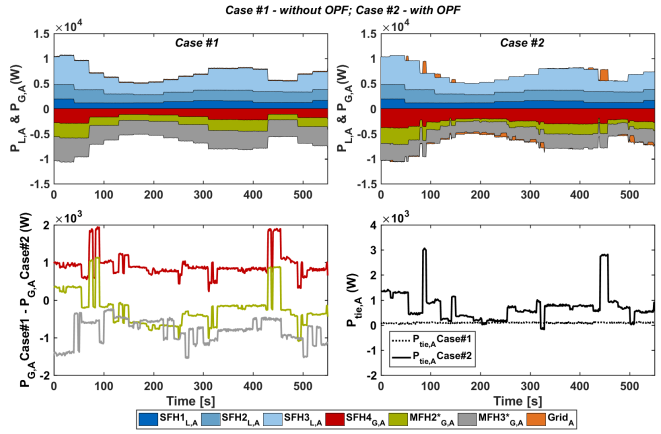

Fig. 7. Comparison of generation mix (top), change in $P_{gen,A}$ (bottom left) and power exchanged between clusters (bottom right) with and without OPF

at Cluser #2, as seen in the bottom left of Fig. 7. The bottom right of Fig. 7 shows the power sent from Cluster #2 towards Cluster #1 due to optimised generation costs in the OPF case. The total generation costs is \$0.233 for Case #1 and \$0.198 for Case #2, with an improvement of $\approx 15\%$.

V. Conclusion

The CoSES microgrid laboratory was established to research microgrid operation through real and emulated multi-energy system grids. In this paper, the electrical network and PHIL capacities of the lab are presented in detail. The philosophies behind the design choices in the electrical and control system network of CoSES are explained. A PHIL control framework is introduced to combine the real-time computation with simulation and optimisation algorithms with an access to commercial communication protocols through an API. The schematic of this framework can be helpful for other laboratories in implementing similar strategies for hardware validation of simulated results with multiple real-time controllers. Experiment validation for the PHIL agents is shown in the results section. One detailed microgrid experiment for implementing distributed OPF validation on PHIL agents is also shown for the reader's understanding of the lab capacities and the potential of the proposed infrastructure choices in a research question context.

References

[1] A. Spina, K. Rauma, C. Aldejohann, M. Holt, J. Maasmann, P. Berg, U. Häger, F. Rettberg, and C. Rehtanz, "Smart grid technology lab – a full-scale low voltage research facility at tu dortmund university," in *2018 AEIT International Annual Conference*, pp. 1–6, 2018.

[2] M. C. Alvarez-Herault, A. Labonne, S. Touré, T. Braconnier, V. Debusschere, R. Caire, and N. Hadjsaid, "An original smart-grids test bed to teach feeder automation functions in a distribution grid," *IEEE Transactions on Power Systems*, vol. 33, no. 1, pp. 373–385, 2018.

[3] G. Lauss, F. Andrén, M. Stifter, R. Bründlinger, T. Strasser, K. Knöbl, and H. Fechner, "Smart grid research infrastructures in austria: Examples of available laboratories and their possibilities," in *2015 IEEE 13th International Conference on Industrial Informatics (INDIN)*, pp. 1539–1545, 2015.

[4] SINTEF, "National Smart Grid Laboratory," Nov. 8, 2021 [Online].

[5] A. Monot, M. Wahler, J. Valtari, M. Rita-Kasari, and J. Nikko, "Real-time research lab in the sundom smart grid pilot," in *CIRED Workshop 2016*, pp. 1–4, 2016.

[6] J. Østergaard, Q. Wu, and R. Garcia-Valle, "Real time intelligent control laboratory (rt-icl) of powerlabdk for smart grid technology development," in *2012 Complexity in Engineering (COMPENG). Proceedings*, pp. 1–4, 2012.

[7] V. S. Perić, T. Hamacher, A. Mohapatra, F. Christiange, D. Zinsmeister, P. Tzscheutschler, and C. Aigner, "CoSES Laboratory for Combined Energy Systems At TU Munich," *IEEE Power and Energy Society General Meeting*, 2020.

[8] Egston Power, "COMPISO Power Hardware in the Loop," Nov. 8, 2021 [Online].

[9] International Electrotechnical Commission, "IEC 60309-1:2021," Nov. 8, 2021 [Online].

[10] NI, "Veristand 2018," Nov. 8, 2021 [Online].

[11] M. Mayer, A. Mohapatra, and V. S. Peric, "IoT Integration for Combined Energy Systems at the CoSES Laboratory," in *2021 IEEE 7th World Forum on Internet of Things (WF-IoT)*, pp. 195–200, 2021.

[12] LEM, "Lem transducers," Nov. 8, 2021 [Online].

[13] E. Sezgin, A. Mohapatra, T. Hamacher, Özgül Salor, and V. S. Perić, "Fast harmonic analysis for phil experiments with decentralized real-time controllers," *Electric Power Systems Research*, vol. 211, p. 108493, 2022.

[14] M. Cornejo, A. Mohapatra, S. Candas, and V. S. Peric, "PHIL implementation of a decentralized online OPF for active distribution grids." accepted for PES GM 2022, http://dx.doi.org/10.36227/techrxiv.17065193.

Concluding remarks on the publication

We raised a question regarding the salient desirable features for an ADG laboratory designed for a research institution and listed some of these qualities in Tab. 2.2. The Tab. 2.3, contextualises the features from the CoSES laboratory's perspective.

Table 2.3: Salient PHIL Hardware and Software features at CoSES.

CoSES Hardware	CoSES Software
Emulation instead of Simulation - Real 1.5 km low voltage grid, commercial PV, EV chargers and battery system, emulated prosumers through the Egston Compiso amplifiers.	**Free choice of toolchain** - NI VeriStand RT environment accepts models in .dll version from a wide range of development tools. Any experiment is controlled by a combination of models from MATLAB/Simulink, LabVIEW, Modelica and object oriented programming.
Flexible grid configuration - CoSES can switch between grid connected and islanded with radial or meshed topology. Connecting cables between buses can be changed in length and diameter. Prosumers can be moved to any LV bus.	**Multiple timescales** - NI VeriStand RT environment decimates RT models for specific execution rates. VeriStand gateway connects software timing to the RT timing domain.
User-friendly reconfiguration procedure - Prosumers and DERs can be safely moved around without LV electrician assistance through CEE plugs and the patch cabinet. Circuit breakers for topology change have remotely controlled circuit breakers.	**Distributed instrumentation** - Six NI PXIe-8880 embedded controllers are distributed over the lab, with access to local measurements and an asynchronously updated data network.
Minimize power losses - A separate 630 kVA feedback transformer loops the prosumer emulator back into the mains grid. Only losses are ohmic drops at full power rating.	**Open to commercial protocols** - NI VeriStand gateway APIs in various programming languages, opens the RT control environment to external communication protocols.

The CoSES ADG laboratory was created to explore ADG operations using real and simulated multi-energy system grids. This paper provides an in-depth look at the lab's electrical network and its PHIL capabilities. We explain the reasoning behind our design choices for both the electrical and control system networks. The PHIL control framework merges RT computation with simulation and optimization algorithms, offering access to commercial communication protocols via a straightforward API. This framework's schematic can serve as a practical guide for other labs seeking to implement similar hardware validation strategies with multiple RT controllers.

This chapter has dealt with commissioning an ADG laboratory, encompassing three distinct papers that contribute to its functionality. The next chapter will leverage these tools and frameworks to address specific ADG research questions, with a focus on illustrating how these tools enable precision in our investigations, while maintaining the near-reality constraints and practical assumptions.

Chapter 3

ADG Laboratory Experiments

In theory, practice is simple

Unknown

The potency of a tool can only be judged by its application. Once established, it is an incumbent challenge for any laboratory to conduct investigations where the experiments justify themselves by adding value to the theoretical claim. It is a widely held belief that experimental validation enhances the credibility of an analysis beyond pure theoretical outcomes. However, CoSES laboratory possesses many degrees of freedom for an experiment design and it is possible to fall into a trap of superfluous experiments without reasonable added benefit. This tendency can inadvertently lead to a repetitive investigative approach, resulting in a lack of diversity in the use of the laboratory's resources.

This redundant tradition could still be acceptable while working with a single test bed but it falls short of fully utilizing the capabilities of a complex ADG facility like CoSES. To reiterate, the lab features five prosumers, twelve RT controllers, an array of commercial DER devices, and diverse grid topology, to name a few of its salient features. Focusing solely on a single use case in such a multi-faceted setting would not fully exploit the laboratory's potential. Therefore, it is imperative that we explore numerous ways in which we can leverage this facility and demonstrate that each distinct application represents significant progress, enhancing the theoretical foundation upon which it is built.

In the current chapter, three distinctly different applications of the CoSES laboratory are presented which use the measurement concept, dashboards and the PHIL framework laid out in the previous chapter.

Software instead of new hardware for ADG operation - The first publication implements a M-Class phasor measurement unit (PMU) as a pure software module within the existing instrumentation of the ADG laboratory. This work challenges the conventional practice of utilizing separate devices for distinct grid functions. It explores the potential of leveraging shared embedded resources within the ADG, which is a popular research topic in the ADG community [103].

Verify popular optimised ADG operation ideas - The second paper demonstrates a RT optimal power flow (OPF) algorithm through a PHIL setup. Unlike conventional papers, working only with simulations, we use the CoSES laboratory to recreate an unbalanced

three-phase ADG environment, utilizing SDP relaxation and ADMM techniques for solving the optimization problem. The experiment goes beyond the idealised simulation confines to scrutinize the practical application of a RT OPF with a real instrumentation network and prosumers. Online OPF is widely researched in ADG communities, due to the increased penetration of fast dispatchable power electronic converters and advent of computing performance. Our work provides insights on the difference between theoretically promised benefit to savings in a real ADG.

A new ADG control hypothesis - In the third paper, we imagine a new ADG research topic based on a completely theoretical control theory tool, with so far limited applications in power systems. We conceptualize a standard grid frequency controller as a reachability analysis problem. This theoretical framework can be used for a reliability tool for operators in the ADG control rooms. While the full integration of RT reachability analysis remains a work in progress, the paper establishes a foundation for reachability analysis of power systems controllers based of standard IEEE test cases and modelled as linear time-invariant systems. Additional to the publication, larger test cases are shown to prove the tractability of the reachability problem. Recent developments of the algorithm has proven that there is a potential for near-RT or online applications for reachability analysis on linear time invariant (LTI) systems. Therefore we provide an experiment concept with emulated synchronous generators through CoSES prosumers and further extend the potential application of this concept in the CoSES laboratory. Laboratory validation of emulated synchronous generators with the Egston prosumers is also provided to showcase the viability of this work.

3.1 Veristand PMU (Publication #4)

PMUs serve as standard measurement units for power grids, capturing voltage, current, and frequency as synchrophasors. These devices adhere to essential standards like IEC/IEEE 60255-118-1 for accuracy [104] and IEEE-SA C37.118.2 for messaging [96].Few commercially available PMUs used in modern power systems are shown in Fig. 3.1. PMUs must pass accuracy tests and deliver messages in the correct format to be classified as such. They come in two classes: Measurement (M) class for higher accuracy with slower reporting, and Protection (P) class for faster reporting with slightly lower accuracy. In this publication, we introduce the concept of implementing an M-Class PMU as a pure software module within the existing instrumentation of an ADG laboratory.

The motivation stems from the idea of shared firmware for grid tasks within ADG and to enhance computational capacity by leveraging the increasing number of embedded controllers in ADG. By sharing resources, there is potential to reduce reliance on individual specialized devices, while also aligning maintenance updates and deployment schedules. This approach is akin to installing new software on a shared operating system, eliminating the need to acquire a new computer for each distinct task.

The paper focuses on showcasing that the control and instrumentation architecture for an inverter current/voltage controller and a phasor measurement unit are fundamentally similar, with differences arising mainly from software variations. We design, implement, and validate an M-Class PMU on a general-purpose PXIe-8880 embedded controller. This

Figure 3.1: Commercial PMUs used in modern power systems. From top left and going clockwise - G5PMU (Elspec Ltd.), MiCOM Agile P847 (GE Grid solutions), SIPROTEC (Siemens Group), VCL-PMU-30 (Valiant Communications).

controller concurrently handles inverter and grid control tasks within a unified RT control environment. The proposed solution demonstrates that various grid control and operation functionalities can actually be unified within the Veristand RT control environment. The PMU is successfully integrated into the NI Veristand control environment at CoSES laboratory, utilizing only the existing instrumentation and controller setup for inverter and prosumer control in an ADG laboratory. The implemented PMU meets the accuracy standards specified by the IEC/IEEE 60255-118-1 standard and produces output compliant with the IEEE-SA C37.118.2 messaging standard.

Publication #4 - M-Class PMU for general purpose embedded controllers in NI Veristand environment

Authors - Anurag Mohapatra, Steffen Büttner, Gerd Bumiller, Thomas Hamacher, Vedran S. Perić

Publication - 2023 IEEE Belgrade PowerTech, 25-29 June, 2023

Digital object identifier - `https://doi.org/10.36227/techrxiv.22658293`

Author	Contribution	Tasks
Anurag Mohapatra	40%	Conceptualization, Methodology, Investigation, Supervision, Visualisation, Writing – original draft
Steffen Büttner	30%	Methodology, Investigation, Validation, Software, Writing - original draft
Gerd Bumiller	5%	Writing - review and editing
Thomas Hamacher	10%	Funding acquisition, Resources, Writing - review and editing
Vedran S. Perić	15%	Conceptualization, Supervision, Writing – review and editing

M-Class PMU for general purpose embedded controllers in NI Veristand environment

Anurag Mohapatra*, Steffen Büttner *, Gerd Bumiller †, Thomas Hamacher*,Vedran. S. Perić*
*Center for Combined Smart Energy Systems (CoSES), Technical University of Munich, Munich, Germany
†Institute of Computer Science, University of Applied Sciences Ruhr West, Mülheim, Germany

***Abstract*—This paper presents the design, implementation and validation of a M-Class PMU on a general purpose embedded controller, concurrently used for inverter and grid control tasks, deployed over a unified real-time control environment. The rising number of embedded controllers in active distribution grid opens an opportunity for shared computation and instrumentation resources. Unified real-time control environments can efficiently coordinate multiple embedded controllers, IOs and models from different toolchain. The PMU in this paper, is implemented within the NI Veristand real-time control environment at CoSES laboratory in TU Munich. It uses the existing instrumentation and controller setup for inverter and prosumer control in an active distribution grid laboratory. The PMU passes all M-class device accuracy tests set by the IEC/IEEE 60255-118-1 standard. The output is compliant to the IEEE-SA C37.118.2 messaging standard and connected to an open source PDC software. The proposed solution demonstrates the possibility of merging different grid control and operation functionalities within the unified Veristand RT control environment.**

***Index Terms*—phasor measurement unit, active distribution grids, M-Class, real-time control, NI Veristand**

I. Introduction

Active Distribution Grids (ADG) are characterised by a proliferation of distributed energy resource (DER) inverters, microgrid controllers, protection schemes, energy management systems and Internet of things (IoT) devices, to name a few. As a consequence, at a distribution grid level, the density of embedded control and communication hardware is rapidly increasing. This opens up opportunities for coordination among individual controllers, shared computation resources, synchronized maintenance updates and improved measurement redundancies. A common environment, which can connect to all the embedded targets, could be beneficial for efficient management of the newly added resources.

Unified real time (RT) environments, such as ETAS [1], SimWB [2] and NI Veristand [3], are popular platforms for control systems with multiple embedded controllers and intelligent devices. These environments are governed by a RT operating system, can coordinate a project over one or multiple embedded controllers, connect to real or virtual IOs and accept compiled models from different toolchain. In our previous works, we have shown that such RT control environments are useful for Power Hardware-in-the-loop (PHIL) validation of sector-coupled ADGs [4], optimised prosumer operation [5] and creating monitoring tools for ADGs [6]. In power systems industry as well, embedded applications are moving towards coordination over a common RT operating system (RTOS) based control environments [7]. Therefore, ADG applications developed over unified RT control environments, can expect an easier transition to industry readiness, as opposed to those developed by directly interfacing with the controller.

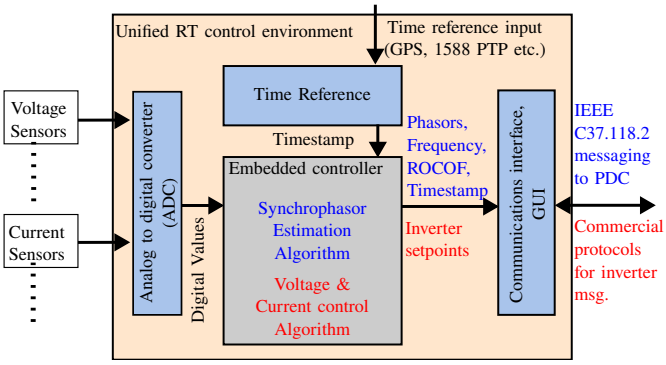

Fig. 1: A generic block diagram for a PMU and an inverter control unit.The common hardware is show in ■, while the specialised software for PMUs are in ■ and those for an inverter control unit are in ■. The common control environment is shown in ■ and the general purpose embedded controller is in ■.

Another direct implication of the increased intelligence at distribution grids, is a possibility to share computation and instrumentation resources between two or more grid functionalities. Thus different grid devices could be morphed into one physical system. A Phasor measurement unit (PMU) is one such device, which has been either marketed as separate unit or bundled together with a protection relay unit [8]. Although specific PMUs can have marginal differences, they can all be described by the generic function blocks as shown in Fig. 1. In the same figure, we compare this structure to a generic inverter controller, another core component for ADGs, and we can observe the functional similarities between the two devices. Extending the philosophy of shared hardware and controller basis in ADG, we can propose an opportunity to integrate a PMU and an inverter controller on general purposed embedded controllers which share a RT control environment. This change

The construction of the CoSES laboratory was supported by Deutsche Forschungsgemeinschaft (DFG) through the project “Flexible reconfigurable microgrid laboratory" under Project number 350746631. The work of Anurag Mohapatra was supported by the German Federal Ministry of Education and Research through the project, "MCube: ComfficientShare" under the Project number 03ZU1105CA. The work of Vedran S. Perić was supported by DFG through the project, “Optimal Operation of Integrated Low-Temperature Bidirectional Heat and Electric Grids (IntElHeat)” under Project number 450821044.

2023 IEEE Belgrade PowerTech | 978-1-6654-8778-8/23/$31.00 ©2023 IEEE | DOI: 10.1109/POWERTECH55446.2023.10202989

in paradigm can be seen as analogous to personal computers serving the different needs of the user through specialised software, which all share the common hardware basis.

In this paper, we present the design, implementation and validation of a M-Class PMU deployed on a general purpose embedded controller and managed over a unified real-time (RT) control environment shared by other network hardware at the CoSES microgrid laboratory in TU Munich. NI Veristand serves as a research proxy in CoSES for the unified RT control environment in the real world [3]. The lab already operates on a unified control environment envisioned in the future active distribution grids, with the benefits such as coordination among individual controllers, shared computation resources, synchronized maintenance updates and improved measurement redundancies. The general purpose controllers in the lab are concurrently used for power electronics device control, optimal energy management schemes and measurement aggregation.

The remainder of this paper is arranged as follows. In Sec. II we describe the synchrophasor estimation algorithm used for our M-Class PMU model. In Sec. III we connect this model with the NI Veristand RT control environment of the CoSES laboratory, an exemplary ADG research facility. In Sec. IV, we validate the model as a M-Class PMU as per the static and dynamic tests stated in IEC/IEEE 60255-118-1 standard [9]. We also combine the PMU with an open source phasor data concentrator (PDC), as per the IEEE-SA C37.118.2 synchrophasor data transfer for power systems standard [10], to demonstrate it as a final product to be used in ADG lab activities.

II. Synchrophasor Estimation Algorithm

The synchrophasor estimation algorithm is the core component for every PMU. It produces the phasor representations of voltage and current, measures grid frequency and rate of change of frequency (ROCOF). These algorithms can be broadly classified as Filter based, Discrete Fourier Transform based and Phase locked loop (PLL) based synchrophasor estimators [11]. Since Phase locked loop's (PLL) are already part of grid inverter synchronization carried out over RT embedded controllers, a PLL based synchrophasor estimation was chosen for this work. This is in the spirit of using generic similarities, as seen in Fig. 1 between a grid inverter and a PMU.

For this work, we have used the single-phase PLL with an improved inverse Park transform based quadrature signal generator (QSG) presented in [12] and shown in Fig. 2. This method was shown to have improved filtering properties for orthogonal signal generation from the input measurement. We also implement a block for phase step detection by comparing the current angular frequency with its 500 ms moving average. On detection of an abrupt phase change, the block adjusts the PID gains and the delay on the phase output filter to compensate the jitter. The performance of this feature is shown in Fig. 3. The final element are the output low-pass filters for phasor magnitude and frequency. This introduces a three

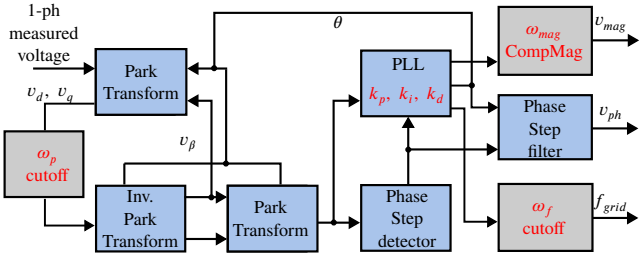

Fig. 2: The filtered inverse Park transform PLL used for synchrophasor estimation in this paper. The elements in ■ are tuned parameters, obtained from the particle swarm optimisation and ■ are low pass filters with their respective cut-off frequencies.

cycle, 60 ms, delay at the cost of higher accuracy on these measurements.

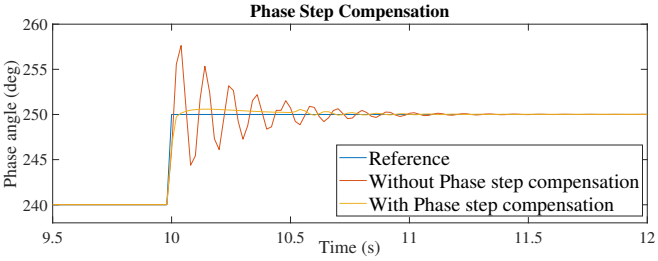

Fig. 3: PLL block response to a phase step change, with and without phase event detector feature.

The emphasis of the present work is towards packaging a M-class PMU grade result as a deployed model on a hardware and software combination meant for inverter control. Therefore, a best case version of the synchrophasor estimation model is not crucial towards this goal. Any known model, which can be tuned within M-Class PMU accuracy range, is suitable for the task at hand. In the next subsection, we present an adequate tuning procedure for the model shown in Fig. 2.

A. Tuning of model parameters

The tunable components in the synchrophasor estimation model shown in Fig. 2 are as follows - k_p, k_i, k_d are the PID controller gains of the single phase PLL, w_p is the cut-off angular frequency of low-pass filters for the inverse Park transform QSG, w_f and w_{mag} are the cut-off angular frequency for the output low-pass filters on phasor magnitude and fundamental frequency respectively and, CompMag is a filter attenuation compensation factor for the voltage magnitude output. The tuning of these mutually dependent parameters is crucial to the adequacy of the SE algorithm for M-class PMU standards.

We use a Particle swarm optimisation (PSO) method [13] to find optimal parameters under the constraint of passing all mandated PMU accuracy tests. The algorithm to find the parameter set for the synchrophasor estimation model is shown in Algo. 1. The parameters are represented as a particle position vector. During its convergence, the optimisation proposes a new value set for the parameter vector and returns them to the synchrophasor estimation model. The model is simulated over

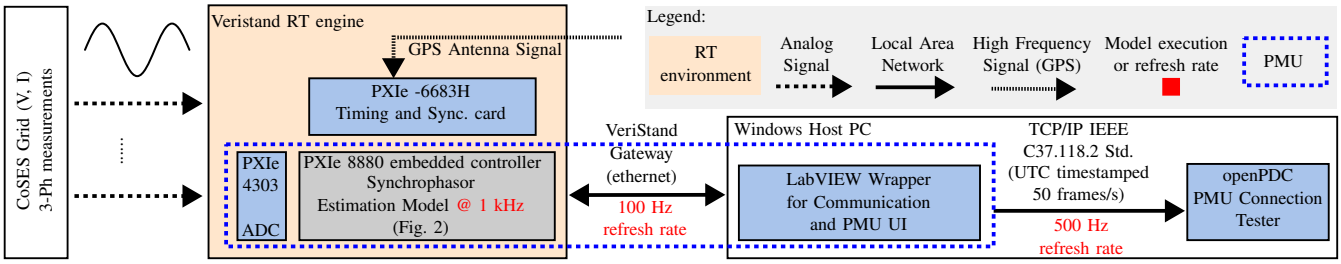

Fig. 4: A schematic for the M-Class PMU developed within NI Veristand at CoSES laboaratory.

a given reference test case, specified in the IEC/IEEE 60255-118-1 standard. The error performance of the output is then compared over different parameter vector sets to select a best fit.

Algorithm 1 PSO algorithm. Initialization taken from [14]

Variables:
simresults, *error*
Initialize:
$20 \leq n \leq 40$; $c_1 \leftarrow 1.2$; $c_2 \leftarrow 1.6$; $w \leftarrow 0.8$
pos $\leftarrow$ *randomised*; vel $\leftarrow$ *randomised*
g_{best}, $p_{best} \leftarrow$ *zeros*; $iter_{warm-up} \leftarrow 100$
while $iter < iter_{warm-up}$ **do**
Warm-up the PSO iterations
end while
while *error* is decreasing **do**
$r_1, r_2 \leftarrow$ *randomised* in $[0, 1]$
vel $\leftarrow w.\text{vel} + c_1.r_1.(p_{best} - \text{pos}) + c_2.r_2.(g_{best} - \text{pos})$
pos $\leftarrow$ pos + vel
for $i = 1$ to n **do**
simresults $\leftarrow$ Simulation(pos)
error $\leftarrow$ costFcn(*simresults*)
end for
$p_{best} \leftarrow \text{best}(p_{best}, error)$
$g_{best} \leftarrow \text{best}(p_{best})$
end while

The cost function in Algo. 1 is of particular interest as it essentially defines the final performance of the model in Fig. 2. The focus of this paper is not on developing the best possible PMU estimation algorithm and therefore, we set the optimisation goal to clearing the accuracy requirements for a M-Class device as mentioned in IEC 60255-118-1 standard.

The cost function used for the PSO is shown below,

$$\text{costFcn} = \left(1 + \Sigma_{Err}\right) + \left(1 + 10 \times \Sigma_{fail}\right)^2 + \left(1 + \Delta\epsilon_{mag}\right) + \left(1 + \Delta\epsilon_{ph}\right) + \left(1 + 10 \times \Delta\tau_{mag}\right) + \left(1 + 10 \times \Delta\tau_{mag}\right) \quad (1)$$

Here, Σ_{Err} represents the sum of all error values from all simulated standard test cases. Σ_{fail} represents the sum of errors, where the simulation results exceeded the maximum allowed error. $\Delta\epsilon_{mag}$ and $\Delta\epsilon_{ph}$ are the overshoots beyond the maximum allowed for magnitude and phase step changes. $\Delta\tau_{mag}$ and $\Delta\tau_{ph}$ are the breaches beyond the maximum allowed settling time for the magnitude and phase step changes. If all accuracy tests are passed, all variables in Eq. 1 except Σ_{Err}, are set to zero. When the average of error, across all the required tests, has stopped decreasing, the PSO iteration is terminated and the best parameter values until then are set as the synchrophasor estimation model parameters.

To reiterate, we present an adequate PMU algorithm (Algo. 1) to satisfies the requirements for M-Class PMU accuracy standard. The crux of the paper lies in repurposing of an inverter controller in NI VeriStand environment, and not on developing a high accuracy PMU algorithm. Any other PMU algorithm, that fits the M-Class description, can also be used without loss of generalisation.

III. PMU IMPLEMENTATION

The PMU design for this paper is centered around placing the tuned Synchrophasor Estimation algorithm from Sec. II on a suitable embedded controller, that is part of a unified RT control environment, NI Veristand, for coordination of controller resources in the grid. It uses a UTC time reference signal, field measurements of voltage and current and provides a messaging interface for a Phasor Data Concentrator (PDC) software. The following subsections explain the key components of the specific PMU implementation for this paper, as shown in Fig. 4.

A. The laboratory setup

The CoSES microgrid research lab at TU Munich uses NI VeriStand RT controller coordination software environment and NI PXIe-8880 embedded controllers upon a PXIe-1065 chassis, with a RT target rate of maximum 10 kHz [15]. These controllers are used to control inverters in the grid, provide power sharing setpoints, implement energy management schemes and to act as real-time simulators. The field measurements are taken by industry standard LEM CV 3-1000 [16] and LF 210S-SP3 [17] transducers, which are brought in over PXIe-4303 analog IO cards at a 24 bit ADC resolution. The time synchronisation is provided by a PXIe-6683H timing card [18] which is connected to a GPS antenna through an in-line amplifier. Thus, referring back to Fig. 1, the CoSES control system structure requires no additional hardware to implement a PMU model.

B. Veristand RT environment

The NI Veristand RT environment can deploy models on multiple embedded controllers, bring together measured signals and modelled IOs and provide a LabVIEW based API access to connect devices through commercial communication protocols [3]. This environment is independent of the modelling toolchains, and can accept compiled models from most

commonly used platforms in research and industry. For the M-class PMU, as shown in Fig. 4, the Veristand API connects the timestamped output from the synchrophasor estimation model to a LabVIEW messaging wrapper VI on a Windows PC. The wrapper converts the output to a message packet as per the IEEE C37.118 communication protocol for PMUs. This packet structure can be connected over a TCP/IP link to any PMU tester software. In this paper, we use the Grid Protection Alliance's openPDC PMU connection tester and Manager [19] to visualise the PMU output.

C. UTC Timestamping in Veristand

The PMU standards recommend a UTC-traceable time reference with a minimum accuracy of $\pm$ 3 μs [9]. This limit refers to the required precision of 1% steady state total vector error (TVE). The implemented PMU uses a GPS tracked time reference over the PXIe-6683H card and it provides an accuracy up to $\pm$40 ns [18]. Additionally, the standards dictate that the phasor measurements should be timestamp aligned to sub-multiples of a whole second. Therefore, for the implemented PMU, the first measurement output should be aligned to the nearest integer second rollover. We chose a 50 frames/s reporting rate and thus the subsequent measurements should be spaced 20 ms apart from the integer second origin.

We use a RT trigger to start the synchrophasor estimation model execution. However, with the unified RT control environment such as NI Veristand, it is often not possible to exactly schedule the start of the execution due to other parallel processes of various priorities in the controller [20]. In this particular case, a 19 μs average offset is observed on the first measurement. This is the average delay between the RT start trigger for the model and the beginning of model execution. However, this mismatch can be easily fixed as both the RT start trigger and the beginning of model execution are timestamped by the same GPS source over the timing card. Therefore, we compensate for this offset by performing a 2-point interpolation. The interpolation leads to an acceptable average relative error of $<$ 0.04%, while fixing a PMU output standard compliance issue for the Veristand RT control environment.

D. Model rates and latency

In Fig. 4, looking from left to right, the synchrophasor estimation model is run at 1 kHz on the RT embedded controller. The model is built in MATLAB/Simulink and compiled as a .dll for the NI Veristand RT environment. Next, the Veristand API, managed through the LabVIEW messaging wrapper and running on a Windows PC, refreshes the data from RT environment at 100 Hz. The PMU output frame rate is set to 50 UTC timestamped frames/s, as is usual for PMUs in 50 Hz systems. The connection to the openPDC tools, made over the standardised PMU messaging protocol, has a 2 ms sleep function for reading the TCP/IP port and thus refreshes at 500 Hz.

According to the standards, the reporting latency of the entire PMU system from the moment of measurement to reporting for the corresponding timestamp to the PDC must not exceed 140 ms for a M-class PMU, reporting at 50 frames/s [9]. The implemented synchrophasor estimator model, in Fig. 2, has a 60 ms calculated group delay from the output low pass filters, as mentioned in Sec. II. Next, the Veristand gateway data transfer from RT controller to Windows PC and LabVIEW to openPDC PMU tester has a maximum delay of 10 ms and 2 ms respectively, due to their corresponding refresh rates shown in Fig. 4. Adding these delays, a maximum total reporting latency of the implemented Veristand PMU is calculated as 72 ms, which is well within the worst allowed delay for the 50 frames/s reporting rate.

TABLE I: Tuned parameters from the PSO algorithm

Parameter	Tuned Value
k_p, k_i, k_d	147, 932, -0.56
ω_p, ω_{mag}, ω_f	54, 115, 70
CompMag	1.008

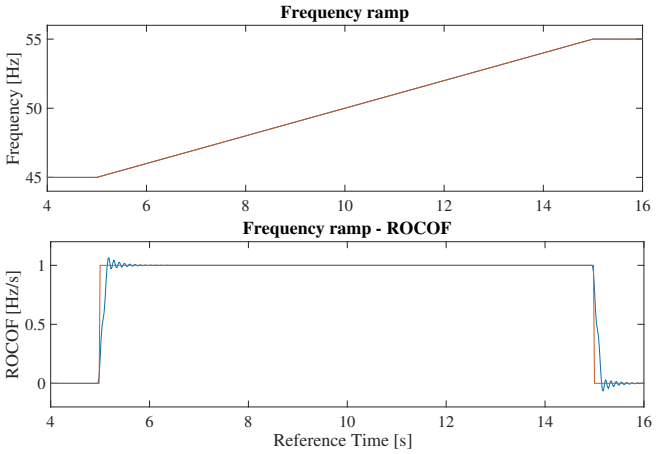

Fig. 5: PMU's response to frequency ramp from 45-55 Hz at 1 Hz/s, as specified in the standards. The reference time-series input signal is shown in and the PMU output is shown in

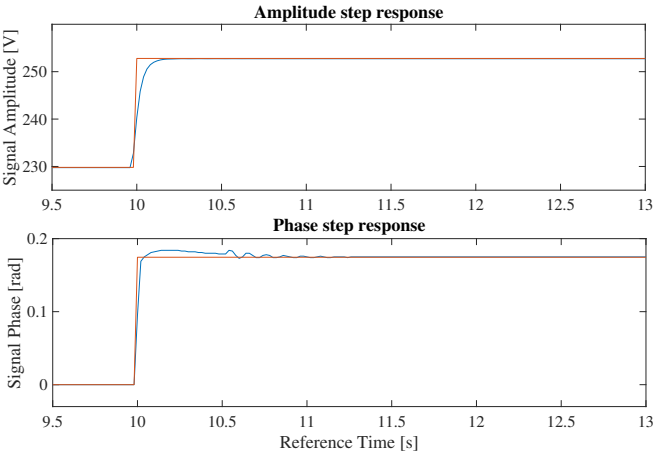

Fig. 6: PMU's response to an amplitude step of 10% and a phase step of 10°, as specified in the standards. The reference time-series input signal is shown in and the PMU output is shown in .

TABLE II: IEC/IEEE 60255-118-1 [9] M-Class PMU accuracy compliance test results for the Veristand PMU.

Accuracy Test Type	**Phasor TVE [%]**		**Frequency Error [Hz]**		**ROCOF Error [Hz/s]**	
	Max. Value	Std. Max.	Max. Value	Std. Max.	Max. Value	Std. Max.
Static tests						
Static frequency	0.2	1	4.78×10^{-8}	0.005	2.15×10^{-4}	0.1
Static magnitude	6.58×10^{-2}	1	3.24×10^{-8}	-	1.54×10^{-10}	-
Harmonic distortion	0.28	1	2.09×10^{-4}	0.025	4.88×10^{-10}	-
Out-of-band interference	1.13	1.3	0.0062	0.01	0.93	-
Dynamic tests						
Amplitude modulation	2.33	3	0.0103	0.3	0.0621	14
Phase modulation	2.95	3	0.0101	0.3	1.93	14
Frequency ramps	0.71	1	0.003	0.01	0.0011	0.2
	Overshoot		**Settling time [ms]**			
	Max. Value	Std. Max.	Max. Value	Std. Max.		
Amplitude step	0	1% of RMS	120	140		
Phase step	0.6°	1°	80	140		

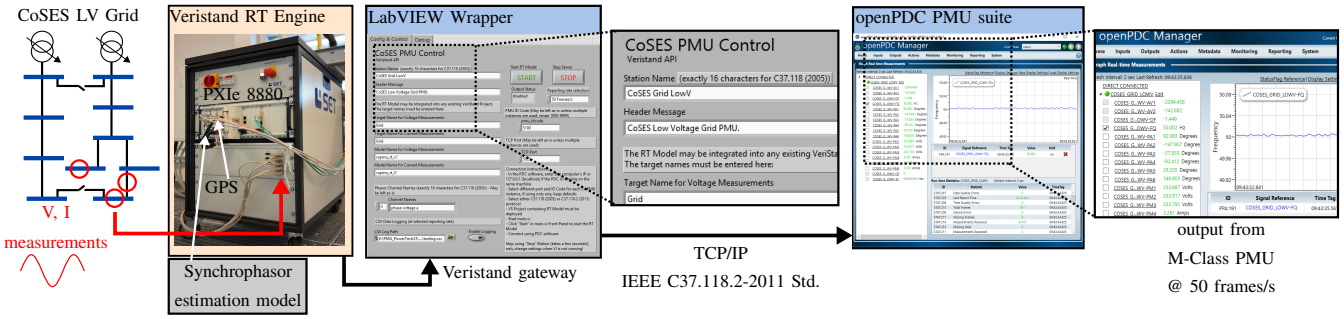

Fig. 7: Demonstration of the Veristand M-Class PMU within the CoSES LV Grid.

IV. PMU Validation and Demonstration

The PMU validation is conducted by comparing the output from the PMU model deployed on the PXIe hardware in the CoSES laboratory with the reference test cases provided in the IEC/IEEE 60255-118-1 standard. The tuned values of the synchrophasor estimation model parameters using the PSO technique described in II-A, is shown in Tab. I. The reference tests explicitly mention the signal range and increment rates for each scenario, which is used to generate a virtual measurement time-series. This time-series is fed as the input signal into the developed PMU.

The tests can be broadly classified into static and dynamic test sets. For both the test sets, the Total Vector Error (TVE), scalar errors on frequency, scalar error on ROCOF are calculated and compared with the limits set by the standard for M-Class accuracy. The results are shown in Tab. II and Fig. 5 shows an exemplary time-series comparison from one of the test routines. Furthermore, the maximum overshoot and settling time for magnitude and phase are considered for the dynamic test scenarios dealing with step changes. This test is shown in Fig. 6. The implemented PMU passes all mandated accuracy tests for a M-Class device as per the IEC/IEEE 60255-118-1 standard. Some rows in Tab. II, do not have a maximum allowed value as these limits are not explicitly specified in the standards.

In Fig. 7 we show the application of the developed PMU within the CoSES laboratory as a measurement unit. Bus voltage and current measurements from the CoSES lab LV grid are processed by the PMU model deployed over the Veristand RT environment, on a PXIe-8880 embedded controller. As a further advantage of this implementation, multiple PMU models can be deployed on all the embedded controllers in the lab. A windows PC connected to this environment, runs the LabVIEW wrapper VI to read the timestamped output from the synchrophasor estimation model. This VI has a front panel to start and stop a specific PMU, label the measurement and for high level network diagnostics. The VI also prepares the IEEE C37.118.2 standard dataframe for PMU data transfer. This is connected to the openPDC Manager software on the Windows PC and it displays the output of the PMU received at 50 frames/s.

V. Conclusion

The increased presence of general purpose embedded controllers in ADGs has created opportunities to coordinate them over an unified RT control environment and share computation resources for grid control activities. We introduce a M-Class PMU which can be deployed on embedded controllers meant for inverter control, energy management schemes or measurement aggregation, without any additional instrumentation and cabling costs. The PMU was implemented on the general

purpose PXI controllers coordinated through NI VeriStand environment and validated at the CoSES microgrid lab at TU Munich. The developed PMU passes all mandated accuracy tests in the IEC/IEEE 60255-118-1 standard and has an output as per the IEEE C37.118.2 messaging standard. While the synchrophasor estimation model used in this work was adequate for M-Class PMU standards, there is significant room for improvement by choosing stricter constraints on the tuning of parameters and investigating other state-of-the-art model structures. Future work will focus on these improvements and exploring other generic intersections in ADG operation and control function to be leveraged as deployed models on a shared hardware and software basis.

REFERENCES

[1] ETAS Group, "COSYM." https://www.etas.com/en/products/cosym-co-simulation-platform-details.php.

[2] Concurrent Real-Time, "SIMulation Workbench." https://concurrent-rt.com/products/software/simulation-workbench/.

[3] National Instruments, "VeriStand." https://www.ni.com/shop/software/products/veristand.html.

[4] V. S. Perić, T. Hamacher, A. Mohapatra, F. Christange, D. Zinsmeister, P. Tzscheutschler, U. Wagner, C. Aigner, and R. Witzmann, "CoSES laboratory for combined energy systems at TU munich," *IEEE Power and Energy Society General Meeting*, vol. 2020-August, 2020.

[5] M. Cornejo, A. Mohapatra, S. Candaş, and V. S. Perić, "PHIL implementation of a decentralized online OPF for active distribution grids," in *2022 IEEE Power Energy Society General Meeting (PESGM)*, pp. 1–5, 2022.

[6] M. Mayer, A. Mohapatra, and V. S. Perić, "IoT Integration for Combined Energy Systems at the CoSES Laboratory," in *2021 IEEE 7th World Forum on Internet of Things (WF-IoT)*, pp. 195–200, 2021.

[7] Wind River, "Intelligent Systems Research - Energy and Utilities." https://www.windriver.com/intelligent-systems/energy-and-utilities.

[8] M. Hojabri, U. Dersch, A. Papaemmanouil, and P. Bosshart, "A comprehensive survey on phasor measurement unit applications in distribution systems," *Energies*, vol. 12, no. 23, pp. 1–23, 2019.

[9] IEC technical committee 95, IEEE Power System Relaying Committee, *IEC/IEEE 60255-118-1 Synchrophasor for power systems - Measurements*. Geneva: International Electrotechnical Commission, 2018.

[10] IEEE-SA, *C37.118.2-2011 - IEEE Standard for Synchrophasor Data Transfer for Power Systems*, vol. 2011. 2011.

[11] R. Teodorescu, M. Liserre, and P. Rodriguez, *Grid Converters for Photovoltaic and Wind Power Systems*. 2011.

[12] M. Ciobotaru, R. Teodorescu, and F. Blaabjerg, "Improved PLL structures for single-phase grid inverters," in *Proc. Power Electronics and Intelligent Control for Energy Conservation Conference (PELINCEC)*, no. February, pp. 1–6, 2005.

[13] J. Kennedy and R. Eberhart, "Particle Swarm Optimization," in *International Conference on Neural Networks (ICNN)*, 1995.

[14] Y. Shi and R. C. Eberhart, "Parameter selection in particle swarm optimization," *Lecture Notes in Computer Science*, vol. 1447, pp. 591–600, 1998.

[15] National Instruments, "PXI Systems." https://www.ni.com/de-de/shop/pxi.html.

[16] LEM, "Voltage Transducer CV 3-100." https://www.lem.com/product-list/cv-31000.

[17] LEM, "Current Transducer LF 210-S/SP3." https://www.lem.com/product-list/lf-210ssp3.

[18] National Instruments, "PXI-6683H Specifications." https://www.ni.com/docs/bundle/pxi-6683-specs/page/specs.html.

[19] Grid Protection Alliance, "openPDC, PMU Connection Tester." https://www.gridprotectionalliance.org/phasor-PDC.html, https://pmuconnectiontester.info.

[20] National Instruments, "Veristand Engine." https://www.ni.com/docs/bundle/veristand/page/vs-engine.html, 2018.

Concluding remarks on the publication

We successfully integrated an M-Class PMU into the CoSES infrastructure, employing the following components,

- **Embedded Hardware** - NI PXIe-8880 with IO cards, GPS time synchronization, and LEM Voltage and Current sensors

- **Installed software** - Inverter control, Prosumer emulation, Energy management hub, Phasor measurement unit

- **Common operating system** - NI VeriStand RT control environment, capable of taking models as .dll or .fmu

The synchrophasor algorithm involved a combination of three single-phase phase-locked loops (PLLs), inverse Park transform, and a phase step filter. The algorithm was fine-tuned using particle swarm optimization and then converted into a .dll file from MATLAB/Simulink for NI VeriStand. The resulting output was connected to a phasor data concentrator software similar to a standard PMU.

Our implemented PMU model has successfully passed all the necessary static and dynamic tests required for M-Class PMUs as specified in the IEC/IEEE 60255-118-1 standard. Notably, this was achieved without any additional wiring or instrumentation costs. The same controller concurrently performs other tasks and multiple PMU instances can be deployed on the same controller. Thus, the CoSES laboratory was used to prove that a PMU can be successfully realized on the general-purpose PXI controllers and managed through a RT control environment such as NI VeriStand.

3.2 ADMM based OPF scheme in CoSES (Publication #5)

In the present landscape of ADG control research, power electronic converters with rapid dispatch capabilities due to no inertia, have garnered significant attention. Similarly, extensive investigations have been conducted on performing OPF in ADG grids. While OPF is conventionally associated with transmission grids, its applicability within distribution grids, especially for local electricity market mechanisms, is gaining prominence. This has lead to a research question where power electronic converters are envisioned as generators, reacting to swift dispatch, post successive OPF iterations [28]. The objective function of the optimisation could deal with direct fuel costs, or could be used as a proxy for congestion management [29][30], self-sufficient generation within a grid, minimizing CO_2 emissions among other things.

The focus on distributed techniques for solving the OPF problem within ADG is driven by concerns related to scalability, robustness, and privacy preservation. Despite substantial exploration into decentralized OPF (D-OPF) methods, at the time of the publication, the authors were unaware of any attempts at implementing online OPF using a PHIL

setup in a realistic grid environment. This gap is critical, as asserting that online D-OPF can serve as a dispatching algorithm in ADG necessitates empirical validation on real hardware. The transition from simulations to real-world scenarios raises challenges related to communication latency, idealized assumptions in the simulation and convex relaxations, and the interface between optimization problems and RT control of inverter-based resources. The substantial capabilities of the CoSES facility offer an opportunity to investigate the potential viability of D-OPF in practical ADG.

This paper introduces a PHIL implementation of a D-OPF algorithm incorporated within the operations of two interconnected ADG. To capture the static behavior of the optimization model, a two-layer control architecture is devised. Beneath the dispatch instructions derived from D-OPF, a primary control mechanism promptly reacts to load dynamics. The proposed framework is examined within the PHIL environment of the CoSES Lab at TUM. In the experimental setup, the two ADG collaboratively optimize their operations through an alternating direction method of multipliers (ADMM)-based unbalanced D-OPF approach. This operational strategy is compared against an exclusive application of primary control, devoid of D-OPF. The results highlight the superior performance of the decentralized approach, although inefficiencies stemming from the integration of optimization methods into RT system operation are also observed.

Publication #5 - PHIL implementation of a decentralized online OPF for active distribution grids

Authors - Martín Cornejo, Anurag Mohapatra, Soner Çandas, Vedran. S. Perić

Publication - 2022 IEEE Power Energy Society General Meeting (PESGM), 17-21 July, 2022

Digital object identifier - https://doi.org/10.1109/PESGM48719.2022.9916705

Author	Contribution	Tasks
Martín Cornejo	40%	Conceptualization, Formal analysis, Investigation, Validation, Software, Visualisation, Writing – original draft
Anurag Mohapatra	30%	Conceptualization, Methodology, Investigation, Validation, Visualisation, Writing - original draft
Soner Çandas	20%	Supervision, Formal analysis, Writing - review and editing
Vedran S. Perić	10%	Supervision, Writing – review and editing

PHIL implementation of a decentralized online OPF for active distribution grids

Martín Cornejo, Anurag Mohapatra, Soner Candaş, Vedran S. Perić
Technical University of Munich
Munich, Germany
{martin.cornejo, anurag.mohapatra, soner.candas, vedran.peric}@tum.de

2022 IEEE Power & Energy Society General Meeting (PESGM) | 978-1-6654-0823-3/22/$31.00 ©2022 IEEE | DOI: 10.1109/PESGM48719.2022.9916705

***Abstract*—This paper demonstrates a Power Hardware-in-the-Loop (PHIL) implementation of a decentralized optimal power flow (D-OPF) algorithm embedded into the operations of two microgrids connected by a tie line. To integrate the static behavior of the optimization model, a two layer control architecture is introduced. Underneath the dispatch commands from the D-OPF, a primary control scheme provides instantaneous reaction to the load dynamics. This setup is tested in the PHIL environment of the CoSES Lab in TU Munich. In the experiment, the two microgrids cooperatively optimize their operation through an Alternating Direction Method of Multipliers (ADMM) based unbalanced D-OPF. The operation is then benchmarked against the exclusive use of primary control, without D-OPF. The decentralized approach outperforms, but also shows minor inefficiencies of integrating optimization methods into the real-time operation of the system.**

***Index Terms*—Optimal power flow, power hardware-in-the-loop, distribution grids, decentralized control, real time control**

I. Introduction

Smart grid and microgrid technologies have emerged as a response to the disruptive integration of distributed energy resources (DER) in power distribution systems. The individual control and optimal coordination of the fast dispatchable inverters connected to the DER makes microgrid operation a challenge. Traditionally in a transmission grid, the optimal power flow (OPF) has been a tool of choice for the operator to dispatch the generators to minimize losses and achieve the best economic performance within the grid constraints. In a distribution grid context, online or real-time OPF can allow fast redispatch of controllable power electronics generation at the household level, in order to leverage local electricity market mechanisms.

However, smart distribution grids also bring their associated concerns with scalability, robustness and privacy, which lends emphasis towards a decentralized implementation scheme [1]. Unlike conventional methods, in which a central controller collects all the data and performs the computations, decentralized algorithms are carried out in multiple local controllers by exchanging limited information to their proximal peers. This allows for an online decentralized OPF (D-OPF) scheme for prosumers who do not want to share information with other neighboring microgrids and yet want to take advantage of an optimal operation of their generation.

While D-OPF has been extensively studied [1], to the best knowledge of the authors, a Power Hardware-in-the-Loop (PHIL) implementation in a realistic grid setting has not yet been attempted. Porting the online D-OPF algorithm into a real time (RT) PHIL application requires further considerations, generally neglected in the simulation models. Another challenge is the integration of the static optimization problem into a RT control scheme for PHIL testbeds. This implementation scheme must be practical and, most importantly, should not depart from reality, to further the claim that online D-OPF schemes can be used in real microgrids.

In this paper we present a PHIL implementation scheme and experimental validation of an online D-OPF method within the Center for Combined Smart Energy Systems (CoSES) lab at TU Munich. CoSES was established to research smart multi-energy systems in an emulated environment [2]. The laboratory emulates a distribution grid through a PHIL system, [3] and therefore lends a valid platform to testbench the online D-OPF implementation in a realistic environment.

The rest of this paper is structured as following. In Section II we introduce the proposed methodology for the validation. The decentralized OPF algorithm is presented, alongside some considerations from the authors to integrate D-OPF in a PHIL environment. Section III gives an insight on the implementation on the CoSES-lab. Section IV presents the experiment, results and discussion. Finally, Section V closes with the conclusions and the outlook for further research.

II. Methodology

A. Decentralized OPF algorithm

Many decentralized methods have been implemented for OPF applications [1]. Arguably, the state-of-the-art in decentralized OPF algorithms constitutes the ADMM-OPF and has been therefore extensively adopted in previous works [4]–[8].

The Alternating Direction Method of Multipliers (ADMM) performs distributed optimization by decomposing an optimization problem into smaller sub-problems and iteratively solving these while sharing information on a few common variables [9]. The advantage over other distributed algorithms is, that consensus-ADMM enables a fully decentralized OPF

The construction of the CoSES laboratory was supported by Deutsche Forschungsgemeinschaft (DFG) through the project "Flexible reconfigurable microgrid laboratory" under Project number 350746631. The work of Vedran Perić was supported by Deutsche Forschungsgemeinschaft (DFG) through the project "Optimal Operation of Integrated Low-Temperature Birdirectional Heat and Electric Grids (IntElHeat)" under Project number 450821044.

implementation with no need of a central controller to orchestrate the optimization [10].

ADMM can be integrated into the OPF by partitioning the power grid, by means of a network decomposition or by splitting it in administrative zones (the independently managed micro-grids and distribution networks). These local power grids can be also referred to as *clusters*. Through the decomposition, each bus of the network is allocated to a specific cluster and to locally replicate the cluster-coupling power lines, each local grid takes a *copy* of the directly neighboring buses.

Over the set of all grid partitions $\mathcal{M}$, each local grid $\{m, n, \dots\} \in \mathcal{M}$ can be individually optimized and the solution will ultimately correspond to the full-grid optimization as long as the voltages of all peripheral buses match among all clusters. ADMM exploits this relation for the distributed optimization of the OPF. First, the common global variables $\bar{v}_i$ are introduced, representing the voltages of all shared buses on cluster periphery. For the global optimum to be preserved, ideally, the peripheral voltages of all cluster $m \in \mathcal{M}$ should be consistent with the global variables:

$$\bar{v}_i - v_i^{(m)} = 0, \qquad \forall\ i \in \mathcal{N}_\varphi^{(m)} \tag{1}$$

The goal is to iteratively optimize the local OPF sub-problems, exchange the resulting peripheral voltages, update the global variables and repeat until all clusters agree on these within a margin of tolerance, hence having solved the global OPF problem.

For the local optimization, the voltage consensus (1) is introduced as a *soft constraint* in the form of an augmented Lagrangian. The objective function of a local OPF is extended from the active power generation cost $f(\mathbf{p_g})$ to the following:

$$\begin{aligned}\mathcal{L}_\rho(\mathbf{p_g}, \mathbf{v}_\varphi, \bar{\mathbf{v}}_\varphi, \boldsymbol{\lambda}) = f(\mathbf{p_g}) + \boldsymbol{\lambda}^T(\bar{\mathbf{v}}_\varphi - \mathbf{v}_\varphi) \\ + \frac{\rho}{2}\ ||\bar{\mathbf{v}}_\varphi - \mathbf{v}_\varphi||_2^2,\end{aligned} \tag{2}$$

where $\rho > 0$, $\boldsymbol{\lambda}$ is the local Lagrangian multipliers, $\mathbf{p_g}$ is the active power generation, $\bar{\mathbf{v}}_\varphi$ and $\mathbf{v}_\varphi$ are the global and local variables of the cluster peripheral bus voltages. Following the consensus ADMM method, for each iteration k, each local-OPF is solved with step-fixed global variables $\bar{\mathbf{v}}_\varphi^{(k)}$ and multipliers $\boldsymbol{\lambda}^{(k)}$.

$$\min_{\mathbf{p_g}, \mathbf{q_g}, \mathbf{v}} \quad \mathcal{L}_\rho(\mathbf{p_g}, \mathbf{v}_\varphi, \bar{\mathbf{v}}_\varphi^{(k)}, \boldsymbol{\lambda}^{(k)}) \tag{3a}$$

$$\text{s.t.}$$

$$\sum_{g \in \mathcal{G}_i} s_g - \sum_{d \in \mathcal{D}_i} s_d = v_i \sum_{k \in \mathcal{N}} Y_{ik}^* v_k^*, \quad \forall\ i \in \mathcal{N}_\chi \tag{3b}$$

$$v_i^l \le |v_i| \le v_i^u, \qquad \forall\ i \in \mathcal{N} \tag{3c}$$

$$p_g^l \le p_g \le p_g^u, \qquad \forall\ g \in \mathcal{G} \tag{3d}$$

$$q_g^l \le q_g \le q_g^u, \qquad \forall\ g \in \mathcal{G} \tag{3e}$$

$$\mathbf{v}_0 = \hat{\mathbf{v}}_0 \tag{3f}$$

The new local peripheral voltages $\mathbf{v}_\varphi^{(k+1)}$, from the local OPF iteration, are collected across all local grids to update the values of the global variables, by taking the average over all local peripheral voltages. A fully decentralized method can be achieved by exchanging the peripheral voltages only between adjacent clusters and locally performing the averaging step.

Multipliers are then updated locally based on the global-local voltage mismatch scaled with the penalty parameter:

$$\boldsymbol{\lambda}^{(k+1)} = \boldsymbol{\lambda}^{(k)} + \rho(\bar{\mathbf{v}}_\varphi^{(k+1)} - \mathbf{v}_\varphi^{(k+1)}) \tag{4}$$

To measure the mismatch error among clusters and between iterations, two indicators are introduced - the *primal residual* r, which highlights the error between global and local variables, and the *dual residual* s, which underlines the deviation of the local variables from the previous to the next iteration.

$$r^k = ||\bar{\mathbf{v}}_\varphi^{k+1} - \mathbf{v}_\varphi^{k+1}||_2 \tag{5a}$$

$$s^k = \rho||\bar{\mathbf{v}}_\varphi^{k+1} - \bar{\mathbf{v}}_\varphi^{k}||_2 \tag{5b}$$

The algorithm stops when both residuals are below a desired tolerance $0 < \epsilon \ll 1$ in all clusters $m \in \mathcal{M}$.

A disadvantage of ADMM is that the convergence speed is highly dependent on the penalty parameter ρ, and a bad choice could critically slow down the convergence. To counter this, an adaptive penalty is introduced via the residual balancing strategy, as proposed in [9] and extended in [11].

B. Unbalanced OPF formulation

The choice of OPF formulation is left on the best approach for the use case as ADMM-OPF implementation is independent of this decision. The SDP-OPF formulation is chosen as it has proven effective and has been extensively adopted for decentralized OPF applications, especially in the context of unbalanced power distribution systems. [1], [6]–[8]. SDP-OPF has the advantage that, thanks to its convexified formulation, for 3-phased radial distribution networks no modeling detail is sacrificed while the global optimum is searched [12], [13]. It also makes it possible to assess the feasibility and the quality of the solutions. This paper follows the *chordal reduced* SDP-OPF formulation [14], which takes advantage of a technique that leverages sparsity and simplifies the computational complexity, significantly reducing the convergence time.

C. PHIL considerations for online D-OPF

Integrating D-OPF into a power system operation requires an interface capable of merging the optimization process with the RT control. The challenge lies in the different time domains for the two processes. The optimization models live in a static world, and it takes some time for the algorithm to compute the results, while the control has to perform the commands in real-time.

The PHIL experiment design must therefore be cognizant of few key considerations for a practical and safe implementation of the online D-OPF scheme.

Local Stability of PHIL layer: The PHIL layer must have a real-time local primary control strategy to provide a safeguard against the slow reacting optimization layer, power mismatch from measurement errors, packet drops and communication latency, by always maintaining the generation equal to the demand.

978-1-6654-0823-3/22/$31.00 ©2022 IEEE

Asynchronous operation of layers: The PHIL and optimization layers have to run asynchronously using common communication interfaces. Thus the two layers are robust to communication adversities and cannot stop or throw an error waiting for the other layer to respond. On the PHIL side, the setpoints from the D-OPF layer should combine with the primary control to give the setpoint to the generator. Thematically this concept is similar to a traditional primary and secondary control for generators. The primary control reacts instantaneously to local load changes and a slower power change command, from any form of secondary control (in this case the D-OPF), redispatches the generators.

Flexibility in system configuration: Multiple experiments would be required to thoroughly investigate the efficacy and consequences of using the online D-OPF to provide generation setpoints. Therefore the PHIL, optimization and interface design should not be rigidly programmed to suit one specific parameter set or one specific grid setup. Furthermore, the interface layer should be ideally flexible to be combined with any other setpoint generation tool, instead of the ADMM based online D-OPF, to increase re-usability of the work in a laboratory.

These points are revisited in the Section III where the specifics of the RT implementation of online D-OPF in CoSES lab is discussed.

III. Implementation in CoSES

A. PHIL setup

Detailed description of the electrical and control setup of CoSES can be found in [2] and [3]. A brief description, relevant to the scope of this paper, is provided in this section. The lab setup emulates a Low voltage (LV) distribution grid of up to seven electrical prosumer households. The grid consists of ten LV buses with cable segments connecting them, which can be rearranged based on the topology needs. The location of the prosumers with reference to the LV buses can be shifted easily in a patch cabinet. Two tap changing transformers connect the lab grid to the Munich public supply grid.

The prosumer behaviour is emulated by seven Egston COMPISO units (CSU) which are bi-directional four leg inverters supplied by a separate power feedback circuit [15]. Each Egston CSU is connected to a prosumer bus and receives setpoints from the CoSES control system through a SFP link. The separation of the CoSES LV grid and feedback grid keeps the power consumption of the lab to only the ohmic losses even while operating at rated power.

The control infrastructure of CoSES comprises of National Instruments (NI) embedded hardware, the RT deployment environment VeriStand (VS) [16] and its associated APIs. Six NI PXI controllers are spread across the lab as distributed RT agents. One controller, denoted henceforth as *grid* controller, collects the LV grid bus voltage and prosumer currents. Two further RT controllers send setpoints to the seven Egston CSUs over a SFP link card. These two controllers can be split as the two clusters used in the D-OPF algorithm and are known as *Egston* controllers in this paper.

The VS environment hosts the different RT targets and the associated field IOs. The *grid* controller runs at $10\,\mathrm{kHz}$ RT execution rate, while the *Egston* controllers operate at $5\,\mathrm{kHz}$. PXI targets cannot inherently exchange information between each other as this cannot be implemented as a RT task. Therefore an asynchronous ring called, *Reflective Memory Network* (RMN) is used to exchange information between CoSES controllers at a maximum jitter of $1\,\mathrm{kHz}$. VS allows compiled models from C/C++, MATLAB, Simulink or LabVIEW and exposes their IOs to the grid measurements and Egston CSU setpoints. The VS Engine maintains the RT execution rate of the models, measurements and setpoints. Time synchronisation is provided between the six RT targets and the seven Egston CSU, which allows for accurate power injection in grid connected mode.

B. D-OPF implementation

The OPF and ADMM-OPF models are implemented in Julia and JuMP, using the interior-point conic solver MOSEK, to solve the SDP-OPF. For the ADMM implementation, the two local OPF models for the clusters shown in Fig. 1 are set up in two Windows PCs running independent Julia instances. The *message exchange* between the two ADMM clusters in Julia during the algorithm execution is achieved through TCP-socket connections and data serialization.

The optimization activity of the operation is enclosed in a static feedback loop. The *clusters* update the loads in the model from grid measurements, then jointly perform the ADMM-OPF and sent the optimal power setpoints to their corresponding *Egston* controllers. To interact with the RT targets, for both measurements and setpoints, the Julia instances rely on a Julia-LabView-VS bridge enabled through the VS API. The Julia instances communicate with the VS API using TCP connections in a JSON format.

Within the VS environment, a Simulink-compiled model for power measurement and PLL is implemented on the *grid* controller. In the *Egston* controllers, Simulink-compiled models are used for each CoSES prosumer in the cluster. These models convert power setpoints to precise current injection waveforms which are sent to the respective Egston CSU. The designated generators within the Egston CSUs, are provided with two setpoints from primary and secondary control respectively. A local cluster control is implemented to reflect the change in the local load from the base load conditions on the primary control power setpoint. If there are more than one generators in a cluster, they jointly share the change in the load. The D-OPF output is taken as a secondary control setpoint, as mentioned in Sec. II. Importantly, when D-OPF is activated and a new setpoint is sent to the cluster, the primary control sets the base load to the current measured load in the cluster. The primary control then dynamically changes the generation to match the load changes with respect to the new base load, until the next D-OPF setpoint arrives. Thus, a combination of the primary and secondary control setpoint, keeps the generation and load balance, irrespective of the rate of load changes or optimization delays.

978-1-6654-0823-3/22/$31.00 ©2022 IEEE

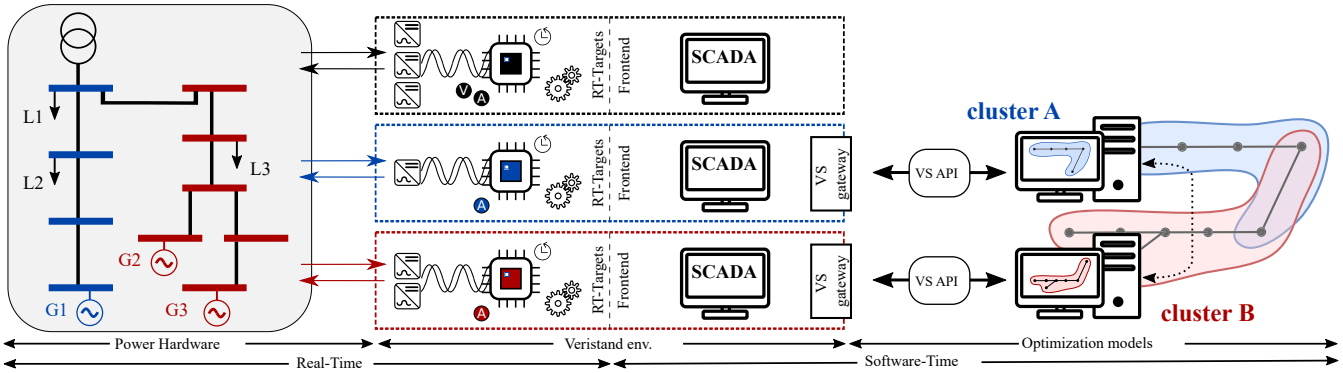

Fig. 1. PHIL implementation of online D-OPF in CoSES: Microgrid clusters with PHIL generator and loads (left), real-time control setup (center), ADMM based D-OPF optimization (right)

IV. Experiment and Results

A. Experiment design

The experiment takes a look into a distribution feeder divided into two clusters, both of which are organized as individual microgrids. Each microgrid has its own loads and generators, as well as an own control and monitoring system. It is assumed that the microgrid operators are interested in minimizing the cost of operating their system. However, the customers in the clusters do not necessarily want to share own information with another operator for a global optimization to work. Such motivations are common in current data privacy landscape and thus online D-OPF can be implemented here as a solution. The grid topology is represented in the leftmost graphic in Fig. 1, and the technical details are summarized in Table I.

Two experiment runs are conducted for this paper to illustrate the PHIL validation of D-OPF. In the first scenario, the optimization is turned off and the two clusters are required to be self-sufficient with their generation needs. The primary control mechanism described in Section III is used for this scenario. The real life analogue can be a microgrid EMS to monitor the loads and adjust the generation setpoints based on a participation factor κ_g and base power p_g^{ref}.

In the second scenario, we activate the online D-OPF layer of secondary control in addition to the primary control for the cluster, for the same load profile. The experiment begins with zero secondary control setpoint and the primary control setpoint set according to the base load conditions. The D-OPF layer takes a snapshot of the loads and returns to the ADMM-based optimization algorithm. Once finished, the optimization returns a secondary control setpoint for the generators. The primary control's base load is now reset to the current measured load. Any subsequent changes to the load from that moment until the new D-OPF setpoints arrive, is handled by the primary control based on the participation factor of the generator.

TABLE I
Generator Data

Gen	Cluster	P_{max} [kW]	Q_{max} [kVAR]	Cost [$/kWh]	κ_g
Grid	A	-	-	$10.0p$	-
G1	A	5.0	$\pm$ 4.0	$6.0p + 0.4p^2$	1.0
G2	B	5.0	$\pm$ 4.0	$4.0p + 0.4p^2$	0.715
G3	B	5.0	$\pm$ 4.0	$3.0p + 0.5p^2$	0.285

The loads are emulated through Egston CSUs and are assembled from the HTW Berlin representative household load profiles [17]. These profiles consist of three-phase active and reactive power timeseries with 1 minute resolution. Each load is the aggregation of 10 individual households of the dataset, with the data time segment for the experiment taken from February 1, starting at 19:00. Both scenarios are run for 30 mins. The generation and load profiles, change in generation in between scenarios and power exchanged between clusters are plotted in the next section.

B. Results

Primary control only: The generators follow the load profile shape, with cluster A covering the internal loads from its only generator and cluster B sharing the local demand between the two generators according to their κ_g, as shown in Fig. 2. As expected, almost no power exchange, P_{tie} between clusters or with the grid is observed and is seen in Fig. 3. The operation is stable but as a consequence of the over-proportional contribution of the generator G1, in covering the total grid demand, the operational expenses grow *unnecessarily* excessive. The total cost at the end of the experiment run is $0.78, from which cluster A contributes about 71%.

With D-OPF: Just as with the previous run, the generation roughly mirrors the load course and is shown in fig. 2. This time however, with a much more balanced distribution of the generator participation, a lower total operational cost of $0.73 (a reduction of about 6%) is achieved. In Fig. 3, we see that the generation from G1 is reduced while the generation from G2 and G3 is increased, when the D-OPF is activated. The exchange between clusters is now prominent in Fig. 3, while the grid exchange is also noticeable in Fig. 2. The P_{tie} power flows mostly from cluster B to A, curtailing the need to produce more from generator G1.

The grid involvement on the other hand is a side effect from the D-OPF wrapping implementation. When the load changes significantly while the optimization is in progress,

978-1-6654-0823-3/22/$31.00 ©2022 IEEE

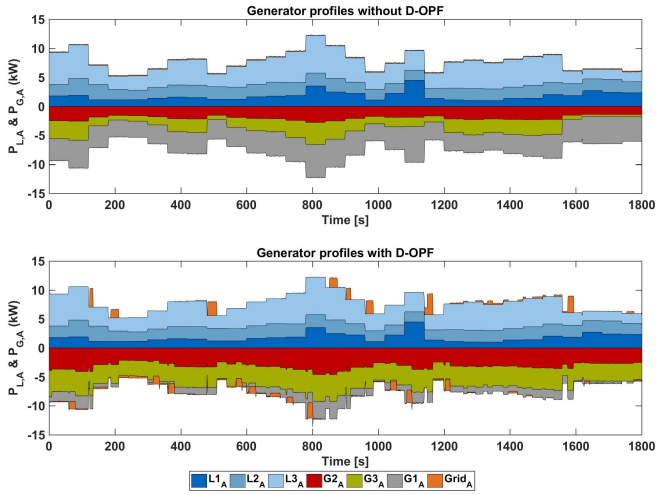

Fig. 2. Comparison of generation profiles with and without OPF (phase-A)

by the time the results arrive these no longer correspond with the actual state and difference has to be compensated from the grid feeder. This mismatch is corrected a few seconds later with the arrival of new optimization results. In our experiment the grid import signifies a great cost penalty. Even though the overall occurrence is short, the cost contribution adds to $\approx$ 15% of total cost. The performance of the optimization algorithm is therefore critical for cost optimal operations. For the case of our implementation, one instance of ADMM-OPF takes in average 18.5 s and $\approx$ 205 iterations to solve, including optimization time and communication overhead. This is significantly more than the central approach SDP-OPF, which takes instead a fraction of a second.

V. Conclusion

We have implemented a D-OPF scheme in a PHIL environment, taking some consideration relevant for a real deployment of the algorithm. The proposed control architecture operates in two layers, the upper level computes the optimal generator setpoints through the D-OPF and sends them to the lower layer, which ensures the system stability through real-time primary control. The interface between both layers should be redundant so that the layers don't depend on each other for their operation. Allowing this interface to be flexible permits to easily interchange optimization models and control algorithms.

The operation scheme is validated through a set of PHIL experiments in the CoSES microgrid-lab. The D-OPF scenario outperformed the individualistic approach consisting of exclusively the primary control. However, there are certain inefficiencies due to changing load as the optimization is getting computed. Even though, the primary control layer provides the D-OPF with a robust operation, with increasing convergence times and communication delay, the strategy's optimal performance would get affected. This serves as an open question to solve in the future work on the topic for a seamless integration of online D-OPF in distribution grids.

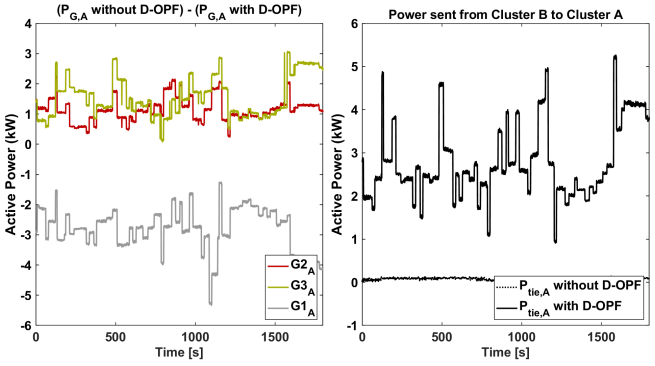

Fig. 3. Change in generator power (left) and tie line power (right) with and without D-OPF (phase-A)

References

[1] D. K. Molzahn, F. Dorfler, H. Sandberg, S. H. Low, S. Chakrabarti, R. Baldick, and J. Lavaei, "A Survey of Distributed Optimization and Control Algorithms for Electric Power Systems," *IEEE Transactions on Smart Grid*, vol. 8, pp. 2941–2962, Nov. 2017.

[2] V. S. Perić, T. Hamacher, A. Mohapatra, F. Christiange, D. Zinsmeister, P. Tzscheutschler, and C. Aigner, "CoSES Laboratory for Combined Energy Systems At TU Munich," *IEEE Power and Energy Society General Meeting*, 2020.

[3] A. Mohapatra, V. S. Peric, and T. Hamacher, "PHIL Infrastructure in CoSES Microgrid Lab," submitted to PES GM 2022, http://dx.doi.org/10.36227/techrxiv.17065184.

[4] T. Erseghe, "Distributed Optimal Power Flow Using ADMM," *IEEE Transactions on Power Systems*, vol. 29, pp. 2370–2380, Sept. 2014.

[5] M. Kraning, E. Chu, J. Lavaei, and S. Boyd, "Dynamic Network Energy Management via Proximal Message Passing," *Foundations and Trends® in Optimization*, vol. 1, no. 2, pp. 73–126, 2014.

[6] E. Dall'Anese, H. Zhu, and G. B. Giannakis, "Distributed Optimal Power Flow for Smart Microgrids," *IEEE Transactions on Smart Grid*, vol. 4, pp. 1464 – 1475, Sept. 2013.

[7] E. Dall'Anese, S. V. Dhople, B. B. Johnson, and G. B. Giannakis, "Decentralized Optimal Dispatch of Photovoltaic Inverters in Residential Distribution Systems," *IEEE Transactions on Energy Conversion*, vol. 29, pp. 957 – 967, Dec. 2014.

[8] Q. Peng and S. H. Low, "Distributed algorithm for optimal power flow on an unbalanced radial network," in *2015 54th IEEE Conference on Decision and Control (CDC)*, (Osaka), pp. 6915–6920, IEEE, Dec. 2015.

[9] S. Boyd, "Distributed Optimization and Statistical Learning via the Alternating Direction Method of Multipliers," *Foundations and Trends in Machine Learning*, vol. 3, no. 1, pp. 1–122, 2010.

[10] S. Candas, K. Zhang, and T. Hamacher, "A Comparative Study of Benders Decomposition and ADMM for Decentralized Optimal Power Flow," in *2020 IEEE Power & Energy Society Innovative Smart Grid Technologies Conference (ISGT)*, (Washington, DC, USA), pp. 1–5, IEEE, Feb. 2020.

[11] B. Wohlberg, "ADMM Penalty Parameter Selection by Residual Balancing," *arXiv:1704.06209 [cs, eess, math]*, Apr. 2017. arXiv: 1704.06209.

[12] S. H. Low, "Convex Relaxation of Optimal Power Flow—Part I: Formulations and Equivalence," *IEEE Transactions on Control of Network Systems*, vol. 1, pp. 15–27, Mar. 2014.

[13] S. H. Low, "Convex Relaxation of Optimal Power Flow—Part II: Exactness," *IEEE Transactions on Control of Network Systems*, vol. 1, pp. 177–189, June 2014.

[14] L. Gan and S. H. Low, "Convex relaxations and linear approximation for optimal power flow in multiphase radial networks," in *2014 Power Systems Computation Conference*, (Wrocław, Poland), pp. 1–9, IEEE, Aug. 2014.

[15] Egston Power, "COMPISO Power Hardware in the Loop," Nov. 8, 2021 [Online].

[16] National Instruments, *"NI Veristand"*, 2018.

[17] T. Tjaden, J. Bergner, J. Weniger, and V. Quaschning, "Repräsentative elektrische Lastprofile für Wohngebäude in Deutschland auf 1-sekündiger Datenbasis." https://pvspeicher.htw-berlin.de/veroeffentlichungen/daten/lastprofile/.

978-1-6654-0823-3/22/$31.00 ©2022 IEEE

Concluding remarks on the publication

The key innovation of the paper is the perspective of visualizing this optimization problem as a PHIL experiment, whose salient features are listed in Tab. 3.1. Incorporating D-OPF into power system operations demands a seamless interface that can harmonize the optimization process with RT control. The challenge arises from the disparate timeframe of these processes. Optimization models reside in a static realm, requiring time to compute outcomes, while control mandates RT execution. Thus the following major changes were made to the standard D-OPF literature dealing with only simulations,

Local Stability of PHIL Layer - The PHIL layer necessitates a RT local primary control strategy to counterbalance the sluggish optimization layer, accommodate power mismatches from measurement inaccuracies, handle communication latency, and account for packet losses by sustaining generation equal to demand.

Synchronous Operation of Layers - The PHIL and optimization layers must run asynchronously via common communication interfaces. This safeguards against communication failure, ensuring neither layer stalls or raises errors waiting for the other's response. On the PHIL side, D-OPF layer setpoints harmonize with primary control, resembling the traditional primary and secondary control paradigm for generators. Primary control swiftly responds to local load changes, while slower power change directives from secondary control (in this case D-OPF) readjust generator dispatch.

Flexibility in System Configuration - Thorough examination of the D-OPF effect for generation setpoints necessitates multiple experiments. Consequently, PHIL, optimization, and interface design should steer clear of rigidity to suit a specific parameter set or grid configuration. Ideally, the interface layer should be adaptable to integrate with any setpoint generation tool, promoting reusability within laboratory setups.

Table 3.1: Salient features of the PHIL online D-OPF experiment in CoSES.

Scope of the experiment	Grid connection – Munich LV grid LV network – 70 & 95mm^2 cables Generators & Loads – Egston Control algorithm – Simulink & LV OPF algorithm – Julia Messaging – JSONs + LV API
Components used	3 x RT Embedded controllers 2 x PCs for distributed optimisation 46 x V, I measurements 6 x Power amplifiers 1 x Veristand RT environment

A notable difference upon activating D-OPF for real experiments is the effect of significant load fluctuations during ongoing optimization. By the time results arrive, they may no longer align with the actual state, prompting grid feeder adjustments. While this mismatch is rectified within seconds with new optimization results, grid import during this interval incurs considerable cost penalties. Although short-lived, these cost contributions aggregate to approximately 15% of the total cost in this publication. The work underlines

the importance of providing demonstrative evidence in a laboratory for simulation studies and thus credibly proving its merit while opening new implementation questions to guide future research.

3.3 Reachability analysis in CoSES (Publication #6)

The last publication in this series of using CoSES as an ADG research facility comes from an ongoing work to implement reachability analysis in RT control systems. Before we begin to discuss the focus on the application of reachability analysis in power systems and the role of an ADG laboratory in this scope of works, we will first look into some preliminaries of reachability analysis in general and its possible transfer as a tool to investigate power system problems. The relevant publication for this section, will demonstrate the conversion of a standard grid frequency control problem using linearized power system models into a linear time invariant reachability analysis problem. The next subsections will expand on this publication, presenting larger test case studies and an outlook on how to organise a RT reachability analysis test in CoSES. The comprehensive nature of this investigation is beyond the scope of this current thesis and will be tackled in a separate research project.

3.3.1 Background: Reachability analysis

Dynamical systems constitute of functions which describe the relationship of a point in the system state space with time. For example, a simple pendulum can be represented as a dynamical system. Here the physical quantities, the angle of pendulum and its angular velocity are considered the system states, while the physical behaviour of the pendulum is governed by Newton's second law of motion. This relationship describes the position of the pendulum at any given moment of time in a two-dimensional coordinate plane.

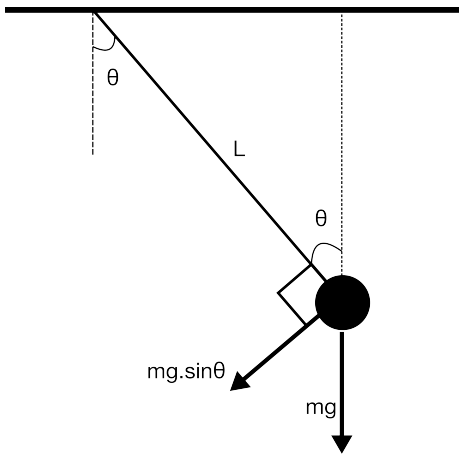

Figure 3.2: A simple pendulum as a dynamical system

For the simple pendulum shown in Fig. 3.2, we can write the newton's second law of motion as, Torque = Moment of inertia x Angular acceleration. With Torque, $T = -mgsin\theta L$, Moment of inertia, $J = mL^2$ and Angular acceleration, $\alpha = \ddot{\theta}$, we can

write this equation as,

$$\ddot{\theta} = -\frac{g}{L} sin\theta \tag{3.1}$$

By taking small angle approximations and cancelling the m on both sides, we get

$$\ddot{\theta} = -\frac{g}{L}\theta \tag{3.2}$$

Now we can introduce the states for the angle and angular velocity as $x_1 = \theta$ and $x_2 = \dot{\theta}$. This leads to an ordinary differential equation (ODE) system,

$$\begin{bmatrix} \dot{x_1} \\ \dot{x_2} \end{bmatrix} = \begin{bmatrix} 0 & 1 \\ -g/L & 0 \end{bmatrix} \begin{bmatrix} x_1 \\ x_2 \end{bmatrix} \tag{3.3}$$

The ODE system is a deterministic description of the simple pendulum system without any external torque and can be solved as an initial value problem. This particular family of linear dynamical systems has been studied extensively and is considered the basis for modern control theory analysis in time domain using state space equations [105]. Such initial value problems can be solved in modern solvers using numerical integration. Given a system of ODEs, $\dot{x} = f(x,t)$ with an initial condition, $x(t_0) = x_0$, numerical integration provides the single trajectory for the evolution of the states x for the specific initial condition, x_0.

Definition of reachability analysis

Reachability analysis is a study to determine the set of *all possible states* a dynamical system can *reach*, from a given set of initial states, when acted upon by a set of inputs and parameters. The input here can be a constant value or a time-series or trajectory value [106]. This can be represented mathematically as,

$$R(x_0, \mathcal{U}) = \{x_1 \in X \mid \exists \tilde{u} \in \mathcal{U} \text{ and } \exists t \in [0, \infty) \text{ such that } x(t) = x_1\}, \tag{3.4}$$

where $R(x_0, \mathcal{U}) \subseteq X$ represents the reachable set, starting from a permissible initial set x_0 under the influence of an input $\tilde{u} \in \mathcal{U}$. Here, $x(t)$ is an integral solution of a linear state space problem expressed as,

$$x(t) = x(0) + \int_0^{t'} f(x(t), u(t))\, dt \tag{3.5}$$

This relationship is a *single state trajectory* caused by an action trajectory $u(t)$, when the state has originated at $x(0)$.

Comparing the two equations 3.4 and 3.5, the essential difference is that they deal with a set of state trajectories vs a single trajectory of a state respectively. The concept of using a set to represent the permissible states, input and parameter ranges is powerful in context of robust control strategies which deal with uncertainties. It is an eminently practical interpretation of real control systems, such as electrical machines, automotives, industrial processes, where the the inputs and parameters are known but with a certain margin of error. It also plays well into other commonly used engineering analysis techniques like

state estimation, which provide their estimates of the possible eigenvalues of a complex plant with a confidence interval around them.

In other words, one could approximate the results of a reachability analysis by discretizing the admissible input, parameter and initial state set, and performing an individual numerical integration to determine the state trajectory evolution based on an unique combination of each of these points. A collection of such individual state trajectories will approximate the reachability analysis, with an infinite number of them needed to be exactly equivalent. This reflection brings us to the most important advantage of performing a reachability analysis, the aspect of a *formal verification*.

Formal verification is a rigorous methodology, mostly used in computer science, to ensure or guarantee model performance through various formal methods, such as model checking, type theory and many others. Reachability analysis is also considered a formal verification strategy and can be used to provide provably safe guarantees for a system [107]. To put things into perspective, if one is able to perform a reachability analysis for a given system of state space equations with bounded uncertainties around inputs, states and parameters, the resulting reachable set of states carries a *formal guarantee*.

Applications of Reachability analysis

The following list is a non-exhaustive indexing of the possible reachability analysis applications in engineering,

Safety sets [108] - Reachability analysis can be used to formally guarantee that the states will not breach outside a given safe set or will avoid a given unsafe set of states, under given bounded initial states, parameters and inputs for a specified time interval.

Control performance assessment [109]- Reachability analysis can show the region of all possible state trajectories under a given controller tuning. This can be used to contrast the performance of two controller settings with formally verified results.

Controller synthesis [110]- Given a list of safety constraints, reachability analysis can provide a control parameter set which guarantee adherence of the feedback controlled plant to the said constraints.

Uncertainty analysis [111] - Reachability analysis can provide a set of reachable sets for a varying degree of uncertainties. Thus, the maximum permissible uncertainty on a given state, input or parameter in the state space system, which keeps the reachable states in the allowed region, can be formally computed.

Reachability analysis in Power systems

Traditional power systems have always dealt with uncertain states, parameters and inputs in steady state and transient analysis. Uncertainties have existed in parameter values for linear power system models, machine models and consumer load profiles. Safety critical constraints such as voltage, frequency, critical clearing time of faults must be maintained regardless of these uncertainties. In a lot of these cases, power system operators simply over-design the system to conservatively remain within the constraints under worst case condition or perform many Monte-Carlo based simulations to cover the uncertainty space with some degree of confidence. In modern power systems with heavy penetration of power

electronics converters for renewable resources, there is a further element of generation uncertainty. Intelligent grid operation, especially at ADG levels with a limited reserve capacity, is required to avoid congestion and grid constraints under intermittent renewable generation.

There have been formal verification methods already in use in power systems, known as direct methods in literature [112]. This involves an explicit solution of the power system differential algebraic equations using Lyapunov candidate functions. The major drawback here being the difficulty in finding the correct Lyapunov function for complex systems and the high computational complexity of the explicit solution. Robust control strategies such H-infinity controller synthesis, which guarantee system stability for bounded uncertainties, have also been extensively studied in power systems [113]. However, they are dependent on the choice of the cost function, which requires prior experience to properly select and tune. Both the direct method and robust control method deal primarily in steady state stability analysis. In other words, they provide a guarantee for asymptotic system convergence to a stable region in the state space under uncertainties. But that might not be a good enough metric for power system operation, as momentary excursions of voltage and frequency to unsafe regions could trigger protection devices, notwithstanding the long term stability perspective of the system.

Given the combined context in traditional and modern power systems, reachability analysis is an attractive tool to provide guaranteed results for reliable operation [109]. There is no requirement to search for optimal Lyapunov functions or cost functions for robust controllers. It avoids the trap of computationally expensive uncertainty modelling methods, by considering the whole uncertainty as a bounded set and continuing all operations with set-based interval arithmetic. The output from such an analysis is therefore an envelope which marks the reachable region for every state trajectory in the time horizon. Additionally, reachability study provides the reachable set at every time-step and can guarantee that states remained in the safe region at every instant of the observation window, on top of converging to a stable operation region.

Qualifiers on performing a reachability analysis

Over-approximation [114] - It has been shown in literature, that the exact reachable set of linear continuous systems can only be calculated for special cases. Thus most reachability analysis tools, calculate the reachable set using over-approximative algorithms. The structure of *over-apprixmation analysis* takes an approximated or relaxed version of the real equation, eg - Taylor series approximation to a certain index for a matrix exponent. The excluded terms are not discarded, but are collected together to provide a bound on the uncertainty caused by their exclusion. After solving the approximate problem for the next time step, the solution is modified in a way which over-approximates the uncertainty from excluding the extra terms. The precision in this over-approximate padding of the result, is an important metric and certain over-approximative methods are considered tight. Tight over-approximation denotes that the enlarged set is still the smallest set which encloses the uncertainty.

Set representation geometry [114] - Reachability analysis uses set-based arithmetic to calculate the reachable sets. Therefore the efficiency of representing higher dimensional

spaces as sets during computation plays a significant role in the feasibility of the problem. *Zonotopes* have been shown to have exception computational efficiency while calculating reachable sets for linear systems with uncertain inputs over long time horizons. A zonotope is a set representation of higher dimensions space around a center, with the new dimensions being added as the Minkowski sum of a new vector representing that dimension as shown in the Fig. 3.3.

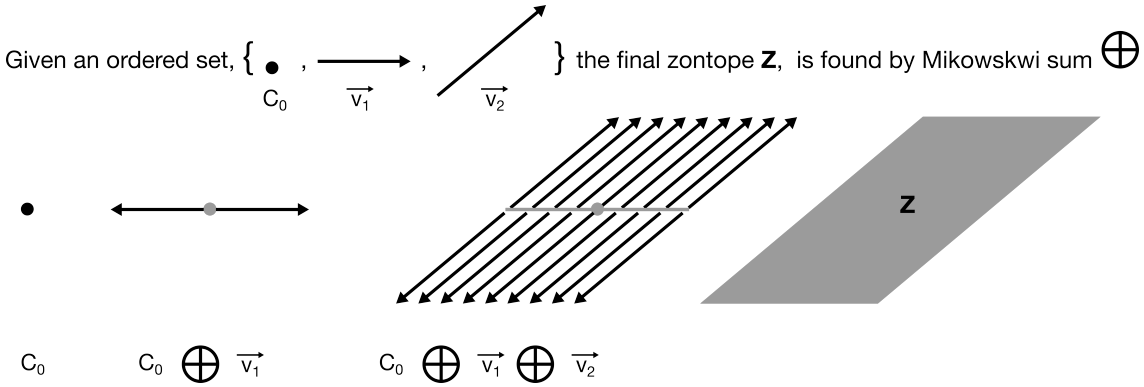

Figure 3.3: A schematic representation of building a zonotope using Minkowski sums.

Tractability - Reachability problems have generally suffered in performance compared to simulation techniques from computation overheads. However in recent times, tools such as COntinuous Reachability Analyser (CORA) [115] and JuliaReach [116] have made tremendous progress in handling large state spaces and over a large time horizon at adequate time-step intervals. The progress has been made through better overhead handling, new zonotope/polytope reduction techniques, and in case of CORA, using adaptive parameter tuning, subspace identification and support functions to quicken the computation time. This is an important point of order in eventually thinking of performing near-RT reachability analysis as an online formal verification tool.

3.3.2 Reachability analysis of grid frequency controllers (Publication #6)

Grid frequency control is an important control problem within power systems, playing a critical role in maintaining system stability by continuously matching generation to the demanded load. Conventionally, classical control approaches like proportional-integral-derivative (PID) control have been extensively employed due to their simplicity and straightforward implementation. The tuning of these control loops has been a subject of thorough investigation in literature, with the evaluation and validation of control performance achieved through simulations that replicate system behavior across varying operational conditions. However, the variety of potential operating scenarios, coupled with the inherent uncertainty surrounding load and renewable energy behaviors, requires a significant number of time-consuming simulation runs to establish sufficient confidence in the safety margins of the controller. Therefore this problem could benefit from an appropriate reachability analysis framework with its formal verification property.

The subsequent publication introduces a new method to formally verify grid frequency control. It uses reachability analysis to calculate reachable sets, including all possible system state or output changes under bounded input load uncertainty. The method is applied to the IEEE 9-Bus system, where we also perform single trajectory simulations with randomised but bounded, input and starting values.The reachable set encompasses these simulations completely, providing an indirect validation. The paper also examines how control parameters and input uncertainties affect reachable sets. The thought being that operators can validate their frequency controllers without extensive simulations, ensuring compliance with grid guidelines.

The main contribution of the paper is in converting a standard power system simulation model into a Linear continuous reachability analysis model. The salient steps are as follows,

- **Step 1** - Power system simulation model with grid frequency controller in the tool of choice. The model is initialised to begin simulation from a steady state condition. Initially, the states are from the choice of power system elements, such as generator, turbine governors and AVRs, the controllable input is the grid frequency setpoint from the controller to all the generator and the uncertain, uncontrolled disturbances are the loads and the grid frequency as output.

- **Step 2** - Linearize the grid model and derive the small signal stability state space model. This would lead to a state space of the following style,

$$\begin{aligned} \Delta\dot{x}(t) &= A\Delta x(t) + B\Delta u(t) + E\Delta d(t) \\ \Delta y(t) &= C\Delta x(t) + D\Delta u(t) \end{aligned} \tag{3.6}$$

  In a grid with N generators, K states per generator unit, M loads whose active and reactive powers (P and Q) are considered inputs, (3.6) has $\Delta x(t) \in^{NK}$ as the states, $\Delta u(t) \in^{K}$ as the designated inputs, $\Delta d(t) \in^{2M}$ are disturbances and $\Delta y(t) \in^{K}$ are the outputs.

- **Step 3** - Write a simple PI control law for the frequency control problem. Assign some preliminary PI gains.

$$\Delta u(t) = K_p\Big(e(t) + \frac{1}{T_i}\int e(t)dt\Big), \tag{3.7}$$

  where, the error is defined as $e(t) = r(t) - \Delta y(t)$, $r(t)$ is the reference to be tracked, K_p is the proportional gain and T_i is the integral time constant.

- **Step 4** - Include the PI controller in a closed loop extended state space. This should leave the controller bundled within the extended state matrix and the disturbance as an uncontrolled input,

$$\begin{aligned} \underbrace{\begin{bmatrix}\Delta\dot{x}(t)\\ \dot{e}_{int}(t)\end{bmatrix}}_{\dot{\widetilde{x}}(t)} &= \underbrace{\begin{bmatrix}A - BC_gK_p & B\frac{K_p}{T_i}\\ -C_g & 0\end{bmatrix}}_{\widetilde{A}} \underbrace{\begin{bmatrix}\Delta x(t)\\ e_{int}(t)\end{bmatrix}}_{\widetilde{x}(t)} + \underbrace{\begin{bmatrix}E\\ O\end{bmatrix}}_{\widetilde{B}} \underbrace{\begin{bmatrix}\Delta d(t)\end{bmatrix}}_{\widetilde{u}(t)} \\ \widetilde{y}(t) &= \underbrace{[C_g \;\; 0]}_{\widetilde{C}}\widetilde{x}(t) \end{aligned} \tag{3.8}$$

where, $\widetilde{A}$ is the extended state matrix and $\widetilde{B}$ is the extended input matrix. The error dynamics is written by rearranging 3.7, as,

$$\dot{e}_{int}(t) = \frac{1}{K_p}\Delta u(t) - \frac{1}{T_i}e_{int}(t) \tag{3.9}$$

This leaves us with a new state space,

$$\dot{\widetilde{x}}(t) = \widetilde{A}\,\widetilde{x}(t) + \widetilde{B}\,\widetilde{u}(t), \quad \widetilde{x}(t) \in^{NK+1}, \quad \widetilde{u}(t) \in^{2M}, \tag{3.10}$$

which takes the grid active and reactive loads as uncontrolled inputs, or disturbances and provides the grid frequency as an output. This treatment can also be rephrased as changing the original problem into a disturbance rejection problem.

- **Step 5** - The final extended state space can be now handled by a reachability analysis tool dealing with linear continuous systems and accepting a time-series of input trajectory. The reachable sets will show the evolution of the grid frequency under specific load time-series with a bounded uncertainty in *every* time-step.

Publication #6 - Formal Verification of Grid Frequency Controllers

Authors - Anurag Mohapatra, Thomas Hamacher, Vedran S. Perić

Publication - 2021 IEEE PES Innovative Smart Grid Technologies Europe (ISGT Europe), 18-21 October, 2021

Digital object identifier - `https://doi.org/10.1109/ISGTEurope52324.2021.9640096`

Author	**Contribution**	**Tasks**
Anurag Mohapatra	60%	Conceptualization, Formal analysis, Methodology, Software, Validation, Visualisation, Writing – original draft
Thomas Hamacher	10%	Funding acquisition, Resources, Writing - review and editing
Vedran S. Perić	30%	Conceptualization, Supervision, Writing – review and editing

Formal Verification of Grid Frequency Controllers

Anurag Mohapatra*, Vedran. S. Perić*, Thomas Hamacher*
*CoSES, Munich School of Engineering, Technical University of Munich, Munich, Germany

***Abstract*—This paper proposes a formal verification strategy of grid frequency control using reachability analysis. Reachability analysis calculates reachable sets, which are all possible evolution of system states, or output variables, given a bounded input uncertainty. Contrary to classical grid frequency control schemes that are generally tuned based on multiple simulations, reachability analysis provides a formal guarantee for the performance of the controller in one computation stage. The proposed method is applied on the IEEE 9-Bus system. The accuracy of reachable sets is validated by simulation results with randomized inputs. In addition, the paper analyses the effect of control parameters and input uncertainties on the reachable sets. Thus, the operator can verify if their tuned frequency controller could violate any mandated grid directives without performing large number of simulations.**

***Index Terms*—Reachable sets, formal verification, reachability analysis, frequency control, load uncertainty**

I. Introduction

Grid frequency control is one of the most important control schemes in power systems. It maintains the system frequency at the nominal level by continuously balancing the generation and load demand. Traditional frequency controllers employ classical approaches such as Proportional-integral-derivative (PID) control, due to its simple implementation [1]. The tuning of such control loops has been extensively studied in literature, where the control performances are assessed and validated by simulating the system behavior in different operating conditions. Due the large number of possible operating conditions and inherent uncertainty of load and renewable energy behavior, this validation requires large number of time-consuming simulation runs to gain sufficient confidence in adequacy of the adopted control scheme [2]. However, despite the multiple simulation runs, there is no formal guarantee that the control scheme will maintain the frequency in the acceptable range under all operating uncertainties.

Reachability analysis is a mathematical algorithm that calculates all possible states that a dynamical system can reach within a given time horizon, taking into account uncertainties in inputs, parameters or initial states. In this sense, the reachability analysis represents a generalization of a dynamic system simulation, where some of the inputs, parameters or initial states are represented by a set instead of a scalar value. Consequently, the resulting states and outputs are expressed as sets evolving in time. Reachability analysis has been used recently in a variety of problems related to dynamic operation of power systems, such as determining critical clearing time during faults under operating uncertainties [3], [4], ensuring safe operation of power plant boiler units [5] and power electronics dominated microgrid [6].

One of the most promising applications of reachablity analysis is a formal verification of controllers, which provides the guarantee that the controller will maintain the system states in the acceptable operating range. In literature, robust control techniques such as H-infinity controllers have been studied which guarantee stability of the system in general, for bounded uncertainties [7]. However, this does not guarantee the position of individual states and outputs in the time-domain. Also, the robustness against uncertainty is dependent on a good choice of the cost functions, which requires prior experience, for the optimisation of the loop tuning. Reachability analysis avoids these requirements by guaranteeing the behaviour in the time-domain and handling the uncertainty directly within the set based solution of the states.

In this paper, we introduce a formal verification strategy for classical grid frequency controllers. In the proposed strategy, an evolution of the reachable set of grid frequency is calculated, assuming the forecast load profile with bounded uncertainty. The calculated reachable set allows grid operator to have a formal guarantee that a dangerous frequency deviation will not occur under expected uncertainty levels over a fixed time interval. In addition, with the use of reachability analysis, the controller parameters can be tuned to avoid excessive frequency deviations. The case studies in this paper demonstrate that the reachability analysis accurately calculates the frequency deviation bounds, which was validated with simulations randomised within the modeled system uncertainties. Finally, the paper demonstrates an example of how the controller parameters affect the size of reachable sets, which provides additional insight during the controller parameter tuning procedure.

The rest of the paper is organized as follows. Section II describes power system model used for reachability analysis. Section III describes the proposed methodology for calculating reachable sets. Section IV shows the validation of the methodology on a standardized test case, with the main conclusions summarised in Section V.

II. Power System Model and Frequency Control

The models for analysis of frequency control in power systems have been used extensively in existing literature [8]. From the perspective of a generator, the speed reference command to the turbine governor is an input and the generator rotor speed is an output, which also determines the grid frequency. The change in load can be modelled as an external disturbance in

978-1-6654-4875-8/21/$31.00 ©2021 IEEE

2021 IEEE PES Innovative Smart Grid Technologies Europe (ISGT Europe) | 978-1-6654-4875-8/21/$31.00 ©2021 IEEE | DOI: 10.1109/ISGTEUROPE52324.2021.9640096

this system. Thus the frequency control problem for the power system can be re-imagined as a disturbance rejection problem where frequency deviations from equilibrium must be removed by change in generator power. A schematic is represented in Fig. 1 and explained in the next subsections.

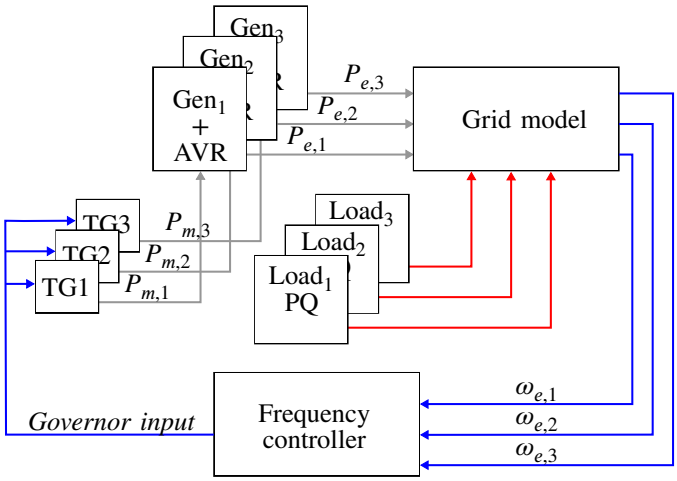

Fig. 1: Schematic for the grid frequency control scheme; where — , are controllable feedbacks and — , are uncontrollable disturbances

A. Power system model

The power system model can be obtained by linearizing a non-linear model around stable operating point, as follows,

$$\begin{aligned} \Delta\dot{x}(t) &= A\Delta x(t) + B\Delta u(t) + E\Delta d(t) \\ \Delta y(t) &= C\Delta x(t) + D\Delta u(t) \end{aligned} \tag{1}$$

In a grid with N generators, K states per generator unit, M loads whose active and reactive powers (P and Q) are considered inputs, (1) has $\Delta x(t) \in \mathbb{R}^{NK}$ as the states, $\Delta u(t) \in \mathbb{R}^{K}$ as the designated inputs, $\Delta d(t) \in \mathbb{R}^{2M}$ are disturbances and $\Delta y(t) \in \mathbb{R}^{K}$ are the outputs.

The states $\Delta x(t)$ involve generator states dependent on the order of synchronous machine being modelled, automatic voltage regulator (AVR) structure and the type of the turbine governor (TG) model. The controllable input, $\Delta u(t)$, is the common governor setpoint for the power system. This is generated from the frequency control block and is dependent on the choice of control algorithm and the participation factor of each generator in the grid. The disturbance, $\Delta d(t)$, is the ΔP, ΔQ load time series which shows deviation from nominal load. The output, $\Delta y(t)$, is a vector of the generator angular speeds which are related directly to the electrical frequency of the grid through participation factors of the generators or the Center of Inertia (COI) considerations. The presented grid model does not include a frequency control scheme which will be described in the next subsection.

B. Frequency control

In this paper we assume that frequency controller has a form of simple Proportional-Integral (PI) scheme in (2) to highlight the potential of reachability analysis. The method can be readily extended to other classical control strategies without any loss of generality.

$$\Delta u(t) = K_p\Big(e(t) + \frac{1}{T_i}\int e(t)dt\Big), \tag{2}$$

where, the error is defined as $e(t) = r(t) - \Delta y(t)$, $r(t)$ is the reference to be tracked, K_p is the proportional gain and T_i is the integral time constant. Since this is a linearized model, the parameters are actually perturbations around nominal value and the reference is therefore set to zero.

Rewriting the error dynamics by defining the integral of error $e(t)$ as the new error $e_{int}(t)$ we get,

$$\dot{e}_{int}(t) = \frac{1}{K_p}\Delta\dot{u}(t) - \frac{1}{T_i}e_{int}(t) \tag{3}$$

We define a new output matrix, $C_g = \begin{bmatrix} p_1 & p_2 & \dots & p_k \end{bmatrix} C$, where p_i is the participation factor of the generator angular speeds to grid frequency. The participating factor of the generators follows $\sum_{i=1}^{K} p_i = 1$. We can replace Δu in (1) with (2). By taking (3) as a second state space model, and adding these to the modified state space equations in (1), we get an extended closed loop state space with PI controller as,

$$\begin{aligned} \underbrace{\begin{bmatrix}\Delta\dot{x}(t)\\ \dot{e}_{int}(t)\end{bmatrix}}_{\dot{\widetilde{x}}(t)} &= \underbrace{\begin{bmatrix} A - BC_gK_p & B\frac{K_p}{T_i} \\ -C_g & 0 \end{bmatrix}}_{\widetilde{A}} \underbrace{\begin{bmatrix}\Delta x(t)\\ e_{int}(t)\end{bmatrix}}_{\widetilde{x}(t)} + \underbrace{\begin{bmatrix} E \\ O \end{bmatrix}}_{\widetilde{B}} \underbrace{\begin{bmatrix}\Delta d(t)\end{bmatrix}}_{\widetilde{u}(t)} \\ \widetilde{y}(t) &= \underbrace{[C_g \;\; 0]}_{\widetilde{C}}\widetilde{x}(t) \end{aligned} \tag{4}$$

where, $\widetilde{A}$ is the extended state matrix and $\widetilde{B}$ is the extended input matrix. This is a multiple input single output (MISO) scheme and the participating generators contribute to one controller output for all the turbine governors. The disturbances in (1) are treated as inputs $\widetilde{u}(t)$ in the extended state space system.

Other outputs such as bus voltage, bus injection current etc. can also be represented in the $\widetilde{C}$ matrix but will not take part in the controller feedback scheme. At this stage the extended state space model, the grid model along with the frequency controller, can be used as it is for the reachability analysis.

III. Continuous Reachability Analysis

Reachability analysis, in context of this paper, is termed as the process of calculating the set of all possible states a system can reach from an initial set of states, when acted upon by a time varying input with bounded uncertainties. The analysis is similar to numerical integration, with that difference that the variables are described by sets instead of scalars. This result of reachability analysis, describes how the uncertain initial state space evolves for the time span under consideration. For a power system model derived in (4),

$$\dot{\widetilde{x}}(t) = \widetilde{A}\,\widetilde{x}(t) + \widetilde{B}\,\widetilde{u}(t), \quad \widetilde{x}(t) \in \mathbb{R}^{NK+1}, \quad \widetilde{u}(t) \in \mathbb{R}^{2M}, \tag{5}$$

the solution space can be divided into two components - a homogeneous system solution, which is the system response without any external input and another, particular solution, which takes the influence of the input state on the system when initial states are all zero [9]. The final reachable set is obtained by union of these two components (homogeneous and particular solutions).

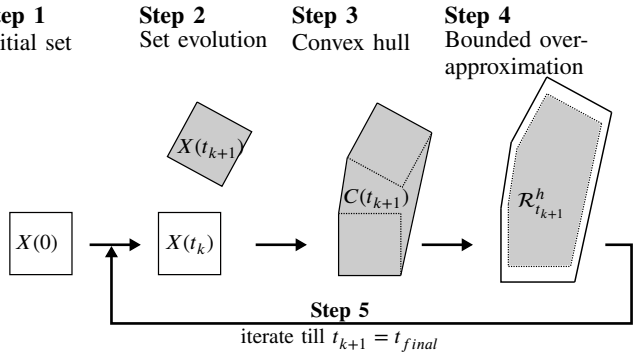

Fig. 2: Steps for reachable set calculation for a linear system without input for a single time step

A. Reachable set for system without input

The steps for reachable set calculation without input are described below and visualized in Fig. 2.

1) Start with a set of initial states at time $t_k = 0$. The initial set, $X(t_k) = X(0)$, is centered at $x(0)$ and bounded by an uncertainty interval.
2) The state solution at a point of time $t_{k+1} = t_k + \tau$ is calculated using the general solution of $X(t_{k+1}) = e^{A\tau} X(t_k)$.
3) A convex hull is created between the initial set of states and set obtained in Step 2.
4) This hull must be enlarged to accommodate all trajectories of the states in the interval $t \in [t_k, t_{k+1}]$. Curvature of the state evolution from $X(t_k)$ to $X(t_{k+1})$ is accounted for by this enlargement. This is done with the smallest enlargement that satisfies the over-approximation criteria [9]. The resulting set, $\mathcal{R}^h_{t_{k+1}}$, is the homogeneous part of the reachable set at t_{k+1}.
5) If $t_{k+1} < t_{final}$, update $X(t_k) = X(t_{k+1})$, $t_k = t_{k+1}$ and go to Step 2.

The final reachable space for all trajectories in the interval $t \in [0, t_{final}]$ is the union of all individual reachable sets, $\mathcal{R}^h_{t_k}$, calculated in Steps 1 to 5.

B. Reachable set of a particular solution

For the particular part of the reachable set $\mathcal{R}^p_{t_k}$ with uncertain inputs $u(t)$, the initial states are taken as $X(t_k) = 0$. The procedure follows the algorithm in the previous subsection, where the general solution in Step 2 is replaced by $X(t_{k+1}) = \int_0^\tau e^{A(\tau - t)} u(t) dt$. On top of the over-approximation in Step 4, an additional correction is applied to cover all possible state trajectories under uncertain input [9]. This is included as Step 6 within the iteration algorithm in the previous subsection.

C. Implementing continuous reachability analysis

Finally, the complete reachable set of the defined power system model is,

$$\mathcal{R}(t_k) = \mathcal{R}^h(t_k) \oplus \mathcal{R}^p(t_k), \tag{6}$$

where, the operator $\oplus$ signifies the Minkowski addition of the sets in accordance with superposition principles.

Few important distinctions have to be made here regarding the particulars of reachability analysis used in this paper -

- The economy in representation of the initial and reachable sets are important towards computational complexity of a reachability analysis. In [10], a zonotope based representation is deemed superior to other set representation forms for linear systems with uncertain inputs. Further description of zonotope generation is shown in [10].
- A wrapping-free algorithm for reachable set calculation is used as demonstrated in [11]. This keeps the over-approximation tight over long horizons and prevents its inflation over time towards a more conservative reachable set.
- Since zonotopes are closed over linear transformation, the reachable set trajectory can be used to calculate reachable sets for any outputs defined as $y = Cx + Du$. In the present work, this property is useful in calculating bus voltage profiles as reachable sets.

IV. Results & Discussion

The standardized IEEE 9 bus model [12] is used to test and validate the methodology described in the previous sections. We use the OpenIPSL [13] toolbox in Dymola, which is a Modelica simulation environment, to create our linearized grid model. The reachability analysis is implemented in the Continous Reachability Analyzer (CORA) MATLAB toolbox [14]. A snapshot of the Dymola model is provided in Fig. 3.

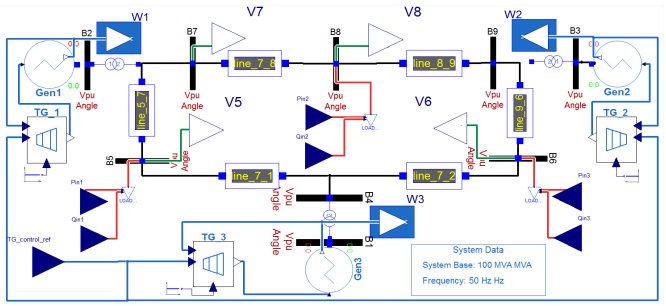

Fig. 3: Modified IEEE 9-Bus OpenIPSL model in Dymola. The ⎯ lines are controllable inputs; ⎯ lines are uncontrollable disturbances; the white icons in shaded ▬ are the generator angular speeds.

Certain updates are made, to the standarized IEEE 9-Bus example provided in OpenIPSL and the settings in CORA, to fit our methodology and are mentioned as follows,

- The electrical machine model of an Order-4 synchronous generator with Type-II AVR is updated to accept P_{mech} as an input parameter

- A Type-II Turbine Governor is added for each generator. A 15% reserve capacity is given on top of nominal governor power output and the block modified to take the ω_{ref} as an input from the frequency controller block.
- The voltage dependent loads are updated to take a time series of active and reactive power as input.
- The generator participation factor in calculating the system frequency is kept equal for all generators. It could also be adjusted based on generator moment of inertia.
- The time step is fixed at 0.001 s. This was initially tuned in Dymola to find the largest fixed time step for the solver while giving accurate results and was later checked with CORA. Smaller time steps, while slowing down the reachability analysis, do not significantly improve the accuracy. Larger time steps lead to instability issues.

The *linearize* function in Dymola is used to create the grid model without the frequency controller. The generator angular speeds are the output feedbacks for the PI frequency controller. Additional bus voltages are also denoted as outputs to observe their reachable sets under influence of the changing loads and the frequency controller. The final model parameters are listed in Table I.

TABLE I: IEEE 9-Bus linear model for reachability analysis

States, $\widetilde{x}$	$[\delta_i,\ \omega_i,\ E_{q_i},\ E_{d_i},\ \mathbf{x}^a_{AVR,i},\ x_{TG,i}]$ for all $i = 1$ to N, e_{int}
Inputs, $\widetilde{u}$	$[\mathrm{P}_i,\ \mathrm{Q}_i]$ for all $i = 1$ to M
Output, $\widetilde{y}$	ω_{grid}

[a]States from the AVR model.

The simulation window is 20 s. The load is varied from the nominal benchmark values with steps at $t = 2$ s, 5 s and 10 s as shown in Fig. 4. The analysis can also include uncertain renewable generation using a similar forecast time series for active and reactive power injection with bounded uncertainties. For brevity reasons, we consider only load perturbation that represents an aggregated load and uncertain renewable generation.

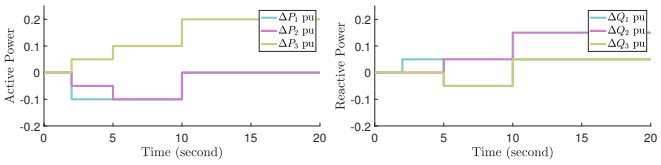

(a) Step changes in active power load. (b) Step changes in reactive power load.

Fig. 4: Load perturbation around nominal value.

All computations were performed on an Intel Xeon E3-1275 processor with 3.6 GHz and 32 GB RAM. The linear reachability algorithm took around 10 s to solve on average for a 28 states and 20,000 step solution, which represents a 20 s simulation. Further ideas on tractability of linear reachability computations can be found in [10] and [15].

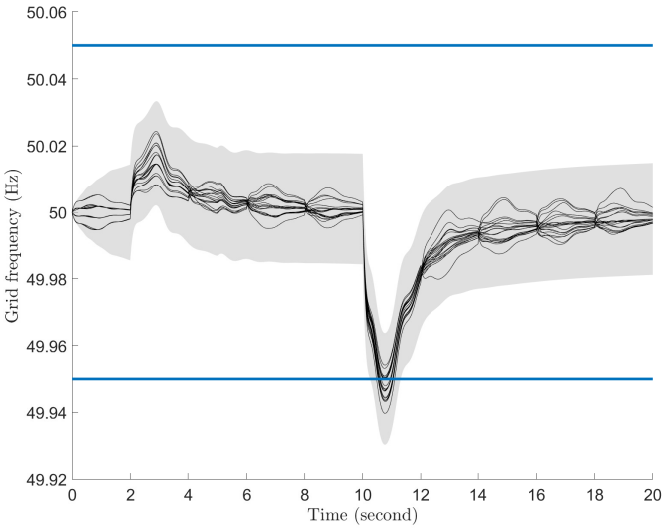

Fig. 5: Reachable sets for grid frequency with randomised simulations

A. LFC verification via Reachable sets

The controller gains, as defined in (2), are set at $K_p = 10$ and $T_i = 5$ s. A $\pm$ 1% load uncertainty exists on top of the pre-forecasted step changes as seen in Fig. 4. The grey envelope in Fig 5 shows the evolution of the reachable set of the grid frequency over 20 s, starting from a balanced condition. The trajectories in black are twenty simulations with randomized input changes sampled within the uncertainty bounds of the reachability problem. It is observed that all the simulation trajectories are all placed within the reachable envelope generated by CORA. This is in line with expectations as the reachable set includes every possible state trajectory.

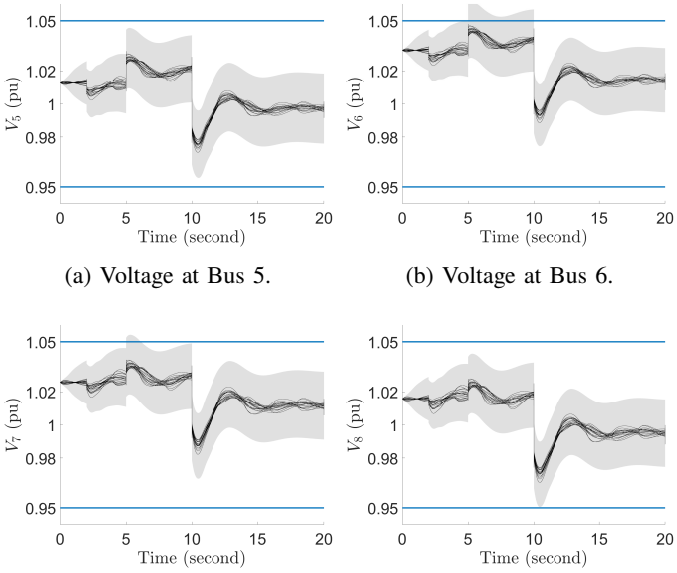

(a) Voltage at Bus 5. (b) Voltage at Bus 6.

(c) Voltage at Bus 7. (d) Voltage at Bus 8.

Fig. 6: Reachable sets for different bus voltages along with random simulations

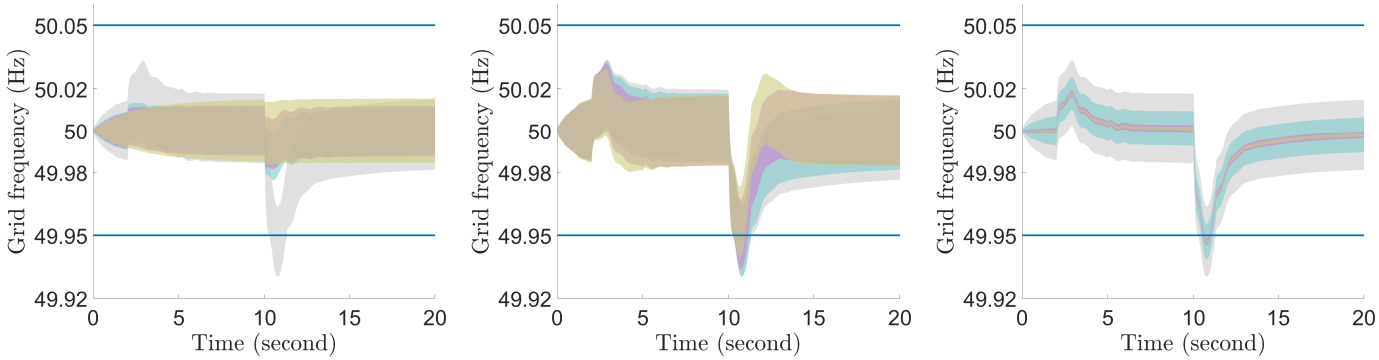

(a) Reachable sets of grid frequency with constant $T_i = 5$ and - $K_p = 10$; $K_p = 50$; $K_p = 100$; $K_p = 500$

(b) Reachable sets of grid frequency with constant $K_p = 10$ and - $T_i = 10$; $T_i = 5$; $T_i = 2$; $T_i = 1$

(c) Reachable sets of grid frequency with different load uncertainties - ±1% p.u.; ±0.5% p.u.; ±0.1% p.u.; ±0.05% p.u.

Fig. 7: Reachable sets of grid frequency under a variety of PI gains and load uncertainties.

An assumption is made that the grid operator wants to regulate against deviations beyond ±50 mHz. This is marked in Fig. 5 with the two blue lines. Therefore, the analysis must reveal if there is a risk of these limits being infringed under the current grid conditions in the next 20 s window. As seen in Fig. 5, while some simulations show that the frequency might dip below 49.95 Hz, some of them do not. Therefore, if the grid operator used only the simulations to plan against the risk of a frequency dip, it is possible that none of the simulations reveal the risk to be so. On the contrary, when observing the reachable set which corresponds to the every possibility of the frequency in a given interval, it is seen that the frequency can go below 49.95 Hz after the second load step change.

The frequency envelope remains in a band around the nominal 50 Hz value after stabilizing against the load step changes. This is a result of the uncertainty in the load. If there were no step changes in the load, the reachable set of the frequency would evolve with the constant width of this band.

The voltages of buses 5 till 8 are shown in Fig 6.The reachable sets of voltage outputs defined by, $y = Cx + Du$, are calculated by projecting from the state reachable sets. Here an assumption is made that the grid operator wants to regulate the bus voltage within a ±10% p.u. range. It is seen that Bus 6 and 7 have a risk of going beyond the maximum allowed voltage. However, a formal guarantee exists for bus 5 and 8, that the voltage will stay within allowable limits for the window under observation. It is worth noting that, as explained in III-C, such treatment can be easily extended to other grid variables due to the linear transformation of reachable sets based on zonotopes.

B. Reachable sets for LFC under different tuning gains and load uncertainties

We validated reachable set calculation algorithm in the previous section. Now we analyse the effect of control parameters on the state reachable sets. Fig. 7a and 7b show the reachable sets for grid frequency under different controller gains with load uncertainty being constant at ±1%. In Fig. 7a, the results of reachability analysis with the proportional gain set to $K_p =$ [10, 50, 100, 500] with the integral time constant fixed at $T_i = 5$ s is shown. Fig 7b, shows the grid frequency with $K_p = 10$ and the integral time constant set to $T_i = [1, 2, 5, 10]$ s. Based on these results, the grid operator can thus have an insight on which controller gains are most suited to avoid unsafe limits. For example, from the results in Fig. 7a, in a gain scheduling regime, the operator could switch the K_p to 50 after realising that $K_p = 10$ could cause a frequency dip into unsafe limits. Similarly, from the results in fig. 7b, the operator could modulate the T_i to minimise the overshoot. In other words, reachability analysis also provides a new approach to tune the gains for frequency controllers without having to run an exponential number of random simulations which are both time consuming and cannot give a formal safety certificate on the performance of the controller.

In Fig. 7c, the reachable sets with load uncertainty per time step, varying in [±1%, ±0.5%, ±0.1%, ±0.05%] is shown with $K_p = 10$ and $T_i = 5$ s. It can be seen that with reduced load uncertainty, the reachable set envelope gets thinner and tends towards a single simulation trajectory. This is expected, as without any input uncertainty the reachable sets do not deviate from a simulation result with fixed initial state.

V. Conclusion

Reachable set computation has recently emerged as a new strategy for studying system dynamics and this paper presents a new application of this method on a conventional power system frequency control problem. Using a standardised test case, it was shown that reachable sets can provably predict frequency safety limits being breached under a specific load time-series with bounded uncertainties, while conventional simulations, representing one out of infinitely many trajectories, may fail to detect these events. The bus voltages were also presented as reachable sets by using linear transformations. The flexibility of the method encourages the use of reachability analysis for other power system control problems as well. In future works, we aim to extend the same approach to a nonlinear grid model, multi-area power systems, and a continuously updating, real-time formal verification strategy for generators.

These approaches can be verified on controllable grid hardware at the Center for Combined Smart Energy Systems (CoSES) [16] at TU Munich.

REFERENCES

[1] R. Shankar, S. R. Pradhan, K. Chatterjee, and R. Mandal, "A comprehensive state of the art literature survey on LFC mechanism for power system," *Renewable and Sustainable Energy Reviews*, vol. 76, pp. 1185–1207, 2017.

[2] E. J. Thalassinakis and E. N. Dialynas, "A Monte-Carlo simulation method for setting the underfrequency load shedding relays and selecting the spinning reserve policy in autonomous power systems," *IEEE Transactions on Power Systems*, vol. 19, pp. 2044–2052, 2004.

[3] M. Althoff, M. Cvetkovic, and M. Ilic, "Transient stability analysis by reachable set computation," in *IEEE PES Innovative Smart Grid Technologies Conference Europe*, 2012.

[4] M. Althoff, "Formal and compositional analysis of power systems using reachable sets," *IEEE Transactions on Power Systems*, vol. 29, no. 5, pp. 2270–2280, 2014.

[5] A. El-Guindy, D. Han, and M. Althoff, "Formal Analysis of Drum-Boiler Units to Maximize the Load-Following Capabilities of Power Plants," *IEEE Transactions on Power Systems*, vol. 31, no. 6, pp. 4691–4702, 2016.

[6] Y. Li, P. Zhang, M. Althoff, and M. Yue, "Distributed Formal Analysis for Power Networks with Deep Integration of Distributed Energy Resources," *IEEE Transactions on Power Systems*, vol. 34, no. 6, pp. 5147–5156, 2019.

[7] N. Chuang, "Robust H-∞ load frequency control in interconnected power systems," *Australasian Universities Power Engineering Conference (AUPEC)*, pp. 1–6, Sep. 2013.

[8] P. Kundur, *Power System Stability and Control*. McGraw-Hill, Inc., 1994.

[9] M. Althoff, O. Stursberg, and M. Buss, "Reachability analysis of linear systems with uncertain parameters and inputs," *Proceedings of the IEEE Conference on Decision and Control*, no. 1, pp. 726–732, 2007.

[10] M. Althoff, *Reachability Analysis and its Application to the Safety Assessment of Autonomous Cars*. PhD thesis, Department of Electrical and Computer Engineering, Technical University of Munich, 2010.

[11] A. Girard, C. Le Guernic, and O. Maler, "Efficient computation of reachable sets of linear time-invariant systems with inputs," *Lecture Notes in Computer Science*, vol. 3927 LNCS, pp. 257–271, 2006.

[12] P. M. Anderson and A. A. Fouad, *Power System Control and Stability*, pp. 37–39. 2003.

[13] M. Baudette, M. Castro, T. Rabuzin, J. Lavenius, T. Bogodorova, and L. Vanfretti, "OpenIPSL: Open-Instance Power System Library âĂŤ Update 1.5 to âĂIJiTesla Power Systems Library (iPSL): A Modelica library for phasor time-domain simulationsâĂİ," *SoftwareX*, vol. 7, pp. 34–36, 2018.

[14] M. Althoff, "An Introduction to CORA 2015 (Tool Presentation)," *Proc. of the Workshop on Applied Verification for Continuous and Hybrid Systems*, vol. 2015, pp. 120–151, 2015.

[15] M. Althoff and B. H. Krogh, "Zonotope bundles for the efficient computation of reachable sets," *50th IEEE Conference on Decision and Control and European Control Conference*, pp. 6814–6821, 2011.

[16] V. S. Perić, T. Hamacher, A. Mohapatra, F. Christiange, D. Zinsmeister, P. Tzscheutschler, and C. Aigner, "CoSES Laboratory for Combined Energy Systems At TU Munich," *IEEE Power and Energy Society General Meeting*, 2020.

Concluding remarks on the publication

The preceding publication takes the reachable set applications in power systems further, applying it to a basic grid frequency control challenge. Using a standard test case, it was shown that reachable sets can predict when frequency safety limits might be exceeded due to specific load scenarios with bounded uncertainties. This is a contrast to typical simulations, which represent just one path among countless possibilities and might miss some or all combinations of inputs and states which would violate a grid operation constraint.

An additional promising aspect of reachable sets is that zonotope representation is closed over linear transformations. This feature allowed us to calculate reachable sets for various outputs, including bus voltages, by operating upon the reachable sets of all the states. We also looked at grid frequency reachable sets under different gains for the PI controller and various load uncertainty ranges. The method's flexibility suggests its potential for tackling other power system control issues too.

3.3.3 Extensions to the work

While the publication [89] shows a promising result, reachability analysis in the form presented in the paper is not fit for online verification of a power system. The observation window of the reachability problem was only 20 s. Using a 32GB RAM, Intel Xeon E3-1275 processor computer, the reachability analysis for 28 states, in the resolution of 1 ms, was solved on average in 10 s using the CORA 2018 version. This means, if used for online verification, the current setup would actually take half of the period of interest to compute the reachable sets itself. Also, the test case used in the publication was only a 9-bus example. The analysis requires to be repeated for larger state spaces to ensure tractability.

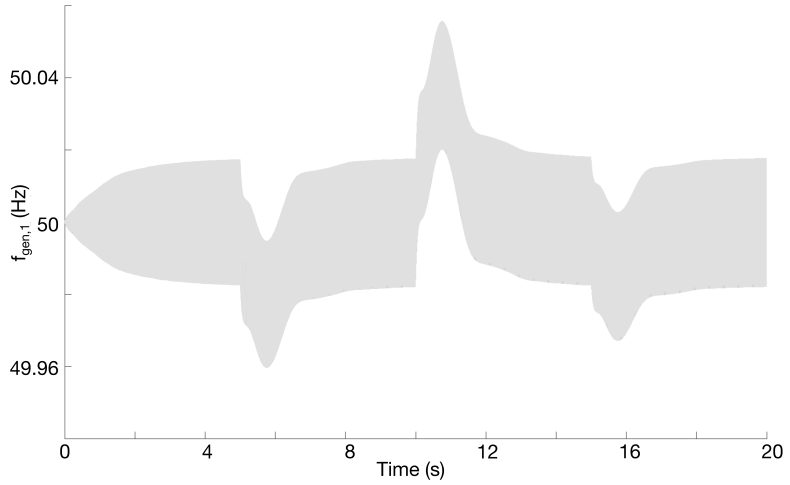

Figure 3.4: Reachability analysis for frequency controller in IEEE 14-bus system.

In the subsequent work, the reachability analysis for grid frequency controller is done for the IEEE 14-bus, shown in Fig. 3.4 and 33-bus cases, shown in 3.5, available in the openIPSL Dymola toolbox [117]. While using a newer version of the toolbox, CORA 2021,

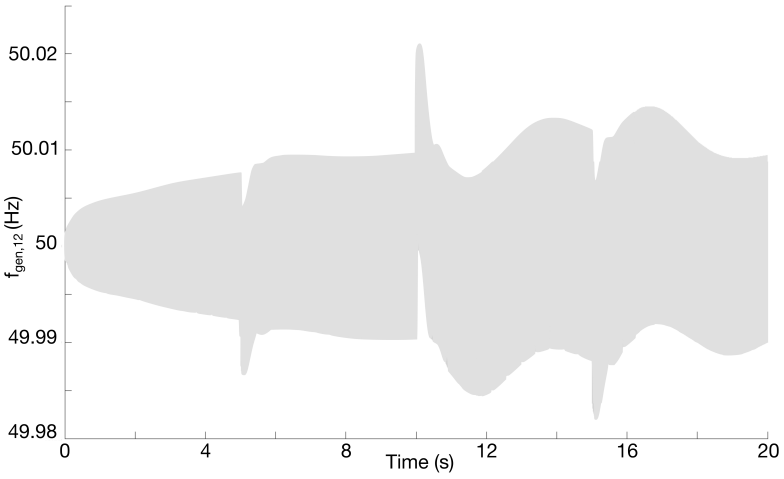

Figure 3.5: Reachability analysis for frequency controller in IEEE 33-bus system.

and worse specifications on the computer with Intel Xeon E-2144G with 16GB RAM, the IEEE 14-bus model with 46 states and 20,000 steps (20 s observation window in 1 ms time-steps) is solved on average in 15 s. The IEEE 33-bus model with 133 states and 20,000 steps is solved in 33 s. The prior IEEE 9-bus model used in the publication still averaged 10 s on the new hardware and software settings. While larger power system state spaces can be accommodated within the CORA reachability framework, the execution time is dependent on the internal overheads of the CORA toolbox and also infeasible for an online application. Similar to the ADMM setpoints in [88], the expectations from an online reachability tool should be to inspect a time horizon in a fraction of that time.

A recent work in the reachability analysis of linear systems through *support functions* and its implementation through CORA has shown an unprecedented potential for using reachability analysis in power system for RT applications [118]. Using the same models as shown in the previous figures and the publication, the authors were able to accelerate the reachability analysis of IEEE 9-bus, 14-bus and 33-bus models to 0.49 s, 0.14 s and 1.3 s respectively. This development completely changes the scope of online verification of linearized power systems using reachability analysis. A PHIL experiment structure for formal verification of grid frequency controllers in CoSES laboratory is provided in the next subsection.

3.3.4 PHIL continuous reachability concept with emulated machines

Before we can describe the PHIL reachability structure, we have to take a short detour on emulation using inverters in ADG laboratories. The prosumer emulators in CoSES laboratory can be programmed to emulate dynamics of different generators and loads. This is a powerful tool at the disposal of the researcher since any equipment can be virtually recreated with precise dynamics due to the high bandwidth control of the emulation inverters. However, there are a few major challenges in such an exercise and it will be illustrated here with the example of a synchronous generator.

Modelling paradigms for dynamical systems

Modelling approaches for dynamical systems can be broadly categorized into two families [119]:

- **Causal modelling** - A Causal model is based on an input-output relationship where the signal flow from input towards the output predicates the execution order of the modelled functions. MATLAB/Simulink and LabVIEW are some commonly known causal modelling tools.
- **Acausal modelling** - Acausal modelling describes the modelled system by implicit differential algebraic equations (DAE), which are solved to describe the state evolution of the dynamic system over time. Modelica language and Modelica based graphical modelling tools such as Dymola are common examples for acausal modelling tools [120].

Generally speaking, physics based modelling is considered to be acausal as it is difficult to separate the cause from the effect in physical systems [121]. Some examples of commonly used physical modelling libraries are mechanical elements, electrical elements, hydraulic elements, thermal models, multi-phase fluid models and gas models. These libraries use physical laws, such as conservation of mass, momentum and energy, to simulate the models rather than signal flow and purely mathematical operators used in causal executions.

Modelling of synchronous generator for emulation

Synchronous generators in the grid, react to the electrical behaviour of the grid and the mechanical behaviour of the shaft. Mathematical modelling of a synchronous generator will contain set of equations concerning the electrical behaviour and another set of equations for the mechanical behaviour. A few equations from either set would carry a coupling element, depending upon the complexity of modelling. In its simplest form, the well known swing equation, is the coupling term in the second order synchronous generator model.

However, there is no strict causality to these two sets of equations, or in other words, the electrical equations do not necessarily follow the execution of the mechanical equations or vice-versa. This is a typical behaviour of a physical system and many simulation tools provide physical modelling interfaces which allow acausal solutions. Emulation models, on the contrary, must follow a causal loop of setpoints leading to measurement feedback.

In the absence of the real equipment, emulation is used to capture the essential characteristics and dynamics of a physical system, allowing the analysis, prediction, and understanding of how the system behaves under different conditions. Therefore, the emulation models recreate the physics of a real device through an equivalent mathematical equation set with defined input and output interfaces. The Fig. 3.6 shows a possible control schematic for emulating, a synchronous generator with its usual control elements, on a grid following inverter. The synchronous generator model in Fig. 3.6 is comprised of a synchronous machine model, controlled through a turbine governor (TG) and an automatic voltage regulator (AVR) block. The control references for the TG and AVR blocks are provided by frequency and voltage control blocks, which could be simple PI controller at this stage.

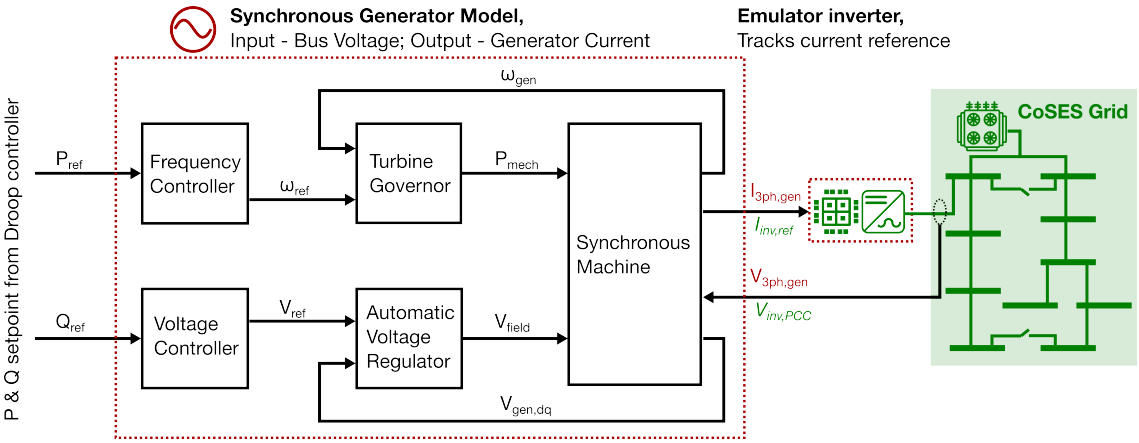

Figure 3.6: Schematic control diagram of emulating a synchronous generator through an inverter emulator connected to a real distribution grid.

Table 3.2: Modelled components for the emulated synchronous generator

Synchronous machine	5th order model, salient pole machine, parameters taken for 50Hz 400V 16KVA 1500RPM machine from [122]
Turbine governor	TG Type II, as mentioned in [117]
Automatic voltage regulator	AVR Type II as mentioned in [117]
Frequency controller	PI controller
Voltage controller	None. The AVR block is provided with a fixed voltage reference.
Modelling environment	Simulink and NI VeriStand RT control environment (compiled models as .dll or .fmu).

Here the synchronous machine block is modelled as a causal block which takes mechanical power and field voltage as an *input* and provides a generator current as an *output*. This *output* current is then fed as the *input* current reference for the grid following inverter. Assuming an idealised, unity gain and infinite bandwidth, inverter control loop, the inverter *output* current is now a proxy for the generator current and should reflect the dynamic properties of the modelled synchronous generator. However, the real PHIL interface has attenuation loss and a finite bandwidth leading to some inaccuracies as seen in the subsequent paragraphs.

Emulated synchronous machines on PHIL

An emulated synchronous generator model, as per the schematic shown in Fig. 3.6 was performed in CoSES using the Egston Compiso PHIL emulators. The modelled components for the experiment as shown in Tab. 3.2.

The model was built in MATLAB/Simulink 2016a and compiled as a .dll for NI VeriStand to be deployed on the PXIe embedded controllers in CoSES. The Egston Compiso unit in the grid following mode is taken as the emulator inverter from Fig. 3.6. The bus voltage measurement at the inverter PCC is fed back into the synchronous

generator model, along with the calculated active power injection. In Fig. 3.7, we see the slew rate of transient step response for the emulated generator over inverter setup. The active power reference to the frequency controller block in Fig. 3.6 is stepped up, leading to a change in the P_{ref} as seen by the synchronous machine block. The electrical power output from the synchronous machine, P_{gen} responds accordingly. The electrical power is defined by,

$$P_{gen} = \frac{3}{2}\omega(\lambda_d i_q - \lambda_q i_d), \tag{3.11}$$

where, ω is the rotor angular speed, $\lambda_{d,q}$ are the direct and quadrature axis stator flux linkages and $i_{d,q}$ are the direct and quadrature axis generator output (stator) current.

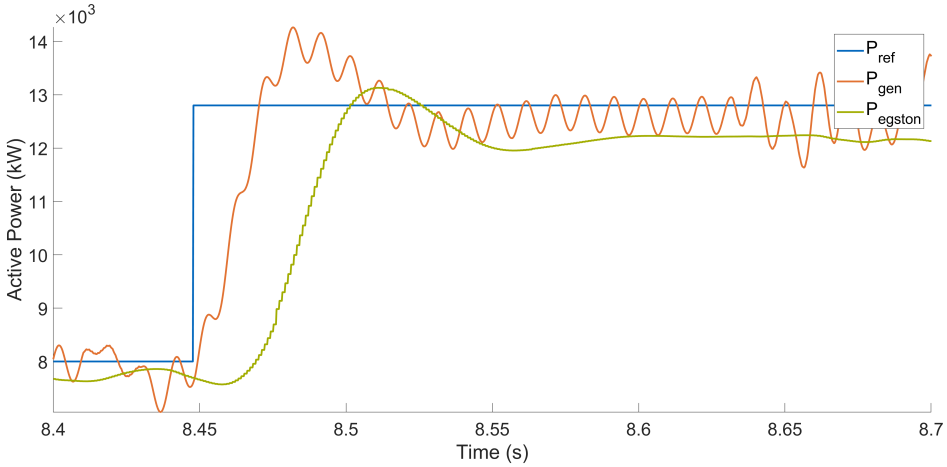

Figure 3.7: Step change in power reference, P_{ref} for the synchronous generator model along with the electrical power output from the synchronous machine block, P_{gen} and the emulated electrical power response as measured from the Egston inverter terminals, P_{egston}. In an ideal emulation, the P_{gen} and P_{egston} graphs would be identical.

The P_{egston} in Fig. 3.7 has a phase delay and an amplitude reduction as compared to the P_{gen} curve, but the overall shape is closely related. The phase delay can be explained by the causal relationship between the generator and the inverter models, where the subsequent model is always reacting to past measurements. This could be mitigated by a fixed phase compensation in the inverter current model with an estimated execution time of the generator model, similar to a feed-forward correction. The amplitude attenuation can also be similarly adjusted by a magnitude gain compensation. However, these are experiment specific adjustments which must be re-tuned in every new setup for best results.

In Fig. 3.8, we see a 20 s window of four step changes on the active power reference. While the P_{egston} and P_{gen} curves are tracking each other, there are intermittent jitters on the P_{gen} which effect P_{egston} as well. These abnormalities are brought by the real voltage measurement being linked to the simulation model as an input. The bus voltage is first analysed and reconciled into a voltage magnitude and phase term, to be shared among the different controllers [85]. The phase term is not constant and the jitters on the raw phase measurement affects the stability of the electrical power calculation from the synchronous machine model.

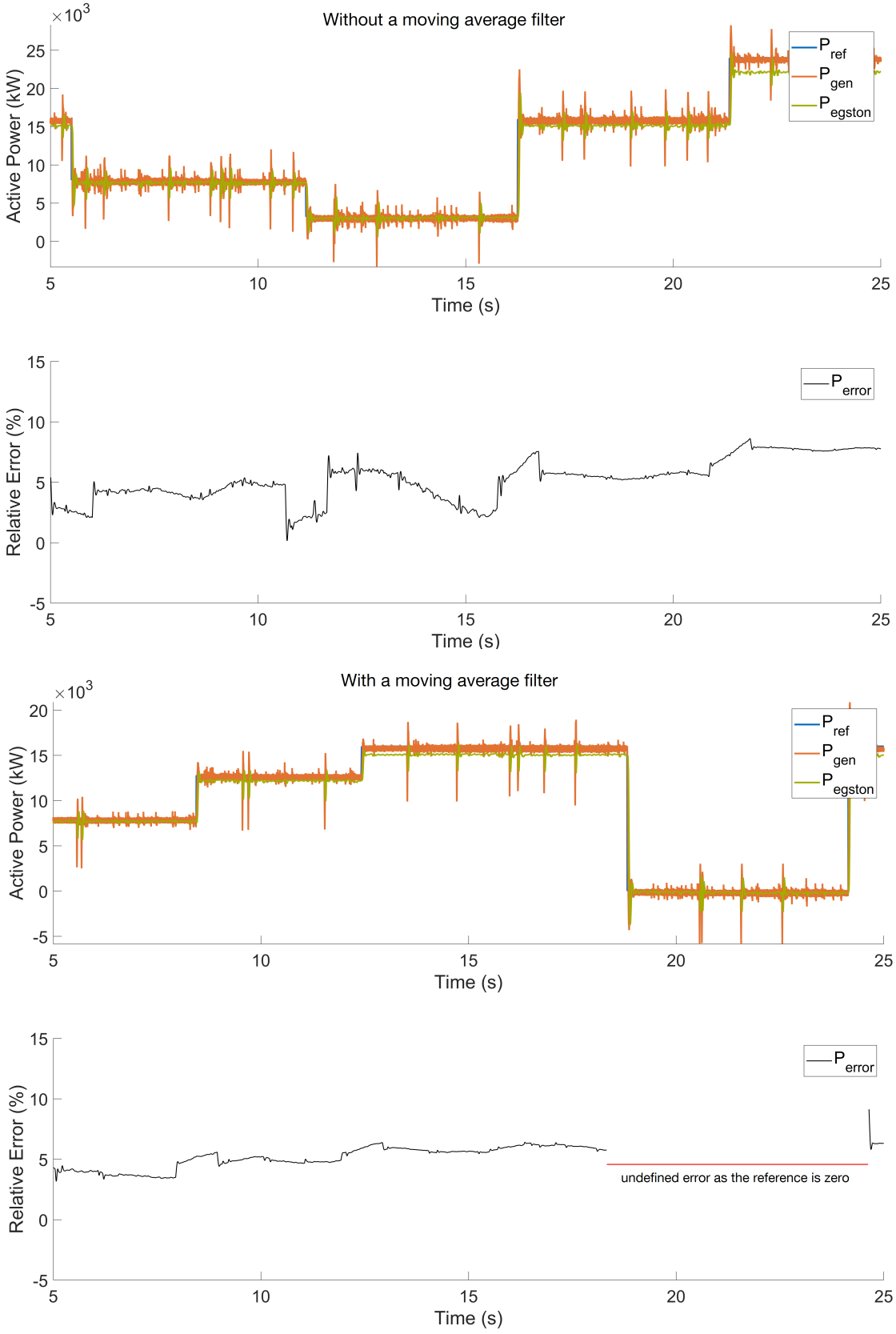

Figure 3.8: Schematic control diagram of emulating a synchronous generator through an inverter emulator connected to a real distribution grid.

Regardless of these phase jumps, the relative error of Egston output, P_{egston} to the reference power, P_{ref} remains under 5%, as long as the P_{ref} is within the rated power, 16 kW, of the emulated generator. After 20 s, in the Fig. 3.8, the reference goes above the rated capacity of the machine and this leads to greater error as the saturation properties were neglected in the machine modelling. In the bottom half of Fig. 3.8, a moving average filter was added to the voltage measurement. This reduces the phase step related errors and the relative error on is still around 5%. This level of error can be considered acceptable for emulation of large physical devices.

RT reachability analysis for emulated machines

The final step is a combination of the emulated synchronous machines on Egston inverters with the CoSES LV grid and the accelerated reachability analysis through support vectors in CORA [118]. A schematic of the experiment design, as a concept, is shown in Fig. 3.9 for a grid reliability tool for online formal verification of grid frequency controllers.

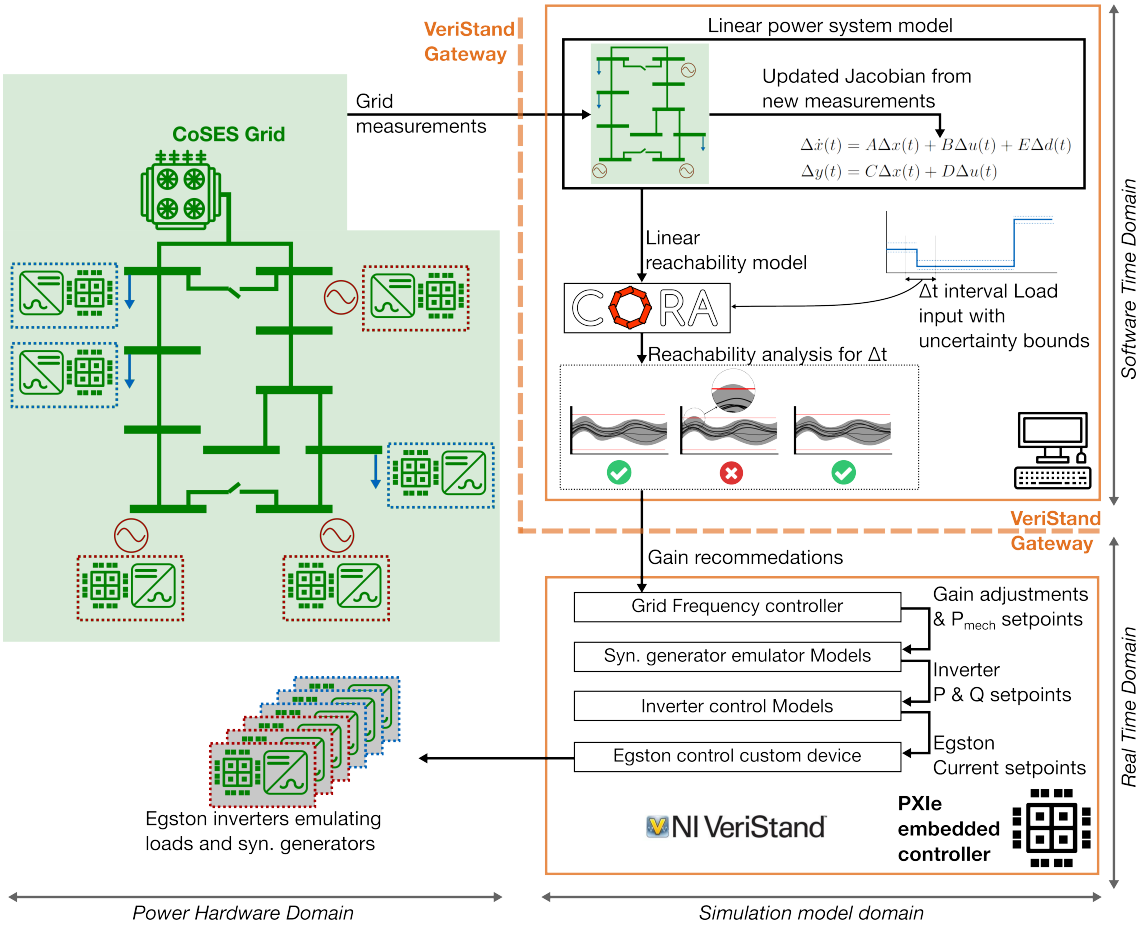

Figure 3.9: Schematic control diagram of emulating a synchronous generator through an inverter emulator connected to a real distribution grid.

We begin with a steady state initialised model of the CoSES LV grid with multiple synchronous generators imagined at specific bus bars and a time-series of three phase active

and reactive power spot loads with a given bounded uncertainty. This model is passed on to CORA for a linear reachability analysis for a given period, Δt. The reachability analysis would reveal if the current tuning of the grid controllers is adequate for the forecasted loads with their uncertainties in Δt. Due to the new accelerated reachability algorithm for linear systems, the problem is expected to be solved in a fraction of seconds, which enables a near-RT implementation.

Based on the reachability analysis pass, gain tuning recommendations are sent to the emulated synchronous generator model from Fig. 3.6. A sequence of interlinked models, deployed on the PXIe controller, transfers the gain tuning to the Egston inverter current reference. The separation of the models allows them to be executed at different rates to manage the RT computation load for the controller. Finally, a new set of grid measurements are passed to the linearized CoSES LV grid model, to update the Jacobian around a new steady state. This experiment design splits the execution of the code between the software and RT timing levels and over simulation, emulation and real LV grid passive components.

The motivation behind such an experiment can be traced back to Fig. 1.1 in the introduction chapter of this thesis, where the drop in the UK grid inertia due to increasing DER generation is shown. Online reliability tools to monitor grid safety and protect against possible grid code violations will carry an important role in future grid research. Following the experiment structure of Fig. 3.9, a system level validation and verification of formally verified frequency controllers can be performed at the CoSES laboratory. The experiment can be readily extended to include DER inverters as well by removing the top two layers within the NI VeriStand domain, which represent the emulated synchronous machine. A new formulation of the reachability problem, with inverter states from an average model, will also be required. However once established, the same experiment design setup of Fig. 3.9, can be re-used for many versions of online reachability analysis in an ADG with minor changes.

In summary, this chapter reveals the various practical application of the ADG laboratory at CoSES. The **first two publications** demonstrate the bridging of the gap between simulation and reality in ADG research through shared embedded resources within the ADG and using PHIL to validate theoretical concepts. The **last publication** explores a theoretical concept of reachability analysis for grid frequency controllers. A true PHIL implementation of reachability analysis in a RT sense is beyond the scope of the current thesis and will be tackled in subsequent research projects at CoSES. However, a way forward with an accelerated linear reachability algorithm and an experiment design concept through PHIL emulated synchronous generators was presented.

Chapter 4

Conclusion

The truth is the whole

G.W.F. Hegel

Power grids are undergoing a necessary evolution to accommodate the fossil fuel free future, hypothesised by the various climate action plans world-wide. Distribution grids will bear the burden of bringing in a vast proportion of the new DER. These ADG represent a new paradigm where, instead of the traditional - upstream generation feeding passive loads, active prosumers will proliferate the distribution grids. These ADGs would not only represent the erstwhile electrical power grid, but also the electrified heating and mobility sectors.

These transitions bring many operational hurdles but at the same time, provide opportunities for optimised operation through sector-coupled flexibilities. A deep integration of ICT and intelligent operations becomes a necessity to mitigate the intermittency and distributed nature of renewable generation resources. Among the various research directions stemming from these requirements, PHIL validation of ADG operation and control concepts represents an important family of investigations. PHIL analyses bring a concept one step closer in the systems engineering process to market readiness by testing it against near real-world conditions in RT.

Power system laboratories with PHIL testbed have been a standard laboratory setup at most grid research institutes worldwide. This thesis was focused on three research questions pertaining to establishing and operating PHIL laboratories for ADG research. The CoSES laboratory at TU Munich, which was commissioned during the doctoral research conducted for this thesis, served as the rubric for a typical ADG research facility. The following paragraphs provide short summaries of the answers provided for these central research questions.

Q1: How should a PHIL laboratory for ADG research be established, with real prosumers, distributed control scheme, limited set of measurements, - Chapter 2 dealt with the commissioning challenges at CoSES laboratory in general to make it a near-realistic representation of an ADG. One of the early challenges was establishing time synchronisation and maintaining the distributed controller structure representative of ADGs without sacrificing measurement fidelity for prosumer emulators in CoSES.

A split measurement concept was introduced which could resolve a continuous power calculation and harmonic analysis in RT, with current and voltages being recorded over separate embedded controllers, connected through an asynchronous link with variable delay. A further challenge was integrating the different measurement points on a graphical representation using open-source monitoring and observability platforms. The lab was therefore extended as an IoT network and connected through to a Grafana dashboard. Finally a PHIL control framework was developed to encompass the best practices to maintain the realistic ADG characteristics, with an option to connect the RT emulators and power hardware of the laboratory to external supervisory agents such as optimisation agents, market frameworks, demand side management signals and weather forecasts.

Various publications in this thesis dealt with experiments which utilised the real prosumers, distributed controllers and limited measurements available on-site for a real ADG, as represented in CoSES. While all the publications in Chapter 2 maintained this focus from a lab establishment perspective, in Chapter 3 two ADG applications were experimentally verified without sacrificing these realistic assumptions. These applications serve as evidence of the potential to design further ADG experiments while preserving real-world characteristics within a laboratory setting.

Q2: to validate concepts on, as realistic as possible, test beds, - As motivated in the introduction to this thesis, the ultimate aim for PHIL based research is to bring concepts closer to fruition to their application cases. To this end, in Chapter 3, multiple ADG research topics were presented with their PHIL implementation evidences to show the possibility in re-imagining simulated results as RT experiments. A purely software M-Class PMU was presented as an addendum to the normally available control infrastructure for an ADG. This work backs the theoretical claim of potentially sharing the computation resources available in ADGs instead of installing specialised devices for different grid control and monitoring activities. Another such theoretical result, the online D-OPF as a secondary control strategy for inverter based resources, has been a popular subject of research in ADG optimisation communities. This concept was implemented over the PHIL hardware in CoSES, with clustered grid groups, privacy preserving information exchange, RT measurement feedback into the optimisation problems, and Egston emulators used as both generation and loads. Translating this problem into a PHIL experiment, required enacting a local group droop controller and showed a sub-optimal operation period when the load setpoints changed, as in reality, while the optimised generation setpoints were awaited. This result showed that the quantum of benefit claimed by such theoretical results might be substantially diminished during a real-world operation and thus requires further investigation. A further publication highlighted the transference of an erstwhile less explored concept of reachability analysis as an investigation tool in power system. The subsequent sections showed a way forward for implementing the formal verification of frequency controllers under uncertain renewable energy generation as a PHIL experiment within CoSES through emulated synchronous generators. Experimental verification results were provided for synchronous generators with common mechanical power and field voltage controllers, emulated over the Egston inverters. Due to complexity of the full RT PHIL implementation of formally verified frequency controllers, a separate research project will be conceptualised for these experiments.

Q3: while promoting efficient experiment design and reduced collaboration pains. - The concept of collaboration friendly laboratory design was highlighted as an important marker for sector coupled ADG research. As an multi-disciplinary field, the ADG control and operation problems must be abstracted to different levels with the perspective of the electrical grid, power electronics, heating grid, control systems, signal processing and energy system optimisation fields. Also it is desirable for the research infrastructure to be conducive to simultaneous experiments, sharing computation and hardware resources without interfering the results and a certain flexibility in using a modelling tool of choice. Through the PHIL framework, the IoT observation platform, and shared computation resources between the software PMU and a grid controller in CoSES, it was shown that the various researchers can interface at different levels of this ADG laboratory. Parallel experiments, abstracted monitoring dashboards, and freedom of modelling tools are enforced through the VeriStand RT environment and its gateway API.

Outlook

The current document is a comprehensive introduction to an extremely powerful laboratory for ADG research, that brings concepts next door to a field test or market readiness.

The CoSES laboratory was borne out of a need to have realistic research installation for low voltage sector-coupled distribution grids. However, in the process of establishing this facility, we uncovered many application cases without a commonly accepted solution, technical gaps which do not allow realistic assumptions within a lab and a general discomfort among the community to work with realistic hardware and commercial devices.

In the opinion of this author, such trepidation remains a hurdle to overcome. We must be willing to take the risks of working with the constraints of reality and not hide behind convenient assumptions to preserve elegance of our theories. It is my hope that the work behind this thesis and future research from CoSES laboratory will contribute in fostering this change in mindset.

Appendix A

Abbreviations

PV	Photovoltaic
DER	Distributed energy resources
ADG	Active distribution grids
ICT	Information and communication technologies
PCC	Point of common coupling
RT	Real-time
RTDS	Real-time digital simulator
DSP	Digital signal processing
EMT	Electromagnetic transient
IO	Input-output
FPGA	Field-programmable gate array
OS	Operating system
DAE	Differential algebraic equations
HIL	Hardware in the loop
CHIL	Controller hardware in the loop
PHIL	Power hardware in the loop
HUT	Hardware under test
IA	Interface algorithm
AGC	Automatic generator control
IEEE	Institute for Electrical and Electronic Engineers
SCADA	Supervisory Control and Data Acquisition
CoSES	Center for Combined Smart Energy Systems
UTC	Coordinated Universal Time
PTP	Precise Time Protocol
GPS	Global Positioning System
SDFT	Sliding Discrete Fourier Transform
DFT	Discrete Fourier Transform
IoT	Internet of Things
PMU	Phasor Measurement Unit
OPF	Optimal Power Flow
PLL	Phase-Locked Loop

ADMM	Alternating direction method of multipliers
SDP	Semi-definite programming
LTI	Linear time invariant
CORA	Continuous Reachability Analyser
PID	Proportional Integral Derivative
TG	Turbine Governor
AVR	Automatic Voltage Regulator
PI	Proportional Integral

Appendix B

Doctoral Journey

Publications

First Author Publications

[1] A. Mohapatra, V. S. Peric, and T. Hamacher, "Formal Verification of Grid Frequency Controllers," in *Proceedings of 2021 IEEE PES Innovative Smart Grid Technologies Europe, Espoo*, IEEE PES, 2021, ISBN: 9781665448758. DOI: 10.1109/ISGTEurope52324.2021.9640096.

[2] A. Mohapatra, T. Hamacher, and V. S. Peric, "PHIL Infrastructure in CoSES Microgrid Laboratory," in *Proceedings of 2022 IEEE PES Innovative Smart Grid Technologies Conference Europe, Novi Sad*, vol. 2022-October, IEEE PES, 2022, ISBN: 9-7816-6548-0321. DOI: 10.1109/ISGT-Europe54678.2022.9960295.

[3] A. Mohapatra, S. Büttner, G. Bumiller, T. Hamacher, and V. S. Perić, "M-Class PMU for General Purpose Embedded Controllers in NI Veristand Environment," in *Proceedings of 2023 IEEE Belgrade PowerTech*, IEEE, Jun. 2023, pp. 1–6, ISBN: 978-1-6654-8778-8. DOI: 10.1109/PowerTech55446.2023.10202989. [Online]. Available: https://ieeexplore.ieee.org/document/10202989/.

Co-authored publications

[1] V. S. Peric *et al.*, "CoSES Laboratory for Combined Energy Systems At TU Munich," in *2020 IEEE Power Energy Society General Meeting (PESGM)*, 2020, pp. 1–5. DOI: 10.1109/PESGM41954.2020.9281442.

[2] E. Sezgin, A. Mohapatra, T. Hamacher, Ö. Salor, and V. S. Perić, "Fast harmonic analysis for PHIL experiments with decentralized real-time controllers," *Electric Power Systems Research*, vol. 211, Oct. 2022, ISSN: 03787796. DOI: 10.1016/j.epsr.2022.108493.

[3] M. Mayer, A. Mohapatra, and V. S. Peric, "IoT Integration for Combined Energy Systems at the CoSES Laboratory," in *Proceedings of 7th IEEE World Forum on Internet of Things, WF-IoT 2021*, IEEE, Jun. 2021, pp. 195–200, ISBN: 9781665444316. DOI: 10.1109/WF-IoT51360.2021.9596000.

[4] M. Cornejo, A. Mohapatra, S. Candas, and V. S. Peric, "PHIL implementation of a decentralized online OPF for active distribution grids," in *Proceedings of IEEE Power and Energy Society General Meeting 2022, Denver*, vol. 2022-July, IEEE PES, 2022, ISBN: 9781665408233. DOI: 10.1109/PESGM48719.2022.9916705.

[5] S. Candas, B. Reveron Baecker, A. Mohapatra, and T. Hamacher, "Optimization-based framework for low-voltage grid reinforcement assessment under various levels of flexibility and coordination," *Applied Energy*, vol. 343, p. 121 147, 2023, ISSN: 0306-2619. DOI: https://doi.org/10.1016/j.apenergy.2023.121147. [Online]. Available: https://www.sciencedirect.com/science/article/pii/S0306261923005111.

Research Projects

Project Name	**Flexibel konfigurierbares Microgrid-Labor**
Funding program	Forschungsgroßgeräte
Funding agency	Deutsche Forschungsgemeinschaft (DFG)
Project identifier	350746631
Project duration	awarded in 2017
URL	https://www.mep.tum.de/en/mep/coses/
Involved as	Project member - Electrical grid and control system team
Duration of involvement	2017/10 - 2019/12
Main tasks	Procurement and billing of components, installation and commissioning of distributed real-time control infrastructure, developing and commissioning of experiment design concept, commissioning of the Power Hardware-in-the-loop prosumer emaulators.

Project Name	**MCube - ComfficientShare** Komfortables und effizientes Elektrofahrzeug- und Ladepunkt-Sharing für städtische Wohnviertel
Funding program	Clusters4Future
Funding agency	Bundesministerium für Bildung und Forschung
Project Agency	Forschungszentrum Jülich GmbH

Project identifier	03ZU1105CA
Project duration	2021/11/01 bis 2024/10/31
URL	`https://www.mcube-cluster.de/projekt/comfficientshare/`
Involved as	Research Associate at academic project partner TUM - ENS
Duration of involvement	2021/11/01 - 2023/11/31
Main tasks	Literature Review, Research Gap Identification, Demonstration site determination, interaction with the citizen participants, Modeling of car sharing as a energy system model, Documentation, Exchange with Research Community, Dissemination of Results, Coordination with MCube project partners, Event Organization and Participation.

Supervision

Bachelor Thesis of Micha Neumann on *Development and Construction of a Weather station for the CoSES Lab.* Garching, March 2019. Examiner: Prof. Thomas Hamacher.

Master Thesis of Miroslav Lach on *Development and Instrumentation of a Weather-Data Acquisition and Management System for Application in an experimental Microgrid.* Garching, September 2019. Examiner: Prof. Thomas Hamacher.

Master Thesis of Timoumi Ghazi on *Design and Construction of a high voltage reference device for CoSES.* Garching, November 2019. Examiner: Prof. Thomas Hamacher.

Master Thesis of Fulei Xie on *Comparison of microgrid architecture for an example smart home network.* Garching, January 2020, Co-supervised with Soner Candas. Examiner: Prof. Thomas Hamacher.

Bachelor Thesis of Tim Ullrich on *Design and Validation of a PV Model for CoSES Microgrid Lab.* Garching, April 2020. Examiner: Prof. Thomas Hamacher.

Master Thesis of Verena Pichler on *Real-time Energy Management System for a Sector Coupled Microgrid.* Garching, May 2020. Examiner: Prof. Harald Lesch.

Bachelor Thesis of Alessandro Pan on *Development of a RevolutionPi based receiver for wireless M-Bus electricity meters.* Garching, July 2020. Examiner: Prof. Thomas Hamacher.

Master Thesis of Zubejr Sedic on *Efficiency optimized Control of a Six-Phase Asynchronous Machine.* Garching, September 2020, Co-supervised with Igor Gusyev, External

thesis at BMW AG, Munich. Examiner: Prof. Thomas Hamacher.

Master Thesis of Daniel Stichtling on *Energy-Based Condition Monitoring in the Context of Industry 4.0.* Garching, September 2020, Co-supervised with Michael Bernard, External thesis at Fortiss. Examiner: Prof. Thomas Hamacher.

Bachelor Thesis of Lucas Kesting on *Design and Construction of an Excitation Source and Grid Synchronizer for a Synchonous Generator Test Bench.* Garching, September 2020. Examiner: Prof. Thomas Hamacher.

Master Thesis of Martin Cornejo on *A decentralized optimal power flow method for real-time applications in power distribution systems.* Garching, January 2021, Co-supervised with Soner Candas. Examiner: Prof. Thomas Hamacher.

Master Thesis of Johannes Weindl on *Design & construction of a four-leg inverter cabinet.* Garching, May 2021. Examiner: Prof. Thomas Hamacher.

Master Thesis of Matthias Mayer on *Development of the CoSES Internet of Things Platform.* Garching, July 2021. Examiner: Prof. Thomas Hamacher.

Research Internship of Steffen Büttner on *PXI Chassis Time Synchronization via GPS.* Garching, July 2021. Examiner: Prof. Thomas Hamacher.

Bachelor Thesis of Max Hock on *Improvement and Extension of a real-time webbased weather station in CoSES Laboratory.* Garching, August 2021. Examiner: Prof. Thomas Hamacher.

Master Thesis of Steffen Büttner on *Implementation of VeriStand Phasor Measurement Unit for the CoSES Laboratory.* Garching, August 2022. Examiner: Prof. Thomas Hamacher.

Master Thesis of Martin Krautloher on *Economic optimization of services-stacking Battery Energy Storage System.* Garching, May 2023, Co-supervised with Gregorio Velasquez, External thesis at Sonnen GmbH, Allgäu. Examiner: Prof. Thomas Hamacher.

Project Lab Renewable and Sustainable Energy Systems Supervision of a student group for *Microgrid test bench Project*, Garching July 2019, and *Load management test bench Project*, February 2020.

Student Research Assistant (Hiwi) Supervision of student research assistants incl. hiring, administration, training, task management and mentorship.

- Max Hock: 2022/4/1 - 2022/9/30
- Samantha Camacho: 2022/9/1 - 2022/11/30

Teaching

Laboratory course Tutor for the block course *Praktikum LabVIEW in der Energiewirtschaft.*, WiSe 2019, SoSe 2020, SoSe 2020, WiSe 2021, SoSe 2021, WiSe 2022

Laboratory course Tutor for the semester lab *Praktikum Dezentrale Energiesysteme.*, WiSe 2018, 2019, 2020, 2021, 2022

Lecture series - Lecture on Electrical Components in Off-grid systems for the series *Renewable Energy Systems in Developing Countries*, WiSe 2018, 2019, 2020

Theory course - Syllabus design and Tutorials for the course *Active Distribution Grid*, WiSe 2020, 2021, 2022

Center for Combined Smart Energy Systems (CoSES)

Continuous operation, maintenance and upgrades for an Active Distribution Grid laboratory and active participation in the associated research group.

- Laboratory
  - Electrical prosumers
  - Low voltage indoor switchroom
  - Measurement devices and synchronisation
  - Experiment framework in VeriStand
  - Experiment design
  - Laboratory framework design
  - Safety Concepts
  - Network Administration
- Research Group
  - Contributing towards research direction
  - Team building
  - Team structures
  - Representation in forums and events
  - Lab tours

Selected Events

Date	**Location**	**Name**	**Type of participation**
2018, July	Garching	*8th Energy Colloquium of the Munich School of Engineering*; Presentation title, "Four-leg inverters for unbalanced grid feed-in from Renewable energy sources"	presenter
2018, September	Waischenfeld	*Netzwerktreffen des BayWISS Verbundkolleg Energie*; Presentation title, "Center for Combined Smart Energy Systems (CoSES) The idea and the possibilities",	presenter
2018, September	Garching	First-aider training	participant
2018, September	Karlsruhe	*Workshop Echtzeitsimulation in der Energietechnik*; Presentation title, "Real-time from off-grid to smart grid"	presenter
2018, October	Garching	*Tag der offene Tür* Microgrid concepts in research	presenter
2018, November	Raitenhaslach	*Kick-off seminar* for the doctorate by TUM Graduate School; Skill course: "Serious Creativitiy"	participant
2019, May	Garching	*VeriStand Fundamentals Course* by National Instruments	participant
2019, July	Garching	Official opening event of the *Laboratory for Combined Smart Energy System* (CoSES) at TUM	host, participant
2019, July	Garching	*Customized VeriStand Integrator Training* by National Instruments	participant
2019, September	Garching	*Modelica Workshop* by the TUM Graduate School and the Modelica Association	participant
2020, February	Garching	Course on *Scientific Paper Writing* by TUM Graduate School	participant
2020, March	Garching	*Risk assessment workshop* by the TUM Hochschulrefrat 6	participant
2020, July	online	*10th Energy Colloquium of the Munich School of Engineering*; Presentation title, "Fast harmonic estimation using real-time embedded controllers in CoSES smart grid"	presenter

2021, April	online	*4th Spring School Data-driven model learning of dynamic systems*; organised by Ecole Centrale de Lyon	participant
2021, July	online	*IEEE 7th World Forum on Internet of Things*; Co-author for presentation on " IoT Integration for Combined Energy Systems at the CoSES Laboratory"	participant
2021, October	online	*IEEE PES Innovative Smart Grid Technologies Europe Conference*; Presentation on "Formal Verification of Grid Frequency Controllers"	presenter
2022, May	Munich	*MCube Cluster Kick-off*;	participant
2022, July	Porto	*XXII Power Systems Computation Conference*; Presentation on "Fast harmonic analysis for PHIL experiments with decentralized real-time controllers"	presenter
2022, October	Novi Sad	*IEEE PES Innovative Smart Grid Technologies Europe Conference*; Presentation on "PHIL Infrastructure in CoSES Microgrid Laboratory"	presenter
2022, November	Karlsruhe	*Workshop Real-time Simulation in Power Engineering 2022*; Presentation title, "Going beyond PHIL"	presenter
2022, November	Garching	*Doctoral Workshop - Energy Informatics*; hosted by the TUM Chair of Informatics, presented the CoSES lab for the participants	host, presenter
2023, April	Berchtesgaden	*Retreat* for the TUM research group for Combined Smart Energy Systems (CoSES)	organizer, presenter
2023, May	Garching	Course on *Good scientific practice* by TUM Graduate School	participant
2023, June	Belgrade	*IEEE PowerTech Conference*; Presentation on "M-Class PMU for general purpose embedded controllers in NI Veristand environment"	presenter
2023, July	Garching	*Doctoral Summer School* ; hosted by the Max Planck Institut für Plasma physics, presented the CoSES lab for the participants	host, presenter

Bibliography

[1] W. Stevenson and J. Grainger, *Power System Analysis*. McGraw-Hill Education, 1994, ISBN: 9780070612938. [Online]. Available: https://books.google.de/books?id=NBIoAQAAMAAJ.

[2] H. Schellnhuber, S. Rahmstorf, and R. Winkelmann, " Why the right climate target was agreed in Paris," *Nature Clim Change*, pp. 649–653, Jun. 2016. DOI: https://doi.org/10.1038/nclimate3013. [Online]. Available: https://www.nature.com/articles/nclimate3013.

[3] F. Milano, F. Dörfler, G. Hug, D. J. Hill, and G. Verbič, "Foundations and challenges of low-inertia systems (invited paper)," in *2018 Power Systems Computation Conference (PSCC)*, 2018, pp. 1–25. DOI: 10.23919/PSCC.2018.8450880.

[4] F. Blaabjerg, Y. Yang, D. Yang, and X. Wang, "Distributed Power-Generation Systems and Protection," *Proceedings of the IEEE*, vol. 105, no. 7, pp. 1311–1331, 2017. DOI: 10.1109/JPROC.2017.2696878.

[5] I. Dytham, "System Inertia Monitoring National Grid ESO," Tech. Rep., 2021. [Online]. Available: https://www.naspi.org/sites/default/files/2021-06/20210630_naspi_webinar_system_inertia.pdf.

[6] Troy Miller. "Bi-Directional Power Flow: The New World Order and What That Means for the Grid," IEEE Smartgrid. (), [Online]. Available: https://smartgrid.ieee.org/bulletins/november-2017/two-way-power-flow-the-new-world-order-and-what-that-means-for-the-grid (visited on 09/15/2023).

[7] R. W. Kenyon *et al.*, "Stability and control of power systems with high penetrations of inverter-based resources: An accessible review of current knowledge and open questions," *Solar Energy*, vol. 210, pp. 149–168, 2020, Special Issue on Grid Integration, ISSN: 0038-092X. DOI: https://doi.org/10.1016/j.solener.2020.05.053. [Online]. Available: https://www.sciencedirect.com/science/article/pii/S0038092X20305442.

[8] B. Lasseter, "Microgrids [distributed power generation]," *2001 IEEE Power Engineering Society Winter Meeting, PES 2001 - Conference Proceedings*, vol. 1, pp. 146–149, 2001. DOI: 10.1109/PESW.2001.917020.

[9] S. Chowdhury, S. P. Chowdhury, and P. Crossley, "Microgrids and active distribution networks," *Microgrids and Active Distribution Networks*, pp. 1–298, Jan. 2009. DOI: 10.1049/pbrn006e. [Online]. Available: https://digital-library.theiet.org/content/books/po/pbrn006e.

[10] N. Hatziargyriou, H. Asano, R. Iravani, and C. Marnay, "Microgrids," *IEEE Power and Energy Magazine*, vol. 5, no. 4, pp. 78–94, Jul. 2007, ISSN: 15407977. DOI: 10.1109/MPAE.2007.376583.

[11] N. Liu, X. Yu, C. Wang, C. Li, L. Ma, and J. Lei, "Energy-sharing model with price-based demand response for microgrids of peer-to-peer prosumers," *IEEE Transactions on Power Systems*, vol. 32, no. 5, pp. 3569–3583, 2017. DOI: 10.1109/TPWRS.2017.2649558.

[12] I. Serban, S. Céspedes, C. Marinescu, C. A. Azurdia-Meza, J. S. Gómez, and D. S. Hueichapan, "Communication Requirements in Microgrids: A Practical Survey," *IEEE Access*, vol. 8, pp. 47 694–47 712, 2020. DOI: 10.1109/ACCESS.2020.2977928.

[13] "Ieee standard for interconnection and interoperability of distributed energy resources with associated electric power systems interfaces," *IEEE Std 1547-2018 (Revision of IEEE Std 1547-2003)*, pp. 1–138, 2018. DOI: 10.1109/IEEESTD.2018.8332112.

[14] Hermann W. Dommel, "Digital Computer Solution of Electromagnetic Transients in Single-and Multiphase Networks," *IEEE Transactions on Power Apparatus and Systems*, vol. PAS-88, no. 4, 1969. [Online]. Available: https://ieeexplore.ieee.org/document/4073845.

[15] T. Berry; A.R. Daniels; R.W. Dunn, "Real time simulation of power system transient behaviour," in *1991 Third International Conference on Power System Monitoring and Control*, 1991. [Online]. Available: https://ieeexplore.ieee.org/document/151763.

[16] M. O. Faruque *et al.*, "Real-Time Simulation Technologies for Power Systems Design, Testing, and Analysis," *IEEE Power and Energy Technology Systems Journal*, vol. 2, pp. 63–73, 2015, ISSN: 23327707. DOI: 10.1109/JPETS.2015.2427370.

[17] Y. Chen and V. Dinavahi, "FPGA-Based Real-Time EMTP," *IEEE Transactions on Power Delivery*, vol. 24, no. 2, pp. 892–902, 2009. DOI: 10.1109/TPWRD.2008.923392.

[18] J. W. S. Liu, "Real-time operating systems," *Wiley Encyclopedia of Computer Science and Engineering*, 2011. DOI: 10.1002/9780470050118.ecse618.

[19] G. Lauss *et al.*, "Smart grid research infrastructures in Austria: Examples of available laboratories and their possibilities," *Proceeding - 2015 IEEE International Conference on Industrial Informatics, INDIN 2015*, pp. 1539–1545, Sep. 2015. DOI: 10.1109/INDIN.2015.7281962.

[20] H. Hanselmann, "Hardware-in-the-loop simulation testing and its integration into a CACSD toolset," *Proceedings of Joint Conference on Control Applications Intelligent Control and Computer Aided Control System Design*, 1996. [Online]. Available: https://ieeexplore.ieee.org/document/555253.

[21] D. Maclay, "Simulation gets into the loop," *IEE Review*, vol. 43, no. 3, pp. 109–112, 1997. [Online]. Available: https://ieeexplore.ieee.org/document/590793.

[22] Santiago Lentijo; Salvatore D'Arco; Antonello Monti, *Comparing the Dynamic Performances of Power Hardware-in-the-Loop Interfaces*, 2009. [Online]. Available: https://ieeexplore.ieee.org/stamp/stamp.jsp?tp=&arnumber=5170073&tag=1 (visited on 11/21/2022).

[23] W. Ren; M. Sloderbeck; M. Steurer; V. Dinavahi; T. Noda; S. Filizadeh; A. R. Chevrefils; M. Matar; R. Iravani; C. Dufour; J. Belanger; "Interfacing Issues in Real-Time Digital Simulators," *IEEE Transactions on Power Delivery*, vol. 26, no. 2, 2010. [Online]. Available: https://ieeexplore.ieee.org/stamp/stamp.jsp?arnumber=5628278.

[24] Felix Lehfuss and Georg Lauss, Panos Kotsampopoulos and Nikos Hatziargyriou, and Paul Crolla and Andrew Roscoe, *Comparison of multiple Power Amplification types for Power Hardware-in-the-Loop Applications*, 2012. [Online]. Available: https://ieeexplore.ieee.org/stamp/stamp.jsp?tp=&arnumber=6242959&tag=1 (visited on 11/21/2022).

[25] Amin Khodaei; Mohammad Shahidehpour, *Microgrid-Based Co-Optimization of Generation and Transmission Planning in Power Systems*, 2013. [Online]. Available: https://ieeexplore.ieee.org/stamp/stamp.jsp?arnumber=6377245 (visited on 11/22/2022).

[26] A. Borghetti *et al.*, "Short-term scheduling and control of active distribution systems with high penetration of renewable resources," *IEEE Systems Journal*, vol. 4, no. 3, pp. 313–322, Sep. 2010, ISSN: 19328184. DOI: 10.1109/JSYST.2010.2059171.

[27] A. Kargarian Marvasti *et al.*, "Optimal Operation of Active Distribution Grids: A System of Systems Framework," *IEEE Transactions on Smart Grid*, vol. 5, no. 3, 2014. DOI: 10.1109/TSG.2013.2282867. [Online]. Available: http://www.ieee.org/publications_standards/publications/rights/index.html.

[28] S. Hanif, T. Massier, H. B. Gooi, T. Hamacher, and T. Reindl, "Cost Optimal Integration of Flexible Buildings in Congested Distribution Grids," *IEEE Transactions on Power Systems*, vol. 32, no. 3, pp. 2254–2266, 2017. DOI: 10.1109/TPWRS.2016.2605921.

[29] S. Hanif, H. B. Gooi, T. Massier, T. Hamacher, and T. Reindl, "Distributed Congestion Management of Distribution Grids Under Robust Flexible Buildings Operations," *IEEE Transactions on Power Systems*, vol. 32, no. 6, pp. 4600–4613, 2017. DOI: 10.1109/TPWRS.2017.2660065.

[30] S. Hanif, K. Zhang, C. M. Hackl, M. Barati, H. B. Gooi, and T. Hamacher, "Decomposition and Equilibrium Achieving Distribution Locational Marginal Prices Using Trust-Region Method," *IEEE Transactions on Smart Grid*, vol. 10, no. 3, pp. 3269–3281, 2019. DOI: 10.1109/TSG.2018.2822766.

[31] S. H. Low, "Convex relaxation of optimal power flow—part i: Formulations and equivalence," *IEEE Transactions on Control of Network Systems*, vol. 1, no. 1, pp. 15–27, 2014. DOI: 10.1109/TCNS.2014.2309732.

[32] J. Huang, B. Cui, X. Zhou, and A. Bernstein, "A generalized lindistflow model for power flow analysis," *CoRR*, vol. abs/2104.02118, 2021. arXiv: 2104.02118. [Online]. Available: https://arxiv.org/abs/2104.02118.

[33] D. Ton and J. Reilly, "Microgrid controller initiatives," *IEEE Power and Energy Magazine*, vol. 15, no. 4, pp. 24–31, 2017, ISSN: 15407977. DOI: 10.1109/MPE.2017.2691238.

[34] A. Maitra *et al.*, "Microgrid controllers: Expanding Their Role and Evaluating Their Performance," *IEEE Power and Energy Magazine*, vol. 15, no. 4, pp. 41–49, 2017, ISSN: 15407977. DOI: 10.1109/MPE.2017.2690519.

[35] IEEE-PES Task Force on Microgrid Control, *Trends in Microgrid Control*, 2014. [Online]. Available: https://ieeexplore.ieee.org/stamp/stamp.jsp?tp=&arnumber=6818494 (visited on 11/22/2022).

[36] Y. Kou, Y. Liu, and X. Wang, "Harmonic Mitigation in Active Distribution Grids Using Inverters: A Review," *IEEE Transactions on Smart Grid*, vol. 9, no. 2, pp. 1046–1057, 2018. DOI: 10.1109/TSG.2016.2616540.

[37] C. Perera and G. Ledwich, "Active power filters for power quality improvement in smart grids," *Energies*, vol. 11, no. 4, p. 747, 2018. DOI: 10.3390/en11040747.

[38] H. Wang and J. Huang, "Incentivizing Energy Trading for Interconnected Microgrids," *IEEE Transactions on Smart Grid*, vol. 9, no. 4, pp. 2647–2657, 2018. DOI: 10.1109/TSG.2016.2614988.

[39] J. M. Guerrero, J. C. Vasquez, J. Matas, L. G. De Vicuña, and M. Castilla, "Hierarchical control of droop-controlled AC and DC microgrids - A general approach toward standardization," *IEEE Transactions on Industrial Electronics*, vol. 58, no. 1, pp. 158–172, Jan. 2011, ISSN: 02780046. DOI: 10.1109/TIE.2010.2066534.

[40] J. Rocabert, A. Luna, F. Blaabjerg, and P. Rodríguez, "Control of power converters in AC microgrids," *IEEE Transactions on Power Electronics*, vol. 27, no. 11, pp. 4734–4749, 2012, ISSN: 08858993. DOI: 10.1109/TPEL.2012.2199334.

[41] E. Noonan and E. Fitzpatrick, "Will distributed energy resources (DERs) change how we get our energy?" en, *European Parliamentary Research Service*, Jul. 2020. [Online]. Available: https://www.europarl.europa.eu/RegData/etudes/ATAG/2020/651944/EPRS_ATA(2020)651944_EN.pdf.

[42] B. Kampman, J. Blommerde, and M. Afman, *The potential of energy citizens in the European Union*, Sep. 2016. [Online]. Available: https://ce.nl/wp-content/uploads/2021/03/CE_Delft_3J00_Potential_energy_citizens_EU_final_1479221398.pdf.

[43] J. W. Simpson-Porco, Q. Shafiee, F. Dörfler, J. C. Vasquez, J. M. Guerrero, and F. Bullo, "Secondary frequency and voltage control of islanded microgrids via distributed averaging," *IEEE Transactions on Industrial Electronics*, vol. 62, no. 11, pp. 7025–7038, 2015. DOI: 10.1109/TIE.2015.2436879.

[44] A. H. Etemadi, E. J. Davison, and R. Iravani, "A decentralized robust control strategy for multi-DER microgrids-part I: Fundamental concepts," *IEEE Transactions on Power Delivery*, vol. 27, no. 4, pp. 1843–1853, 2012, ISSN: 08858977. DOI: 10.1109/TPWRD.2012.2202920.

[45] O. Ouramdane, E. Elbouchikhi, Y. Amirat, and E. S. Gooya, "Optimal sizing of domestic grid-connected microgrid maximizing self consumption and battery lifespan," *IFAC-PapersOnLine*, vol. 55, no. 12, pp. 683–688, 2022, 14th IFAC Workshop on Adaptive and Learning Control Systems ALCOS 2022, ISSN: 2405-8963. DOI: https://doi.org/10.1016/j.ifacol.2022.07.391. [Online]. Available: https://www.sciencedirect.com/science/article/pii/S2405896322007923.

[46] S. Ayasun; R. Fischl; T. Chmielewski; S. Vallieu; K. Miu; C. Nwankpa, *Evaluation of the static performance of a simulation-stimulation interface for power hardware in the loop*, 2003. [Online]. Available: https://ieeexplore.ieee.org/stamp/stamp.jsp?tp=&arnumber=1304513&tag=1 (visited on 11/21/2022).

[47] S. Alzate-Drada, K. Montano-Martinez, and F. Andrade, "Energy Management System for a Residential Microgrid in a Power Hardware-in-the-Loop Platform," *IEEE Power and Energy Society General Meeting*, vol. 2019-Augus, Aug. 2019, ISSN: 19449933. DOI: 10.1109/PESGM40551.2019.8974002.

[48] K. Prabakar *et al.*, "Site-Specific Evaluation of Microgrid Controller Using Controller and Power-Hardware-in-the-Loop," *IECON Proceedings (Industrial Electronics Conference)*, vol. 2019-Octob, pp. 6463–6468, Oct. 2019. DOI: 10.1109/IECON.2019.8927354.

[49] R. Stanev, K. Viglov, K. Nakov, and T. Asenov, "A Real Time Power Hardware in the Loop Test Bed for Power System Stability Studies," *2020 12th Electrical Engineering Faculty Conference, BulEF 2020*, Sep. 2020. DOI: 10.1109/BULEF51036.2020.9326020.

[50] J. Roldan-Perez *et al.*, "Emulation of Complex Grid Scenarios by using Power Hardware in the Loop (PHIL) Techniques," *IECON Proceedings (Industrial Electronics Conference)*, vol. 2021-Octob, Oct. 2021. DOI: 10.1109/IECON48115.2021.9589168.

[51] E. Bompard *et al.*, "Latency and Simulation Stability in a Remote Power Hardware-in-the-Loop Cosimulation Testbed," *IEEE Transactions on Industry Applications*, vol. 57, no. 4, pp. 3463–3473, Jul. 2021, ISSN: 19399367. DOI: 10.1109/TIA.2021.3082506.

[52] M. Ferrari, B. Park, and M. M. Olama, "Design and evaluation of a model-free frequency control strategy in islanded microgrids with power-hardware-in-the-loop testing," *2021 IEEE Power and Energy Society Innovative Smart Grid Technologies Conference, ISGT 2021*, Feb. 2021. DOI: 10.1109/ISGT49243.2021.9372219.

[53] "Ieee standard for the specification of microgrid controllers," *IEEE Std 2030.7-2017*, pp. 1–43, 2018. DOI: 10.1109/IEEESTD.2018.8340204.

[54] A. S. Vijay, S. Doolla, and M. C. Chandorkar, "Real-Time Testing Approaches for Microgrids," *IEEE Journal of Emerging and Selected Topics in Power Electronics*, vol. 5, no. 3, pp. 1356–1376, Sep. 2017, ISSN: 21686785. DOI: 10.1109/JESTPE.2017.2695486.

[55] DERlab, "European Distributed Energy Resources Laboratories: Activity Report 2012/13," Tech. Rep., 2016. [Online]. Available: https://der-lab.net/wp-content/uploads/2016/05/derlab_activity_report_2012_2013_LQ.pdf.

[56] M. Barnes *et al.*, "MicroGrid laboratory facilities," *2005 International Conference on Future Power Systems*, vol. 2005, 2005. DOI: 10.1109/FPS.2005.204229.

[57] L. Meng, M. Savaghebi, F. Andrade, J. C. Vasquez, J. M. Guerrero, and M. Graells, "Microgrid central controller development and hierarchical control implementation in the intelligent microgrid lab of Aalborg University," *Conference Proceedings - IEEE Applied Power Electronics Conference and Exposition - APEC*, vol. 2015-May, no. May, pp. 2585–2592, May 2015. DOI: 10.1109/APEC.2015.7104716.

[58] B. Xiao *et al.*, "Development of hardware-in-the-loop microgrid testbed," *2015 IEEE Energy Conversion Congress and Exposition, ECCE 2015*, pp. 1196–1202, Oct. 2015. DOI: 10.1109/ECCE.2015.7309827.

[59] C. Patrascu, N. Muntean, O. Cornea, and A. Hedes, "Microgrid laboratory for educational and research purposes," *EEEIC 2016 - International Conference on Environment and Electrical Engineering*, Aug. 2016. DOI: 10.1109/EEEIC.2016.7555682.

[60] A. Monot, M. Wahler, J. Valtari, M. Rita-Kasari, and J. Nikko, "Real-time research lab in the sundom smart grid pilot," *IET Conference Publications*, vol. 2016, no. CP686, 2016. DOI: 10.1049/CP.2016.0726.

[61] I. Serban and C. P. Ion, "A PHIL system designed for testing the dynamic response of microgrid units," *Conference Proceedings - 2017 17th IEEE International Conference on Environment and Electrical Engineering and 2017 1st IEEE Industrial and Commercial Power Systems Europe, EEEIC / I and CPS Europe 2017*, Jul. 2017. DOI: 10.1109/EEEIC.2017.7977763.

[62] P. C. Kotsampopoulos, V. A. Kleftakis, and N. D. Hatziargyriou, "Laboratory Education of Modern Power Systems Using PHIL Simulation," *IEEE Transactions on Power Systems*, vol. 32, no. 5, pp. 3992–4001, Sep. 2017, ISSN: 08858950. DOI: 10.1109/TPWRS.2016.2633201.

[63] M. C. Alvarez-Herault *et al.*, "An Original Smart-Grids Test Bed to Teach Feeder Automation Functions in a Distribution Grid," *IEEE Transactions on Power Systems*, vol. 33, no. 1, pp. 373–385, Apr. 2017, ISSN: 0885-8950. DOI: 10.1109/TPWRS.2017.2695401.

[64] S. Bruno, G. Giannoccaro, M. L. Scala, and G. Lopopolo, "First activities and power-hardware-in-the-loop tests at the public research laboratory LabZERO," *2018 110th AEIT International Annual Conference, AEIT 2018*, Dec. 2018. DOI: 10.23919/AEIT.2018.8577373.

[65] A. Krontiris, I. Jeromin, S. Pfeffer, and M. Pfeffer, "Smart Grid Lab Hessen - a real-life test environment for active distribution grids," *2021 9th International Conference on Modern Power Systems (MPS)*, 2021. DOI: 10.1109/MPS52805.2021.9492637. [Online]. Available: https://eit.h-da.de/forschung/forschungsprojekte/smart-grid-lab.

[66] F. Gielnik *et al.*, "Establishing a Power Hardware-in-the-Loop Environment with a Smart Energy Complex," *2022 57th International Universities Power Engineering Conference: Big Data and Smart Grids, UPEC 2022 - Proceedings*, 2022. DOI: 10.1109/UPEC55022.2022.9918012.

[67] O. Gehrke and H. Bindner, "Building a test platform for agents in power system control: Experience from SYSLAB," *2007 International Conference on Intelligent Systems Applications to Power Systems, ISAP*, 2007. DOI: 10.1109/ISAP.2007.4441635.

[68] D. Surendra and K. N. Shubhanga, "Development of a power system laboratory supported by real-time systems," *2011 International Conference on Power and Energy Systems, ICPS 2011*, 2011. DOI: 10.1109/ICPES.2011.6156686.

[69] J. Østergaard, Q. Wu, and R. Garcia-Valle, "Real Time Intelligent Control Laboratory (RT-ICL) of PowerLabDK for smart grid technology development," *2012 IEEE Workshop on Complexity in Engineering, COMPENG 2012 - Proceedings*, pp. 61–64, 2012. DOI: 10.1109/COMPENG.2012.6242948.

[70] O. Antoine, P. Janssen, Q. Jossen, and J. C. Maun, "A laboratory microgrid for studying grid operations with PMUs," *IEEE Power and Energy Society General Meeting*, 2013, ISSN: 19449925. DOI: 10.1109/PESMG.2013.6672891.

[71] F. Guo *et al.*, "Design and development of a reconfigurable hybrid Microgrid testbed," *2013 IEEE Energy Conversion Congress and Exposition, ECCE 2013*, pp. 1350–1356, 2013. DOI: 10.1109/ECCE.2013.6646862.

[72] G. Messinis *et al.*, "A multi-microgrid laboratory infrastructure for smart grid applications," *IET Conference Publications*, vol. 2014, no. CP665, 2014. DOI: 10.1049/CP.2014.1670.

[73] F. Huerta, J. K. Gruber, M. Prodanovic, and P. Matatagui, "A power-HIL microgrid testbed: Smart Energy Integration Lab (SEIL)," *2014 IEEE Energy Conversion Congress and Exposition, ECCE 2014*, pp. 3998–4003, Nov. 2014. DOI: 10.1109/ECCE.2014.6953945.

[74] Y. Liao, X. Shi, C. Fu, and J. Meng, "Hardware in-the-loop simulation system based on NI-PXI for operation and control of microgrid," *Proceedings of the 2014 9th IEEE Conference on Industrial Electronics and Applications, ICIEA 2014*, pp. 1366–1370, Oct. 2014. DOI: 10.1109/ICIEA.2014.6931381.

[75] L. L. Jansen, N. Andreadou, I. Papaioannou, and A. Marinopoulos, "Smart grid lab research in Europe and beyond," *International Journal of Energy Research*, vol. 44, no. 3, pp. 1307–1336, 2020. [Online]. Available: https://onlinelibrary.wiley.com/doi/epdf/10.1002/er.4818.

[76] O. Heussen, Kai; Gehrke, "State of the Art Smart Grid Laboratories - A Survey about Software Use," Tech. Rep., 2014. [Online]. Available: https://backend.orbit.dtu.dk/ws/portalfiles/portal/104280207/D1.2_survey_evaluation_final.pdf.

[77] Leon Osborne; Jeffrey Brummond; Robert Hart; Mohsen Zarean; P.E Steven Conger, "Clarus: Concept of Operations," Tech. Rep., 2005. [Online]. Available: https://rosap.ntl.bts.gov/view/dot/3710.

[78] EPFL. "Smart grid EPFL." (2022), [Online]. Available: https://smartgrid.epfl.ch (visited on 11/30/2022).

[79] J.-T. Gao, C.-H. Shih, C.-W. Lee, and K.-Y. Lo, "An Active and Reactive Power Controller for Battery Energy Storage System in Microgrids," *IEEE Access*, vol. 10, pp. 10 490–10 499, 2022. DOI: 10.1109/ACCESS.2022.3145009.

[80] *Einweihung des CoSES-Labors*. [Online]. Available: https://www.mep.tum.de/mep/aktuelles/news-single-view/article/einweihung-des-coses-labors/.

[81] V. S. Peric *et al.*, "CoSES Laboratory for Combined Energy Systems At TU Munich," in *2020 IEEE Power Energy Society General Meeting (PESGM)*, 2020, pp. 1–5. DOI: 10.1109/PESGM41954.2020.9281442.

[82] A. Mohapatra, T. Hamacher, and V. S. Peric, "PHIL Infrastructure in CoSES Microgrid Laboratory," in *Proceedings of 2022 IEEE PES Innovative Smart Grid Technologies Conference Europe, Novi Sad*, vol. 2022-October, IEEE PES, 2022, ISBN: 9-7816-6548-0321. DOI: 10.1109/ISGT-Europe54678.2022.9960295.

[83] D. Zinsmeister *et al.*, "A prosumer-based sector-coupled district heating and cooling laboratory architecture," *Smart Energy*, vol. 9, p. 100 095, 2023, ISSN: 2666-9552. DOI: https://doi.org/10.1016/j.segy.2023.100095. [Online]. Available: https://www.sciencedirect.com/science/article/pii/S2666955223000023.

[84] H. Lund *et al.*, "Perspectives on fourth and fifth generation district heating," *Energy*, vol. 227, p. 120 520, 2021, ISSN: 0360-5442. DOI: https://doi.org/10.1016/j.energy.2021.120520. [Online]. Available: https://www.sciencedirect.com/science/article/pii/S0360544221007696.

[85] E. Sezgin, A. Mohapatra, T. Hamacher, Ö. Salor, and V. S. Perić, "Fast harmonic analysis for PHIL experiments with decentralized real-time controllers," *Electric Power Systems Research*, vol. 211, Oct. 2022, ISSN: 03787796. DOI: 10.1016/j.epsr.2022.108493.

[86] M. Mayer, A. Mohapatra, and V. S. Peric, "IoT Integration for Combined Energy Systems at the CoSES Laboratory," in *Proceedings of 7th IEEE World Forum on Internet of Things, WF-IoT 2021*, IEEE, Jun. 2021, pp. 195–200, ISBN: 9781665444316. DOI: 10.1109/WF-IoT51360.2021.9596000.

[87] A. Mohapatra, S. Büttner, G. Bumiller, T. Hamacher, and V. S. Perić, "M-Class PMU for General Purpose Embedded Controllers in NI Veristand Environment," in *Proceedings of 2023 IEEE Belgrade PowerTech*, IEEE, Jun. 2023, pp. 1–6, ISBN: 978-1-6654-8778-8. DOI: 10.1109/PowerTech55446.2023.10202989. [Online]. Available: https://ieeexplore.ieee.org/document/10202989/.

[88] M. Cornejo, A. Mohapatra, S. Candas, and V. S. Peric, "PHIL implementation of a decentralized online OPF for active distribution grids," in *Proceedings of IEEE Power and Energy Society General Meeting 2022, Denver*, vol. 2022-July, IEEE PES, 2022, ISBN: 9781665408233. DOI: 10.1109/PESGM48719.2022.9916705.

[89] A. Mohapatra, V. S. Peric, and T. Hamacher, "Formal Verification of Grid Frequency Controllers," in *Proceedings of 2021 IEEE PES Innovative Smart Grid Technologies Europe, Espoo*, IEEE PES, 2021, ISBN: 9781665448758. DOI: 10.1109/ISGTEurope52324.2021.9640096.

[90] "Time Synchronization in the Electric Power System," North American SynchroPhasor Initiative, NASPI Technical Report NASPI-2017-TR-001, 2017.

[91] M. Surprenant, I. Hiskens, and G. Venkataramanan, "Phase locked loop control of inverters in a microgrid," in *2011 IEEE Energy Conversion Congress and Exposition*, Sep. 2011, pp. 667–672. DOI: 10.1109/ECCE.2011.6063833.

[92] N. Instruments. "PXIe-8880 - PXI Express Controller." Accessed: September 18, 2023. (2023), [Online]. Available: https://www.ni.com/de-de/shop/model/pxie-8880.html.

[93] N. Instruments. "PXI-6683 Specifications." Accessed: September 18, 2023. (2023), [Online]. Available: https://www.ni.com/docs/de-DE/bundle/pxi-6683-specs/page/specs.html.

[94] N. I. of Standards and T. (NIST). "IEEE 1588 - Precision Timing for Sync and Time Stamps." Accessed: September 18, 2023. (2021), [Online]. Available: https://www.nist.gov/el/intelligent-systems-division-73500/ieee-1588.

[95] A. E. Saldaña-González, A. Sumper, M. Aragüés-Peñalba, and M. Smolnikar, "Advanced Distribution Measurement Technologies and Data Applications for Smart Grids: A Review," *Energies*, vol. 13, no. 14, 2020, ISSN: 1996-1073. DOI: 10.3390/en13143730. [Online]. Available: https://www.mdpi.com/1996-1073/13/14/3730.

[96] "IEEE Standard for Synchrophasor Data Transfer for Power Systems," *IEEE Std C37.118.2-2011 (Revision of IEEE Std C37.118-2005)*, pp. 1–53, 2011. DOI: 10.1109/IEEESTD.2011.6111222.

[97] R. S. Singh, H. Hooshyar, and L. Vanfretti, "Assessment of time synchronization requirements for Phasor Measurement Units," in *2015 IEEE Eindhoven PowerTech*, 2015, pp. 1–6. DOI: 10.1109/PTC.2015.7232728.

[98] E. P. Electronics. "CSU100 - Compact Standby Unit." Accessed: September 18, 2023. (2023), [Online]. Available: https://www.egstonpower.com/portfolio/csu100/.

[99] Xilinx. "Aurora 8B10B IP Core." Accessed: September 18, 2023. (2012), [Online]. Available: https://www.xilinx.com/products/intellectual-property/aurora8b10b.html.

[100] "IEEE Standard for Harmonic Control in Electric Power Systems," *IEEE Std 519-2022 (Revision of IEEE Std 519-2014)*, pp. 1–31, Aug. 2022. DOI: 10.1109/IEEESTD.2022.9848440.

[101] N. Instruments. "What Is VeriStand?" Accessed: September 18, 2023. (2018), [Online]. Available: https://www.ni.com/de/shop/data-acquisition-and-control/application-software-for-data-acquisition-and-control-category/what-is-veristand.html.

[102] G. Bedi, G. K. Venayagamoorthy, R. Singh, R. R. Brooks, and K.-C. Wang, "Review of Internet of Things (IoT) in Electric Power and Energy Systems," *IEEE Internet of Things Journal*, vol. 5, no. 2, pp. 847–870, Apr. 2018, ISSN: 2327-4662. DOI: 10.1109/JIOT.2018.2802704.

[103] S. Karnouskos, "The cooperative Internet of Things enabled Smart Grid," presented at the 14th IEEE International Symposium on Consumer Electronics (ISCE2010), Braunschweig: IEEE, Jun. 7, 2010. [Online]. Available: https://citeseerx.ist.psu.edu/viewdoc/download?rep=rep1&type=pdf&doi=10.1.1.208.3773.

[104] "IEEE/IEC International Standard - Measuring relays and protection equipment - Part 118-1: Synchrophasor for power systems - Measurements," *IEC/IEEE 60255-118-1:2018*, pp. 1–78, 2018. DOI: 10.1109/IEEESTD.2018.8577045.

[105] R. E. Kalman, "Mathematical Description of Linear Dynamical Systems," *Journal of the Society for Industrial and Applied Mathematics Series A Control*, vol. 1, no. 2, pp. 152–192, Jan. 1963. DOI: 10.1137/0301010. [Online]. Available: https://doi.org/10.1137/0301010.

[106] S. M. LaValle, *Planning Algorithms*. Cambridge, U.K.: Cambridge University Press, 2006, Available at http://planning.cs.uiuc.edu/.

[107] Y. Kukimoto. "Introduction to Formal Verification." Accessed: September 18, 2023. (1996), [Online]. Available: https://ptolemy.berkeley.edu/projects/embedded/research/vis/doc/VisUser/vis_user/node4.html.

[108] F. Gruber and M. Althoff, "Computing Safe Sets of Linear Sampled-Data Systems," *IEEE Control Systems Letters*, vol. 5, no. 2, pp. 385–390, 2021. DOI: 10.1109/LCSYS.2020.3002476.

[109] M. Althoff, "Formal and Compositional Analysis of Power Systems Using Reachable Sets," *IEEE Transactions on Power Systems*, vol. 29, no. 5, pp. 2270–2280, Sep. 2014, ISSN: 0885-8950, 1558-0679. DOI: 10.1109/TPWRS.2014.2306731. [Online]. Available: http://ieeexplore.ieee.org/document/6750746/ (visited on 08/30/2023).

[110] B. Schürmann, N. Kochdumper, and M. Althoff, "Reachset Model Predictive Control for Disturbed Nonlinear Systems," in *2018 IEEE Conference on Decision and Control (CDC)*, 2018, pp. 3463–3470. DOI: 10.1109/CDC.2018.8619781.

[111] A. El-Guindy, D. Han, and M. Althoff, "Estimating the region of attraction via forward reachable sets," in *2017 American Control Conference (ACC)*, 2017, pp. 1263–1270. DOI: 10.23919/ACC.2017.7963126.

[112] M. Ribbens-Pavella and F. Evans, "Direct methods for studying dynamics of large-scale electric power systems—A survey," *Automatica*, vol. 21, no. 1, pp. 1–21, 1985, ISSN: 0005-1098. DOI: https://doi.org/10.1016/0005-1098(85)90095-0. [Online]. Available: https://www.sciencedirect.com/science/article/pii/0005109885900950.

[113] H. Bevrani, *Robust Power System Frequency Control*. Boston, MA: Springer US, 2009, ISBN: 978-0-387-84877-8 978-0-387-84878-5. DOI: 10.1007/978-0-387-84878-5. [Online]. Available: https://link.springer.com/10.1007/978-0-387-84878-5 (visited on 09/19/2023).

[114] M. Althoff, "Reachability Analysis and its Application to the Safety Assessment of Autonomous Cars," en, Ph.D. dissertation, Technische Universität München, 2010, p. 221.

[115] M. Althoff, "An Introduction to CORA 2015," in *Proc. of the Workshop on Applied Verification for Continuous and Hybrid Systems*, 2015, pp. 120–151. DOI: 10.29007/zbkv.

[116] S. Bogomolov, M. Forets, G. Frehse, K. Potomkin, and C. Schilling, "JuliaReach: A toolbox for set-based reachability," in *Proceedings of the 22nd ACM International Conference on Hybrid Systems: Computation and Control*, Montreal Quebec Canada: ACM, Apr. 16, 2019, pp. 39–44, ISBN: 978-1-4503-6282-5. DOI: 10.1145/3302504.3311804. [Online]. Available: https://dl.acm.org/doi/10.1145/3302504.3311804 (visited on 09/19/2023).

[117] M. Baudette, M. Castro, T. Rabuzin, J. Lavenius, T. Bogodorova, and L. Vanfretti, "OpenIPSL: Open-instance power system library — update 1.5 to "iTesla power systems library (iPSL): A modelica library for phasor time-domain simulations"," *SoftwareX*, vol. 7, pp. 34–36, Jan. 2018, ISSN: 23527110. DOI: 10.1016/j.softx.2018.01.002. [Online]. Available: https://linkinghub.elsevier.com/retrieve/pii/S2352711018300050 (visited on 09/19/2023).

[118] M. Wetzlinger, N. Kochdumper, S. Bak, and M. Althoff, "Fully-Automated Verification of Linear Systems Using Reachability Analysis with Support Functions," in *Proceedings of the 26th ACM International Conference on Hybrid Systems: Computation and Control*, San Antonio TX USA: ACM, May 9, 2023, pp. 1–12, ISBN: 9798400700330. DOI: 10.1145/3575870.3587121. [Online]. Available: https://dl.acm.org/doi/10.1145/3575870.3587121 (visited on 08/30/2023).

[119] G. Schweiger *et al.*, "District energy systems: Modelling paradigms and general-purpose tools," *Energy*, vol. 164, pp. 1326–1340, Dec. 2018. DOI: 10.1016/j.energy.2018.08.193. [Online]. Available: https://doi.org/10.1016/j.energy.2018.08.193.

[120] M. Wetter, M. Bonvini, and T. S. Nouidui, "Equation-based languages – A new paradigm for building energy modeling, simulation and optimization," *Energy and Buildings*, vol. 117, pp. 290–300, Apr. 2016. DOI: 10.1016/j.enbuild.2015.10.017. [Online]. Available: https://doi.org/10.1016/j.enbuild.2015.10.017.

[121] F. E. Cellier, H. Elmqvist, M. Otter, *et al.*, "Modeling from physical principles," *The Control Handbook, 1996 by CRC Press, Inc., ed. William S. Levine*, pp. 99–108, 1996.

[122] MathWorks. "Synchronous Machine pu Standard." Accessed: September 18, 2023. (2006), [Online]. Available: `https://de.mathworks.com/help/sps/powersys/ref/synchronousmachinepustandard.html`.